2022

New insights into *Staphylococcus aureus* cell cycle and cell wall stress response

Pedro Baptista Fernandes

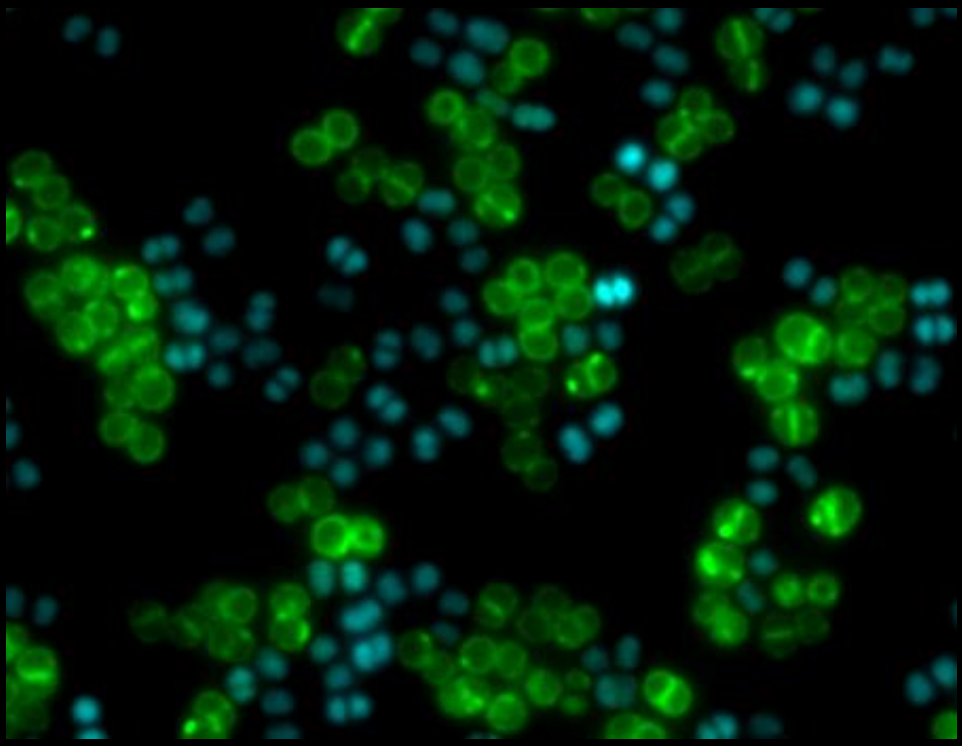

Dissertation presented to obtain the **Ph.D degree in**

Molecular Biosciences

Oeiras, July 2022

INSTITUTO DE TECNOLOGIA QUÍMICA E BIOLÓGICA ANTÓNIO XAVIER | UNIVERSIDADE NOVA DE LISBOA

New insights into *Staphylococcus aureus* cell cycle and cell wall stress response

Pedro Escada Cardoso Baptista Fernandes

Dissertation presented to obtain the Ph.D degree in Molecular Biosciences

Oeiras, July, 2022

Acknowledgments

I would like to thank Professor Mariana Pinho, my thesis supervisor. I still remember the first day I came to the lab. I am always sceptical about my achievements but when I look back, I realize how much I grew as a person and as a researcher. This whole journey wouldn't have been possible without your guidance and support. I can't express enough my gratitude for the opportunity you gave me and for believing in me all the time. Sometimes I felt that I didn't fit your high standards and that made me push my limits, to become a better person and a better scientist. Thank you for that! And specially for all the opportunities that arose during all this time, the collaborations I got involved in and for all the fascinating people I met along the way! Thank you Mariana!

To Professor Sérgio Filipe, for all the passionate discussions. To be completely honest, your mind fascinates me, it's like a volcano always erupting with ideas. Thank you for all the input you had to this PhD and for your dedication in planning experiments and interpreting the results. I will miss our Lab Meetings and the moments when you were actually right about something, after suggesting a non-conventional model or mechanism "I knew it!". Thank you Sérgio!

To my thesis committee, Prof. Adriano Henriques and Dr. Jorge Carneiro for helpful discussions on how to improve my work and specially for questioning everything I presented. It made me a better and more rigorous researcher.

To Dr. Marcos Pires, my supervisor at Lehigh University, for allowing me to come to his lab. It was a very pleasant and challenging experience. It was the first time I was living abroad and I learned a lot while I was there, despite the trip back to Portugal (which was probably the worst flight I ever had in my life!).

After all these years working in the Bacterial Cell Biology Laboratory, I had the opportunity to meet so many incredibly intelligent and fascinating people. There are so many people I must acknowledge that I have to write another PhD thesis just for that. Ok, here we go! João Monteiro was probably the first person I met, when I arrived, you were the one teaching me how things were done in the lab, and you had to have a colossal patience for my 1000000000 questions every second: How do I do this? How do I do that? How do I turn this on? How do I turn this off? And after all of this, you still ask me to be part of the groomsmen, at your wedding!? To Pedro Matos… Where do I start? You are basically ubiquitous in my life, you are always there! Anytime, anywhere I need! You are like the Power Rangers of my life (you can pick your favourite colour)! I owe you a lot! And *Ovos em número ímpar*! Never forget this! Raquel Pereira, my housemate for 3 years (?), you are probably now one of my closest friends. Sometimes, you know me better than I know myself! We shared so many things and you taught me so much! From microscopy to how to cook (or, at least, you tried)! Or how not to use a vacuum cleaner! Bruno Computer Genius Saraiva, knowing you restored my faith in Mankind! You made our lives so much easier in the lab! And outside the lab, as well! You are probably the best life coach ever and you do your job for free! Nathalie, the definition of Virtue and Integrity. That is why you became our Pelican of Justice! Thank

you for setting such high standards at work and in life (and sorry for the brownie…). Trish, the “firefighter”, who helped me whenever my work looked like a Californian wildfire. You were there with your fire truck every time I was being consumed by the flames of despair! Ok, this sounds super dramatic, but you know what I mean! Helena, I know you don’t like to be called Molecular Biology expert, but that is the truth. You are one of those people that never talk much, but when you do, all the thoughts you share are wise. You are a wise Molecular Biology expert! Ambre, the example that working hard in life pays off! Your example was really inspiring to me! And I miss our political (and less political) discussions! Andreia Tavares, a person with such a great determination in life and at work. Your work discipline was impressive! Learned a lot with you (and sorry for asking for the breath alcohol test)! Mário, my partner in so many occasions, from Star Wars discussions, to gaming, working, you also had your fire truck ready whenever I needed to extinguish a fire (or anyone in the lab, in fact). Sara, I think my truck is finally moving out of the garage (so many truck analogies in these acknowledgments). I might be out of fuel, after so many manoeuvres, though! If I can do it, you can do it, this is 100% true! Your resilience and hard-working skills will have to pay off!!! Also, don’t forget that we need to publish our paper about the existence of the “Evil Genius”. For Descartes, it was just an academic hypothesis, but we confirmed it exists!! Andreia Duarte, my Krav Maga and 日本語 partner, but specially my “little mother”, thank you for taking care of me and for being the invisible hand that holds me, when I need! And... リボソーム and ゲノム, but probably your favourite is 木曜日. ありがとうございます。 Moritz, I will be always amazed with your general knowledge and for you being

always so helpful, despite liking Star Wars: The Last Jedi (that's outrageous). We are going to cross the finish line at the same time! Marta, a.k.a. Dr. Sporniak, the person who discovered phage λ, I will never forget your bench with 200000000 test tubes and your astonishing sense of humour. Think I've never laughed so hard in my life, before meeting you! Remember that joke that made me laugh non-stop, I couldn't pipette for a week? Lucia (Santa Lucia), hope you still have the flag! You were always so polite, well behaved and always available to discuss everything from science to architecture (yes, I still remember your Art Nouveau lecture). Vincent, my favourite statistician, you taught me so much and I was so impressed with your coding skills that I had to take a R Programming Course! I still remember those endless afternoons and evenings we spent at the microscope! Nils, our FLIMist, a.k.a. FLIMstone! Thank you for all the time we spent discussing science and for that amazing Christmas gift! Those cards were truly inspiring. I miss our talks at the cafeteria queue, waiting for our turn to ask *menina* for soup. Simon, my bench neighbour, and our plasmid machine gun, you make more plasmids per second than any other human being alive. I will always admire your very methodical procedures! Daniel Vega, probably the strongest man in the Solar System, and the one who tested the response of all bacteria on Earth to copper! "*If you don't know who did it, blame the Peruvian*!" Vanessa, the lab's chemist, and my partner in all the pranks! You were always fun to be with! António and Leonor were two very recent acquisitions to the lab, but I enjoyed every second I was with you two! From the Wordle/Worldle/Flagle contests with António to the hours spent looking at white/blue colonies with Leonor (and running away from wasps)! Oh, and our gastronomic discussions at lunch! Barquetes for the win!!! Good luck to you both

for your PhDs! Adrián, you will inherit this Holy Site called Pedro's bench. Not sure if Holy Site or Cursed Site, to be honest. Take care of it and I wish you all the best! Same for you, Dominik! I am part of the Past, you are the Future! And to all the past lab members, whom I had the pleasure to meet, before starting the PhD: Teresa, Bernardino, Gabriela and Ana Jorge.

To all the people in the Bacterial Cell Surfaces and Pathogenesis laboratory, but specially Magda, Rita Narciso, Denise, Joana and Gonçalo. You all left already! I miss you! Though Magda comes back, sometimes, when she takes holidays from her Post-Doc in the U.K. and comes to work at ITQB.

I would like to thank ITQB NOVA, the institution where I developed my research, basically my second home during this period. Thank you for providing all the equipment, the excellent working conditions, and the amazing environment. A special thanks to Teresa Baptista, for all the help! Also, I would like to thank the financial support from Fundação para a Ciência e Tecnologia (FCT) and from the European Research Council (ERC).

To my friends from Lisbon, Oeiras, Cascais and my FCUL friends! Thank you for all the support and for being always there for me when I needed the most. And thank you for cheering me up, when I was grumpy and complaining about life.

To the teachers I've had throughout my life, this thesis belongs to you, as well. I only got this far because of you! I need to highlight a few names: prof. Lucinda, prof. Paula (Primary School), prof. Maria José Monteiro (History - 5thgrade), prof. Maria Laura (Natural Sciences – 6th grade), prof. Filomena Limão (History – 7th and 8th grades), prof. Maria Helena Ferreira (Mathematics – 10th, 11th and

12th grades) and prof. Ângela Rocha (Philosophy – 10th and 11th grades). During College years, I need to highlight prof. Rogério Tenreiro, prof. Mário Santos, prof. Lélia Chambel and prof. Ana Reis.

To my Japanese teacher, イネス, thank you for the amazing lessons. 日本語のクラスはたのしくておもしろいです。

To my Discord friends, for all the amazing gaming night sessions. From Garry's Mod Prop Hunt to Golf With Your Friends or RuneScape. These moments were especially refreshing for my soul, after those frustrating days at work. Thank you!

To my Krav Maga friends, for all the punches and kicks we've exchanged. Those classes were super tiring, but I felt extremely good afterwards!

And finally, to my family. You were always there for me. You always believed in me, even when I did not! My deepest and most heartfelt thank you to you all! If there is one goal in my life, it is to never disappoint you!

Publications in International Peer-reviewed Journals as result of this thesis:

Monteiro JM***, Fernandes PB***, Vaz F, Pereira AR, Tavares AC, Ferreira MT, Pereira PM, Veiga H., Kuru E, VanNieuwenhze MS, Brun YV, Filipe SR and Pinho MG. Cell shape dynamics during the staphylococcal cell cycle. Nature Communications 6, 8055, doi:10.1038/ncomms9055 (2015) *J.M.M. and P.B.F. contributed equally to this work

Fernandes PB, Reed, P, Monteiro JM, Pinho MG, Revisiting the role of VraTSR in *Staphylococcus aureus* response to cell wall targeting antibiotics. (Under revision)

Contents

ABBREVIATIONS AND ACRONYMS 1

ABSTRACT 4

RESUMO 6

CHAPTER I - General Introduction 9

CHAPTER II - Cell shape dynamics during the staphylococcal cell cycle 71

CHAPTER III - Preliminary studies on variability of *vraTSR* expression in *Staphylococcus aureus* cells exposed to cell wall targeting antibiotics 129

CHAPTER IV - Revisiting the role of VraTSR in *Staphylococcus aureus* response to cell wall targeting antibiotics 163

CHAPTER V - Discussion and future perspectives 205

Abbreviations and Acronyms

AFM	Atomic force microscopy
Amp	Ampicillin
ATP	Adenosine triphosphate
BCIP	5-bromo-4-chloro-3-indolyl phosphate, toluidine salt
CA	Catalytic and adenosine triphosphate (ATP) binding domain
CAMPs	Cationic antimicrobial peptides
CDFI	2-(2-Chlorophenyl)-3-[1-(2,3-dimethylbenzyl)piperidin-4-yl]-5-fluoro-1H-indole
Cryo-TEM	Cryo transmission electron microscopy
CW	Cell wall
CWSS	Cell wall stress stimulon
C55P	Undecaprenyl phosphate
D-Ala	D-Alanine
D-Glu	D-Glutamic Acid
DHp	Histidine phosphorylation domain
DS	Dissacharide units
Ery	Erythromycin
FACS	Fluorescence-activated cell sorting
FR	Fluorescence ratio
FSC	Forward scattering
Glc*N*Ac	*N*-acetylglucosamine
HADA	HCC-amino-D-alanine
HK	Histidine kinase
HMM	High molecular mass
IMHK	Intramembrane-sensing histidine kinase

IM	Inner membrane
IPTG	Isopropyl-β-D-thiogalactopyranoside
IWZ	Inner wall zone
L-Ala	L-Alanine
L-Lys	L-Lysine
LMM	Low molecular mass
LA	Luria-Bertani agar
LB	Luria-Bertani broth
LPS	Lipopolysaccharides
LTA	Lipoteichoic acids
mDAP	*meso*-diaminopimelic acid
MIC	Minimum inhibitory concentration
MRSA	Methicillin resistant *Staphylococcus aureus*
Mur*N*Ac	*N*-acetylmuramic acid
MZ	Middle zone
NADA	NBD-amino-D-alanine
OD	Optical density
OM	Outer membrane
ORF	Open reading frame
OTF	Optical transfer function
OWZ	Outer wall zone
PALM	Photoactivated localisation microscopy
PBP	Pencillin binding protein
PBS	Phosphate buffer saline
PDMS	Polydimethylsiloxane
PG	Peptidoglycan
PI	Propidium iodide
PM	Plasma membrane
PS	Periplasmic space

REC	Receiver domain
RR	Response regulator
Sb	Size at birth
Sd	Size at division
sfGFP	superfast green fluorescent protein
SEM	Scanning electron microscopy
SIM	Structured illumination microscopy
TA	Teichoic acids
TCS	Two-component system
TG	Transglycosylation
TGase	Transglycosylase
TM	Transmembrane
TP	Transpeptidation
TPase	Transpeptidase
TSA	Tryptic soy agar
TSB	Tryptic soy broth
Tsp	Transcription start point
VRSA	Vancomycin-resistant *Staphylococcus aureus*
WGA	Wheat germ agglutinin
WTA	Wall Teichoic Acids
X-gal	5-Bromo-4-chloro-3-indolyl β-D-galactopyranoside
YFP	Yellow fluorescent protein

Abstract

The Gram-positive *Staphylococcus aureus* is considered one of the most prominent pathogens worldwide, presenting a global health concern. Particularly, the multi-drug resistant methicillin-resistant *S. aureus* (MRSA) is well known for causing nosocomial infections, as well as across the community. *S. aureus* capacity to survive antibiotic treatment, which makes MRSA infections very difficult to treat, prompts the need for further studies of its biology, so that new approaches for treatment can be devised.

S. aureus cells are coccoid bacteria with roughly 1 µm diameter, a feature that has impaired a precise characterization, not only of its cell cycle, but also of the morphological changes that occur during this process. In this work, we explored these two fascinating aspects of *S. aureus* – the strategies this pathogen employs to respond to antibiotics, especially those that target the cell wall (CW), and its cell cycle.

We started by investigating the cell cycle of this pathogen, using super-resolution microscopy, a technique that allowed us to observe that *S. aureus* increased in volume and elongated throughout its cell cycle. After cell division, turgor pressure and autolytic enzymes were required to reshape the flat septum into a curved surface, a process that generated less than one hemisphere of each daughter cell. This proportion was kept during the whole cycle, which allowed us to conclude that cell growth required peptidoglycan (PG) synthesis and remodelling in the entire CW surface.

Given that the CW is an essential bacterial structure and thus the target of several antibiotics, we proceeded to study the response of

S. aureus to CW targeting antibiotics, especially the response mediated by the VraTSR regulatory system, a sentinel system that is activated whenever CW damage is inflicted. We observed that VraTSR activation was variable within an isogenic population and that cells which presented higher *vraTSR* expression levels seemed to be more susceptible to the presence of the CW targeting antibiotic oxacillin. Interestingly, we found that VraTSR responded, albeit to low levels, to conditions where no CW targeting antibiotic was present, such as when *S. aureus* cells were subjected to an osmotic shock.

This intriguing result led us to revisit the conundrum of what is the signal perceived by VraTSR. We found that VraT, a protein suggested to be responsible for signal detection, was localised at the membrane and that its C-terminal domain was extracellular. We found that the molecule that triggered VraTSR was not an intermediate in the CW synthesis pathway, contrarily to what was previously thought. We observed that penicillin-binding protein (PBP) 2, an enzyme with both transglycosylase (TGase) and transpeptidase (TPase) activities, had a critical role in maintaining VraTSR in the off state, since its depletion led to a strong activation of this regulatory system. Although both activities of this enzyme seemed to be required for keeping the system off, we favour the hypothesis that TGase activity has a prominent role, as mutants in other TPases, which have severe defects in peptidoglycan crosslinking, did not trigger the VraTSR system.

This thesis contributed to a better understanding of how *S. aureus* grows, divides and responds to antibiotics that target the CW, generating knowledge that in the future may contribute to the design of new antimicrobial therapies.

Resumo

A bactéria Gram-positiva *Staphylococcus aureus* é considerada um dos mais relevantes microorganismos patogénicos, a nível mundial, representando um problema de saúde global. Em particular, as estirpes multi-resistentes de *Staphylococcus aureus* resistentes à meticilina são conhecidas por causarem infeções a nível hospitalar e na comunidade. A capacidade de sobrevivência de *S. aureus* a tratamentos com antibióticos, facto que torna infeções por MRSA difíceis de tratar, torna crucial o estudo da biologia deste microorganismo, com o objectivo a longo prazo de desenvolver novas estratégias de tratamento.

S. aureus é uma bactéria aproximadamente esférica com cerca de 1 µm de diâmetro, facto que impossibilitou uma caracterização detalhada do seu ciclo celular, bem como a análise das alterações morfológicas que ocorrem durante este processo. Neste trabalho, explorámos estas duas fascinantes características de *S. aureus*: as estratégias usadas para responder aos antibióticos, especialmente os que têm como alvo a parede celular, e o seu ciclo celular.

Começámos por investigar o ciclo celular deste microorganismo patogénico, usando microscopia de super-resolução. Esta técnica permitiu-nos observar que *S. aureus* não só aumenta o seu volume, como alonga durante o ciclo celular. Após a divisão da célula-mãe em duas células-filhas, é necessária não só a atividade de enzimas autolíticas que cortam o peptidoglicano, mas também a pressão de turgescência, para remodelar a superfície septal de modo a que esta se converta numa superfície curva, um processo que gera menos do que um hemisfério de cada célula-filha. Esta

proporção é mantida ao longo de todo o ciclo celular, o que nos permitiu concluir que o crescimento das células requer, em simultâneo, síntese e remodelação do peptidoglicano ao longo de toda a superfície da celular.

Considerando que a parede celular é uma estrutura essencial para a sobrevivência das bactérias e, deste modo, o alvo preferencial de muitos antibióticos, decidimos estudar a resposta de *S. aureus* a antibióticos que têm como alvo esta estrutura bacteriana. O nosso estudo incidiu sobretudo na resposta mediada pelo sistema VraTSR, um sistema que é ativado sempre que a parede celular sofre algum dano. Observámos que a sua ativação era variável numa população de células geneticamente iguais e que as células que apresentavam maiores níveis de expressão de *vraTSR* eram tendencialmente mais suscetíveis à presença de oxacilina, um antibiótico que tem como alvo a parede celular. Surpreendentemente, constatámos que o sistema VraTSR respondia, mesmo que em níveis mais baixos, a condições em que não usávamos antibióticos, por exemplo, quando as células sofriam um choque osmótico.

Este resultado inesperado fez-nos revisitar a questão relativa à natureza do sinal detetado pelo sistema VraTSR. Conseguimos concluir que VraT, a proteína proposta como sendo o sensor do sistema, se localiza na membrana celular e o seu domínio C-terminal está localizado na região extracelular. Concluímos também que a molécula responsável pela ativação do sistema VraTSR não era nenhum intermediário da síntese enzimática da parede celular, contrariamente ao que se pensava até então. Observámos que a proteína de ligação à penicilina 2 (PBP2), uma enzima com as atividades de transglicosilase e transpeptidase na

síntese do peptidoglicano, tinha um papel crucial na manutenção do sistema VraTSR no seu estado não ativo, uma vez que a sua depleção levava a uma ativação pronunciada deste sistema. Apesar de ambas as atividades desta enzima parecerem ser necessárias para manter o sistema inativo, pensamos que a atividade de transglicosilase tem um papel predominante, uma vez que mutações em outras enzimas com atividade de transpeptidase, com defeitos visíveis no grau de “crosslinking” do peptidoglicano, não ativavam o sistema VraTSR.

Esta tese contribuiu para um maior conhecimento relativo ao crescimento e divisão de *S. aureus*, bem como à forma como esta bactéria responde à presença de antibióticos que têm como alvo a parede celular. Este conhecimento pode ser usado futuramente no desenvolvimento de novas estratégias terapêuticas contra este microorganismo.

.

Chapter I

General Introduction

Chapter contents

General considerations regarding the bacterial cell cycle 11
Cell size and division regulation during the cell cycle 13
The cell cycle of *Staphylococcus aureus* 17
The cell cycle as a source of variability 21
Noise in gene expression 23
The Bacterial Cell Envelope 26
Gram-negative envelope 27
Gram-positive envelope 29
Peptidoglycan structure and architecture 30
Peptidoglycan biosynthesis 35
Cytoplasmic reactions of peptidoglycan biosynthesis 36
Lipid-linked reactions of peptidoglycan biosynthesis 37
Incorporation of peptidoglycan precursors into the cell wall 38
Antibiotic resistance in *Staphylococcus aureus* 39
Bacterial two-component systems 40
The sensor histidine kinase 41
The response regulator 44
Histidine kinase - response regulator interaction 47
Two-component systems in *Staphylococcus aureus* 48
VraTSR regulatory system 48
Concluding remarks 53
References 54

General considerations regarding the bacterial cell cycle

In the History of Life on Earth, bacteria were amongst the first organisms, with the first records dating back to the Devonian Period (419.2 million to 358.9 million years ago), but believed to be present since early Precambrian time, about 3.5 billion years ago[1]. One of the main features of this primordial life was the property of making copies of itself, known as reproduction[2]. Generally, bacteria are able to reproduce through a mechanism known as binary fission, involving the division of a single cell into two independent and similar compartments, separated by a septum[2]. These independent compartments detach, giving rise to two new daughter cells[3]. This process allowed microorganisms to grow and spread across the planet, colonizing different ecological niches[4]. Since cell division is a critical step in the bacterial cell cycle, it requires tight coordination between cell growth and genome replication, and timing of division[3]. Cell division is carried out by a protein complex called divisome, whose elements interact and assemble in a ring at the division site, the structure that ultimately performs cytokinesis[5]. In the case of *Escherichia coli*, the division machinery includes several essential proteins[6]. The first step of divisome assembly involves recruitment of three proteins- FtsZ, FtsA and ZipA- that form a ring-like structure that is used as scaffold for the sequential recruitment of later division proteins to the division site[5]. One of the most important proteins in this process is the tubulin homolog, FtsZ, a cytoplasmic protein that attaches to the membrane through its partners FtsA and ZipA[7]. To ensure that the division plane is formed at mid cell and that genomic DNA is not bisected by the division septum, bacteria possess regulatory mechanisms like the Min system and nucleoid occlusion[8]. Briefly, the Min system negatively regulates the assembly of the FtsZ

ring at the poles of the cell, by oscillating between those two positions[8], while nucleoid occlusion prevents genomic DNA from being bisected by preventing FtsZ ring assembly near the nucleoid, a structure that contains DNA and DNA-binding proteins[9].

Bacteria are able to maintain their shape and their volume relatively stable across several generations, even after thousands of division events[10]. This implies that cell growth is tightly regulated during the cell cycle. If not, cells that divided before doubling their volume would progressively become unsustainably small and cells that divided long after doubling their volume would constantly increase in size and filament[11].

Typically, the bacterial cell cycle can be divided into three different stages: B, C and D[10,11]. The B period comprises the time between one division (when a new cell is formed) and the initiation of chromosome replication; C period corresponds to the time that the cell takes to replicate the chromosome; D period is the time between the end of chromosome replication and the next division (Figure1).

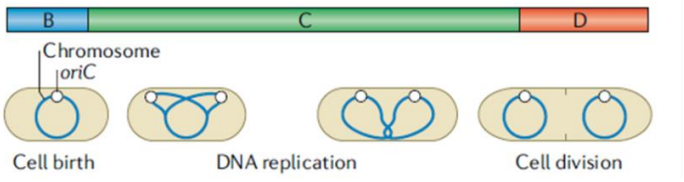

Figure 1. Stages of cell cycle. Bacterial cell cycle can be divided in three different stages: B, C and D. The time spent between cell birth and the beginning of chromosomal replication is called B period. C period comprehends the whole process of DNA replication, after which there is a D period before the next round of division. Adapted from[10].

In both *E. coli* and *Bacillus subtilis* the replication of chromosomal DNA begins at a single origin of replication, *oriC*, and proceeds bidirectionally, until it reaches the terminus[10,11]. When chromosome replication is completed and the two chromosomes are already segregating, the cell prepares for the next round of division through the formation of the FtsZ ring at the division site[10,11]. According to Cooper and Helmstetter's model, in slow-growing bacterial cells, there is only a single round of DNA replication per division[11]. However, in fast-growing cells, the generation time tends to be shorter than the time to replicate the chromosome and therefore the replicating chromosomes re-initiate replication before the previous round of this process is complete[11,12]. As an example, the doubling time for *E. coli* in rich media at 37 °C is close to 20 min, while 60 min are needed for DNA to replicate before division[12].

Cell size and division regulation during the cell cycle

The bacterial cell size is regulated during the cell cycle and may link cell growth to the initiation of chromosome replication[11,13]. This model was suggested by Donachie in 1968[13], who proposed that a new round of DNA replication only occurs once the cell mass/number of chromosome origins ratio reaches a particular value. In other words, the cell mass per replication initiation is constant. The hypothesis that reaching a specific size triggers initiation of chromosome replication provided a model for cell size regulation during the cell cycle, thus explaining cell size homeostasis in a specific population[11]. This model implies that smaller cells take longer time to divide, while larger cells take less time to initiate the next round of division. This size control model has been named "sizer"[14,15]. This "sizer" model was verified for

example in *B. subtilis*, where cell size is regulated in a nutrient dependent manner[16]. According to Weart and colleagues, *B. subtilis* cells are able to perceive when they reach a certain mass for a specific growth rate and modulate the division machinery accordingly[16]. This depends on presence of the metabolic sensor UgtP that links FtsZ assembly to cell mass and chromosome segregation, in a nutrient dependent fashion. This mechanism allows small cells to inhibit FtsZ assembly and/or prolong the temporal length of the FtsZ assembly until they reach a certain mass, while larger cells are able to initiate division sooner[16]. However, in the same work, the "sizer" model fails to explain why timing of replication initiation is unaltered in mutants that are 35% shorter than wild type[11,16], clearly showing that the mechanisms governing the coordination between division and cell size are more complex.

An alternative cell division control model is the so-called "timer" model, which takes into consideration the age of the cell[14,17,18]. Basically, the timer model posits that cell division is dependent on the age of the cell, or the time elapsed since its birth. This model implies a lack of control over the size of the cells, as variance of the size will grow constantly, over several generations[14]. However, according to recent data the newborn cell size and the generation time of individual cells are negatively correlated, completely ruling out the "timer" model[19]. Nonetheless, the case of morphological and functional asymmetry in alphaproteobacteria, namely *Caulobacter crescentus*, between the old and new poles, can be viewed as a contribution of the time factor towards the cell fate[20,21].

Giving that none of the models can, individually, comprehensively explain the regulation of cell size and division, there are models combining the sizer and timer mechanisms, like the bilinear model[14,22]. According to this hypothesis, cells grow linearly in time,

until achieving a threshold length, after which cells keep growing for a fixed amount of time[14,22]. There are reported cases where both size and time variables play a role in the regulation of the cell division, like in *Methylobacterium extorquens*[23]. In *M. extorquens* cell size increases with increasing pole age, while the time between each division decreases[23]. Although, no substantial inconsistencies can be found between experimental data and a model where the division rate depends simultaneously on the size and age of cells, a new simpler model, called the "adder", explains these and further observations (Figure 2)[14,19,24] .

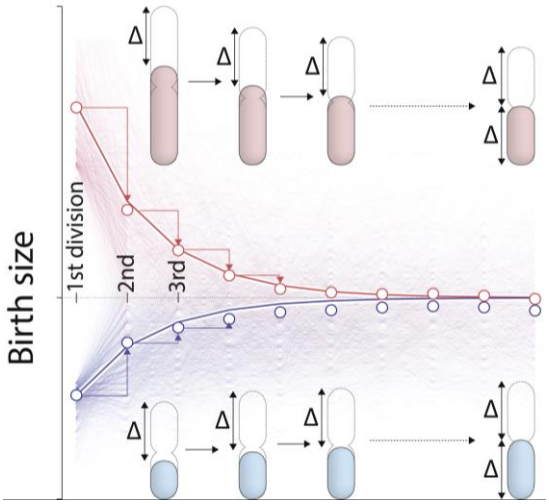

Figure 2. Proposed model for cell size control and homeostasis in bacteria. Bacterial cells maintain size homeostasis by adding a constant size (Δ) and dividing at the middle. According to this model, the newborn cells size, regardless of their initial value, will automatically converge to Δ, if these criteria are met. Adapted from[19].

The "adder" model, a paradigm first proposed in 1993 as "incremental size model", postulates that cells add a constant size (Δ) between birth (sb) and division (sd) for a given growth condition (Δ = sd−sb)[14,19,25]. Also, according to Taheri-Araghi and colleagues, the distribution of the size added to each cell, Δ, in each generation, is

independent of the cell size at birth[19]. One of the first outcomes of this model is that it ensures cell size homeostasis, since after every division, each cell comes closer to the population average[19]. Moreover, the "adder" paradigm agrees with previous models describing initiation of cell division based on the accumulation of cell cycle initiators up to a certain threshold, which triggers the process[26]. The variable added size Δ, together with the growth rate (λ) are enough to explain the distribution of all growth and division parameters, such as relative septum position, division size, newborn size and generation time of both *E. coli* and *B. subtilis*, in all growth conditions[19]. As a result, Taheri-Araghi and colleagues claim that Δ and λ are the two basic parameters that control physiology and size homeostasis in bacteria[19]. Since the "adder" model was proposed, several hypotheses were raised to explain its mechanistic basis. The "adder" may be controlled by the initiation of replication, as suggested in the "adder per origin" model[27]. It states that a new round of DNA replication can only occur once the cell accumulates a critical volume per origin of replication, raising the possibility of an accumulation of an initiator protein[27]. Alternatively, the "adder" may be regulated by the event of division[28]. This approach proposes that bacteria achieve cell size homeostasis by growing on average the same amount between divisions, independently of cell size at birth, suggesting that the "adder" is regulated close to or at division[28]. A third hypothesis considers that the surface-to-volume ratio governs cell size[29]. According to recent data, the two model organisms *E. coli* and *B. subtilis* share a common mechanism of size homeostasis[25]. The authors show that the "adder" mechanism in these microorganisms involves both the accumulation of division percursors, like FtsZ, up to a certain level, per cell, and that their synthesis is proportional to the

growth of cell volume[25]. As a result, the division process regulates size homeostasis in both microorganisms.

The cell cycle of *Staphylococcus aureus*

Staphylococcus aureus is a pathogen widely known for causing nosocomial antibiotic resistant infections. Its clinical relevance and the way it divides make this microorganism an important model for cell division. Most bacteria grow and divide, by elongating and building a new septum at mid cell, perpendicularly to the long cell axis, that divides the mother cell into two independent daughter cells, typical of rod-shaped bacteria[30]. On the contrary, *S. aureus* is a spherical organism that was thought, since the 1970s, to divide in three sequential alternating orthogonal planes over three consecutive division cycles[31,32]. According to this model, to maintain information about the previous division planes, *S. aureus* had to rely on spatial cues and since this spatial reference varies with each division, it could be encoded by DNA[32]. The source of epigenetic information was attributed to peptidoglycan (PG) thick “piecrust” structures, that are formed at the cell surface upon each division, on the division plane[32]. These structures are interpreted as remnants of PG remodelling during division events, thus retaining the spatial information of previous divisions[32]. However, recent published data from our laboratory suggests that *S. aureus* divides in two alternating perpendicular planes, but not necessarily in three[33]. Like *E. coli* and *B. subtilis*, *S. aureus* segregates the replicated chromosomal DNA to the daughter cells, before septal closure[34]. However, unlike the two model microorganisms, *S. aureus* lacks a Min system, relying only on a nucleoid occlusion mechanism to ensure that FtsZ polymerization only occurs at the middle of the cell[35]. Another important

characteristic of the *S. aureus* cell cycle is that it was proposed to synthesize cell wall mainly at the division septum, dependent on one cell wall synthesis machinery[34]. This is strikingly different from rod-shaped microorganisms like *E. coli* and *B. subtilis*, that harbour two different cell wall synthesis machineries, one for incorporation of cell wall mainly at the division septum and the other for elongation of the lateral wall[36]. Due to the small size of *S. aureus* cells, with around 1 μm diameter[37], the morphological changes that may happen during the cell cycle are beyond the resolution of conventional microscopy techniques. There is, however, evidence that cells experience a volume increment, doubling the size, after the split of the mother cell into the two independent daughter cells, accounting for an increase in the surface area[32]. This hypothesis suggested that cells must reshape the septal PG, from a flat surface into a curved one, if no elongation machinery was present. The role of reshaping of the septal region to account for volume duplication has been attributed to enzymatic hydrolysis of PG and cell internal turgor pressure[32,38].

Splitting of the mother cell into two daughter cells requires the sequential events of septation and cell separation. Cryo Transmission Electron Microscopy (cryo-TEM) observations indicate the septum is composed of two septal planes (one per daughter cell) separated by a middle zone of lower electron density[39]. According to Matias and Beveridge, the two daughter cells start the synthesis of two wall layers as soon as the septum starts growing inwards (septal ingrowth), with the integrity of the division septum being maintained by a high-density zone at its initiation point, at the periphery of the cell (Figure 3)[39].

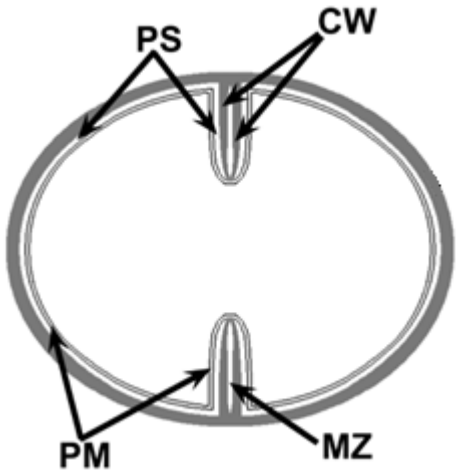

Figure 3. Proposed model for septum structure in *S. aureus.* Septum synthesis results in the generation of distinct layers within the septum: a cryo-TEM low density middle zone (MZ), flanked by high density cell wall (CW) layers. A low-density periplasmic space (PS) can be found not only between the plasma membrane (PM) and the peripheral cell wall, but also in the septum. Adapted from[39].

The septum of *S. aureus* has been described to have five distinct zones of different densities between the membranes of the two future compartments (Figure 3)[39,40]. These five regions consist of two high electron density zones in between three low electron density zones (cryo-TEM), with the high density zones being composed of cell wall matrix while the low density zones have no distinguishable structures within them[39,40]. The low density zones adjacent to the membranes were proposed to be the periplasmic space of Gram-positive bacteria, while the low density zone at the middle of the septum would correspond to a soluble zone trapped between the septal cell walls[39]. As the tip of the septum grows inwards, the two cell wall (CW) layers corresponding to the high density zones grow as two separate planes, though one cannot exclude that these two layers come from a single CW layer, that is immediately hydrolysed[39]. When the septum

is finally closed the daughter cells are kept together, through a cell wall layer at the periphery, at the base of the septum[39]. Although, the thickness of the septum was described to be homogeneous after septal closure, further analysis revealed that, during septum synthesis, the leading edge is thinner and it gradually becomes thicker towards the base of the structure[41]. This configuration is maintained after the closure of the septum, with the centre being thinner than the base, but it progressively becomes homogeneous through PG insertion, performed by cell division machinery[41]. The regions at the base of the closed septum are then further processed by PG hydrolases for complete separation of the daughter cells[39]. *S. aureus* possesses several PG hydrolases[42]. The role of PG hydrolysis in cell daughter separation has been attributed to two enzymes called Atl and Sle1[43]. Atl is a bifunctional enzyme, that undergoes proteolytic processing, generating a 59 kDa endo-beta-N-acetylglucosaminidase and a 62 kDa N-acetylmuramyl-L-alanine amidase, localising as a ring around the zone of division[39,44]. Sle1 is a 32 kDa N-acetylmuramyl-l-alanine amidase that is also implicated in cell separation of *S. aureus*[43]. In the absence of both of these enzymes cell separation is heavily impaired, leading to the formation of cellular clusters[43].

The cell cycle as a source of variability

Much of the phenotypic variability observed at the bacterial population level can be explained by genetic differences, as well as by the effects of the surrounding environment[45]. However, even genetically identical cells, with identical history of exposure to the same environmental conditions may display striking phenotypic variability[45]. The cell cycle has been described as one source of phenotypic variability[45]. One example is the replication-associated gene dosage effect but also, along the bacterial cell cycle, several proteins and enzymatic complexes are recruited to perform specific tasks, like chromosome replication or septum synthesis[46,47,48]. This implies that different proteins are active only at particular time window. As a consequence, while in a synchronized population of cells, the progression of the cell cycle produces predictable changes in protein activity, in an asynchronized population, the cell cycle generates variability[45]. One extreme case of cell cycle-driven variability is the generation of functionally different cells. *Caulobacter crescentus* is an interesting model regarding the generation of cellular asymmetry, since it produces, after every division, two morphologically and functionally different cells: a non-replicating swarmer cell and a replicating stalked cell[49]. This phenotypic dimorphism is intrinsic to the cell cycle[50]. One mechanism used by *C. crescentus* to enable this phenotypic variability is DNA methylation, a process required for cell cycle regulation in this microorganism[51,52]. Chromosome replication occurs in the stalked cell, after binding of the replication initiation protein DnaA to the methylated origin of replication[50]. During early steps of chromosome replication, the DNA is fully methylated but as replication progresses, the replicated chromosome becomes hemi-methylated, since the CcrM methylase

activity is restricted to the end of DNA replication, prior to cell division[50]. In turn, transcription of *dnaA* is inhibited when its promoter is in the hemi-methylated state, soon after chromosome replication[53]. This way, DNA replication acts as a timer for coordination of *C. crescentus* cell cycle[52]. DnaA activates the transcription of *gcrA*, whose product leads to the transcription of *ctrA*[54]. CtrA is a cell cycle transcription regulator and a chromosome replication inhibitor, which is selectively degraded in the stalked cell compartment, but not in the swarmer cell compartment, after the division event has occurred[55,56]. Hence, chromosome replication is restricted to the stalked cell, generating functionally different cells, while sharing the same genetic information.

It is also documented that *C. crescentus* cells may experience metabolic fluctuations, during the cell cycle[57]. Additionally the intracellular redox potential oscillates with the bacterial cell cycle, which may be caused by proteins linking cell cycle stages to metabolism[58]. Examples include the NADH-dependent cell division regulator KidO, a known inhibitor of FtsZ[59] or the glutamate dehydrogenase GdhZ that interferes with FtsZ polymerization by promoting its GTPase activity[60]. Multifunctional enzymes that perform different autonomous and often unrelated functions without partitioning these functions into different domains are called moonlighting enzymes, which is the case of enzymes regulating metabolism and the cell cycle, in *C. crescentus*[61]. Moonlighting enzymes coordinating the cell cycle and metabolism were also identified in *E. coli*, such as the UDP-glucose activated inhibitor of FtsZ ring, OpgH and in *B. subtilis*, such as, the sugar transferase UgtP, also an FtsZ inhibitor[62].

Controlling cell cycle progression is crucial for bacteria to maintain the correct order of events and preserve the integrity of the cell[63].

Therefore, understanding this process is a key aspect of antibiotic development.

Noise in gene expression

The random nature of the chemical reactions that govern biological processes inside a cell influences the way it operates[45,64]. One of such biological processes is gene expression, whose control involves a series of reactions that ultimately regulate most cellular behaviors[45]. To describe variation in gene expression amongst isogenic cells, subjected to the same environmental conditions, the terms noise or stochasticity in gene expression are often used[45]. There are four main sources of noise: (i) the random nature of chemical reactions inside a cell; (ii) differences in the internal states of a population, like the cell cycle phases; (iii) subtle environmental variations; (iv) ongoing genetic mutations[45].

Effects of noise can be minor when large amounts of molecules are present, but may become notable when only a few molecules exist in a cell, which is the case for DNA, RNA and other important regulatory molecules[45,65]. Stochasticity in gene expression, rendering different amounts of protein produced by a specific gene in two isogenic cells, can account for an important fraction of the observed cell-to-cell variation[65,66]. The total noise in a cell (defined as the standard deviation divided by the mean in a given distribution, such as gene expression) can be further decomposed into two different components: extrinsic and intrinsic noise. The extrinsic noise accounts for oscillations in the output of a particular gene, considering that its expression is dependent on fluctuations in the amount, activity and location of regulatory proteins, polymerases or any other factor that interferes with gene expression[45,65]. This concept can be easily

explained if we monitor two reporters for the same regulatory sequence of a given gene, an experimental setting followed by Elowitz and colleagues[65]. Extrinsic noise affects the two reporters equally at the single cell level, but generates differences between different cells (Figure 4A)[45,65]. Some authors consider that the extrinsic noise can be further divided into two categories: (i) global noise, accounting for oscillations of rates of the reactions that affect expression of all genes (Figure 4B); (ii) gene or pathway-specific extrinsic noise, caused by concentration fluctuations of transcription factors or stochasticity inherent to a specific pathway (Figure 4C)[67,68]. On the other hand, if we consider a population of isogenic cells with the same concentration and chemical states of their cellular components, the rate of expression of a given gene would still be different between two cells, due to the random nature of chemical reactions that govern genetic expression[65]. This causes intrinsic noise, which creates differences between two reporters of the same regulatory sequence of a particular gene, in the same intracellular environment (Figure 4D)[45,65].

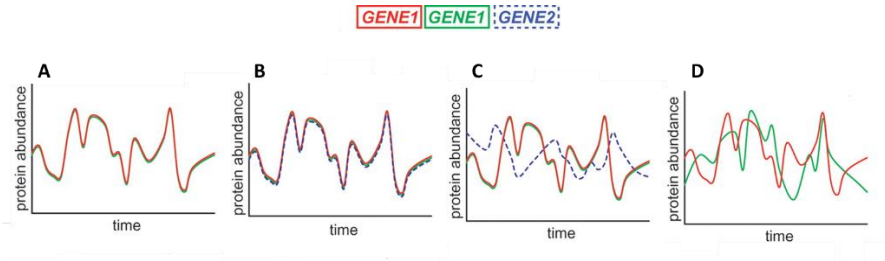

Figure 4. Characteristics of noise in genetic expression. Expression levels of two reporters of the same gene (GENE1), on the same prokaryotic chromosome, are presented in green and red respectively, while GENE2 reporter expression levels are presented in a dashed line **(A)** Extrinsic noise affects two reporters of the same gene in the same extent but generates differences between cells or in the same cell over time. **(B)** Global noise, a component of extrinsic noise, affects the expression of all genes equally, in a single cell, but differs from cell to cell. **(C)** Gene or pathway-specific extrinsic noise is the inherent stochasticity of a specific genetic circuit, thus varying between different genes in the same cell. **(D)** Intrinsic noise causes differences between two reporters of the same gene, in a single cell. Adapted from[45].

Fluctuations in gene expression longer than the cell cycle can have substantial effects on cellular processes, while rapid fluctuations may not have a significant impact[69]. This is due to the fact that fast fluctuations average out quickly while slow oscillations can introduce errors in the genetic circuits, compromising their accuracy[69]. The fact that the time scale of oscillations attributed to intrinsic noise is shorter than that of extrinsic noise, may indicate that cellular phenotypes are more dependent on the extrinsic component of noise than the intrinsic one, even if the latest is known to be the main source of noise[45,69,70]. Given that genetic noise causes inaccuracy on biological systems, this phenomenon is expected to be under selective pressure to be tightly controled[45]. Consequently, various cellular mechanisms have been suggested to mitigate noise effects, such as lowering the intrinsic noise in protein levels by implementing inefficient translation succeeding frequent transcription, which comes at the energetic cost of producing few proteins from several mRNAs[45]. Inefficient translation has been suggested to occur in some regulatory genes in *E. coli* , like *malT*, a gene coding the regulator of maltose regulon[71].

Noise is not always harmful for the biological systems, as systems can take advantage from stochasticity[72]. In bacterial clonal populations the expression of a gene follows an unimodal variation, due to noise effects yet, in some conditions, noise can give rise to a second type of variation that is not unimodal[73]. In this non-unimodal variation, an isogenic population bifurcates into different coexisting subpopulations, a process named bistability[73]. Bistability was proposed to occurs stochastically, since it can be triggered in isogenic populations grown in the same environmental conditions[73]. Two noticeable examples are sporulation and natural competence. The mechanisms underlying bistability involve the effect of noise on a master regulatory gene, allowing the cell to pass a threshold in gene

expression, triggering a qualitative change that ultimately bifurcates the population[73]. One condition in which bistability, and consequently noise, prove to be beneficial for bacterial populations is in the presence of antimicrobial agents, like antibiotics[73]. This strategy involves the generation of a subpopulation, called persisters, that can withstand antibiotic treatment and then resume growth, once the antibiotic is removed[73,74]. Persisters can be distinguished from other cells by their reduced growth rate, a state that they enter stochastically, prior to antibiotic treatment[74]. The existence of a subpopulation of persisters explains why bacterial cell death linked to antibiotic treatment shows a biphasic killing curve[75]. In the presence of antibiotics, persisters and antibiotic susceptible cells coexist. However, while the susceptible population is eliminated swiftly, corresponding to the fast-killing phase, the small persisters subpopulation survives, corresponding to the slow or non-killing phase[75]. The cost of generating slow or non-growing cells is compensated by the capacity of survival of the whole population with the same genetic information. Hence, persisters formation and bistability in general, pose a significant advantage to cells that deal with frequent environmental fluctuations[73].

The Bacterial Cell Envelope

To cope with an often hostile environment, bacteria developed a complex structure, called cell envelope, that surrounds the cytoplasm and allows selective passage of nutrients from the outside and waste products from the inside[76]. In 1884, the Danish bacteriologist Hans Christian Gram developed a staining method that allowed him to classify almost all bacteria into two different groups[77]. This procedure is based on the differential staining with a crystal violet-iodine

complex and a safranin counterstain, with Gram-positive bacteria retaining this complex, while Gram-negative bacteria lose the coloration[77]. The fundamental principle of the Gram stain lies on the structural differences of the cell envelope of these two groups of microorganisms[76].

Gram-negative envelope

In Gram-negative bacteria, the cell envelope is composed of three major layers: the outer membrane (OM), the cell wall (CW), comprised of peptidoglycan (PG) layers, and the cytoplasmic or inner membrane (IM) (Figure 5)[76].

The OM, a specific attribute of Gram-negative bacteria, is the outermost layer of the envelope structure, separating the external environment from the periplasm[76,78]. The OM is composed of phospholipids, proteins and lipopolysaccharides (LPS). Its lipid distribution is asymmetric, with the periplasmic leaflet containing phospholipids and the surface-exposed outer leaflet being mainly composed of LPS[76,78,79]. LPS confers a highly charged property to the OM, enabling several interactions with cations in the outside environment[80].

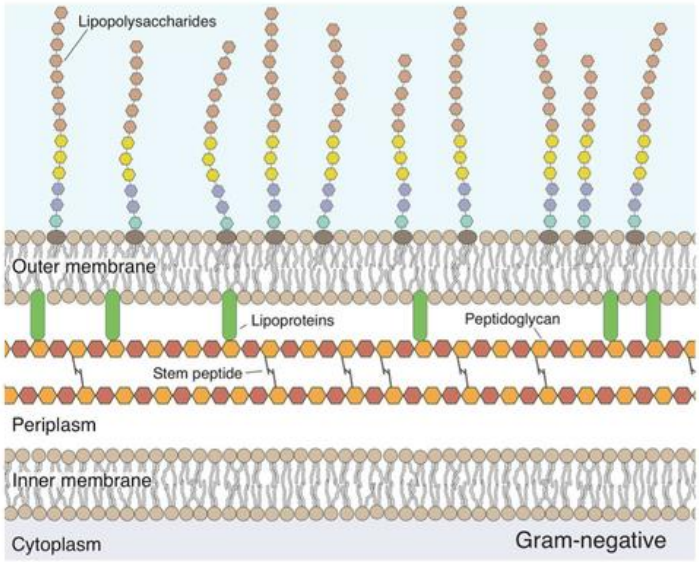

Figure 5. Typical structure of the Gram-negative envelope. In Gram-negative bacteria, the envelope is composed of an outer membrane enclosing the CW (see text), composed of a thin layer of PG (see text) (~4 nm), and the periplasmic space, that separates these structures from the inner membrane. The outer membrane can be coated with LPS (see text) and is connected to the CW via lipoproteins. Adapted from[81]

Underlying the OM, there is a thin layer of PG, typically ranging from around 2.5 nm in *Pseudomonas aeruginosa* to 6.5 nm in *E. coli*[82]. This PG layer is linked to the OM through a lipoprotein called, Lpp or Braun's lipoprotein[83]. The PG layer is immersed in an aqueous compartment, called periplasm, which is more viscous than the cytoplasm and with a high content of proteins[84]. Proteins located in this compartment display different functions, such as sugar and amino acid transport, chemotaxis or envelope biosynthesis[85].

Gram-positive envelope

The Gram-positive envelope has a different layout, when compared to the Gram-negative one. One key aspect is the absence of OM[82] (Figure 6). Cryo-TEM allowed to differentiate two layers within the Gram-positive envelope, besides the membrane: a low-electron density inner wall zone (IWZ) and a high-electron density outer wall zone (OWZ) [39,40,82.] The IWZ has been proposed to be the equivalent of the Gram-negative periplasm, with similar composition and function[86]. The OWZ is a layer containing PG with glycopolymers known as teichoic acids (TA) either covalently anchored to the PG, the Wall Teichoic Acids (WTA), or anchored to the head groups of membrane lipids, the Lipoteichoic Acids (LTA), and cell surface proteins[82,87].

The PG structure in Gram-positive bacteria is considerably thicker than the Gram-negative counterpart, ranging from 20 to 80 nm, with 40-80 individual layers of this polymer[88,89,90]. As for the periplasmic space, in Gram-positive bacteria it is much narrower than in the Gram-negative cells[90]. Some authors argue that the periplasmic space is dynamic, depending on the external conditions that alter the internal cellular volume, since the CW appears to be stiff[91]. Removal of WTA was demonstrated to reduce the thickness of the OWZ in *B. subtilis*, but not in *S. aureus*[39,40]. These polymers can represent over 60% of the mass of the Gram-positive CW, constituting a major structural component[76]. Besides their structural importance, WTA and LTA contribute to the negative surface charge, a similar function to the LPS in Gram-negative bacteria[90,92]. WTA were proposed to bind extracellular metal cations as well as protons, creating local changes in the pH, thus regulating the functions of some extracellular enzymes[93,94].

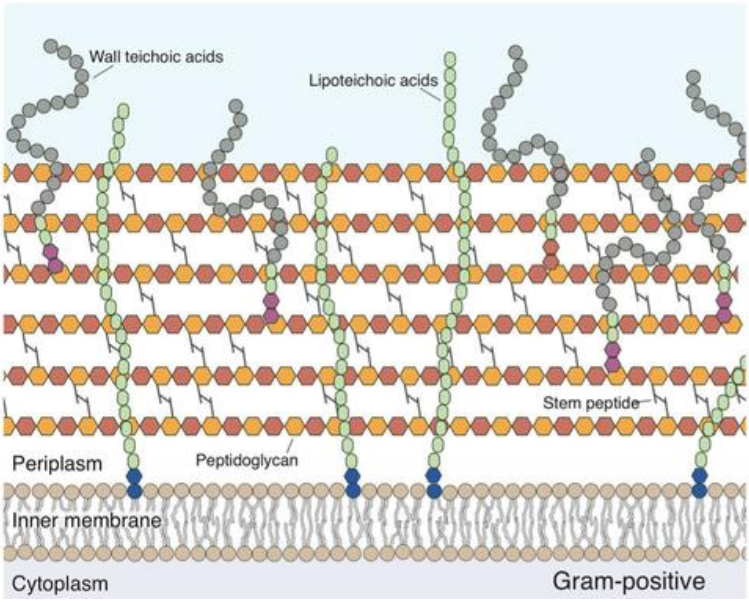

Figure 6. Typical structure of the Gram-positive envelope. In Gram-positive bacteria, the CW represents the major component of the envelope, with a very thick layer of PG. A small periplasm is present between the PG and the cytoplasmic membrane. WTA are covalently attached to PG while LTA are anchored to the membrane. Both polymers can decorate the Gram-positive envelope, spanning through the CW. Adapted from[81]

Peptidoglycan structure and architecture

The CW of bacteria is mainly composed of peptidoglycan (PG), also known as murein. The PG coating can withstand the internal osmotic pressure, preserves cell shape and integrity and serves as a scaffold for anchoring proteins and other cell envelope components[95,96,97]. PG is present in almost all bacteria, with some exceptions, like *Mycoplasma* spp[95].

As its name suggests, PG is a macromolecule comprised of linear glycan chains, cross-linked to each other through short peptides[98].

The glycan chains are composed of alternating *N*-acetylglucosamine (Glc*N*Ac) and *N*-acetylmuramic acid (Mur*N*Ac) residues, linked by β-1,4 bonds[95]. In each Mur*N*Ac residue, the D-lactoyl group is substituted by a small peptide stem, composed of different amino acids that connect to other stem peptides of adjacent glycan strands, performing a cross-link between those strands[95,99]. The general amino acid sequence of stem peptides is L-Alanine (L-Ala), γ-D-Glutamic Acid (γ-D-Glu), *meso*-diaminopimelic acid (mDAP) or L-Lysine (L-Lys), D-Alanine (D-Ala), D-Alanine[95,96]. The cross-linking reaction occurs between the carboxyl group of D-Ala in the fourth position of one stem peptide and the amino group of the diamino acid at the third position of another stem peptide, directly or through a peptide bridge, generating a three-dimensional multi-layered mesh structure (Figure 7)[95,96].

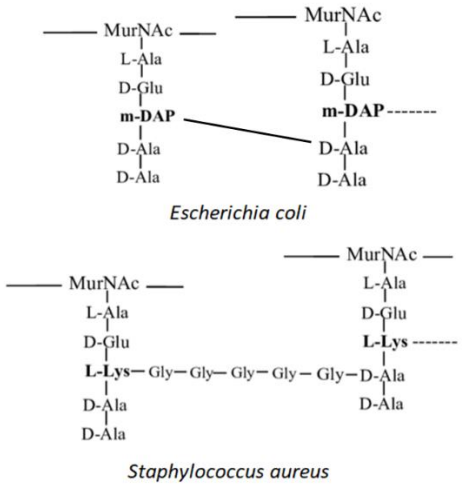

Figure 7. Peptide cross-linking in Gram-negative and Gram-positive bacteria. The cross-linking reaction occurs between the carboxyl group of D-Ala in the fourth position and the amino group of the diamino acid at the third position. In most Gram-negative bacteria, like *E. coli* the reaction happens directly between the aforementioned groups, while in some Gram-positive bacteria, like *S. aureus*, this can occur through a peptide bridge. Adapted from[100].

This architecture is conserved in most bacteria, although there is a certain level of variation regarding the chemistry of the residues of the stem peptides, the glycan chains and the position or composition of the interpeptide bridge[95]. This variability in PG structure and composition confers different properties and allows structural diversity, regarding the CW[95,96,101].

PG glycan chains can suffer secondary alterations such, as *N*-deacetylation of either Mur*N*Ac or Glc*N*Ac, performed by PG deacetylases, most likely on already polymerized PG[102]. *O*-acetylation, a more common modification than deacetylation, has also been documented in Mur*N*Ac residues, most probably on already polymerized PG[103]. Mur*N*Ac residues can also be *N*-glycolylated, a process most commonly found in bacteria with mycolic acids, like *Mycobacterium* spp[102,104]. Contrary to *N*-deacetylation and *O*-acetylation, *N*-glycolylation is performed on PG percursors[102]. Acetylation, deacetylation and O-acetylation alter the properties of PG, allowing the macromolecule to become resistant to the hydrolytic activity of certain enzymes[102,105,106]. Other examples of glycan variability include the termination of the glycan chains with a 1,6-anhydroMur*N*Ac residue that occurs in Gram-negative and some Gram-positive bacteria, like *B. subtilis*, albeit in a low proportion (0.4% of the residues), while most of Gram-positive microorganisms display a reducing end containing either Mur*N*Ac or Glc*N*Ac[95,107].

The glycan chain length is variable between bacterial species and its average value does not seem to correlate with the thickness of the PG layer[95]. *E. coli* and most other Gram-negative bacteria have an average glycan length between 19 and 38 dissacharide units (1 DS equals 1.03 nm), but the length of the glycan chains can depend on growth conditions, being longer in newly synthesized strands and

shorter in PG of cells in stationary phase[82,108,109]. In Gram-positive bacteria, like *B. subtilis*, the glycan chains are extremely long, containing more than 500 DS[82,110]. A model named “coiled cable”, based on Atomic Force Microscopy (AFM) images of fragmented PG sacculi was proposed to explain how these long glycan chains were arranged around the cell, stating that bundles of glycan chains wrap around each other, generating 50 nm wide “cables” (Figure 8A) that go around the cell, perpendicularly to the long axis[91]. However, an alternative model was later proposed based on electron cryo-tomography, which provides full 3-D information, in contrast with 2-D images of AFM, stating that glycan strands run circumferentially around the cell, cross-linked by stem peptides parallel to the long cellular axis, an observation previously reported for Gram-negative bacteria (Figure 8B)[91,111].

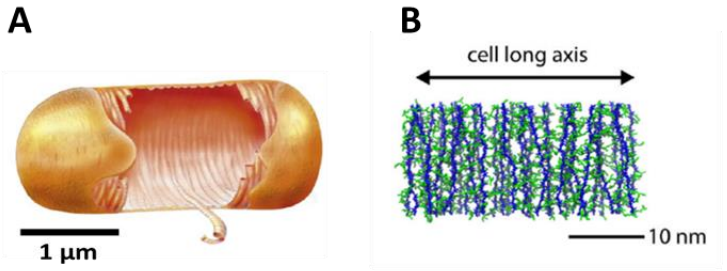

Figure 8. Peptidoglycan macrostructure models. A) The cable model proposes that PG chains wrap into coiled cables that go around the cell, perpendicular to the long axis of the cell. **B)** Glycan strands (in blue) go circumferentially around the cell, cross-linked by stem peptides (in green) parallel to its long axis. Adapted from[82,91].

Nevertheless, this organized orientation of glycan strands around the cell has been recently challenged by Pasquina-Lemonche and colleagues, who claim that the external surfaces of *B. subtilis* and *S. aureus* are disordered and have glycan strands of variable thickness[112]. Yet, in *S. aureus*, the glycan strands are notably shorter

than in *B. subtilis*, with an average length of only 6 dissacharide units, but with a higher degree of peptide cross-linking[113,114].

Cross-linking also presents high variability between microorganisms, with most variations being attributed to the mode of cross-linkage and the length and chemical composition of the interpeptide bridge[95]. Cross-linking (3-4) occurs between the amino acid in the third position of one stem peptide (acyl acceptor) and the D-Ala at fourth position of the other stem peptide (acyl donor), the most common type[99]. This reaction can occur directly between the two referred amino acids or through the presence of an interpeptide bridge[95,99]. A less common mode of cross-linkage requires the reaction between the D-Glu amino acid at second position of one stem peptide and D-Ala at position four of another (2-4)[95]. In specific cases, like *Mycobacteria*, the carboxyl group of the third amino acid can be used as acyl donor, instead of the D-Ala at position four, resulting in (3-3) cross-linking[115].

The structure and architecture of the PG sacculus confers elastic properties, enabling PG to expand and shrink without compromising its integrity[95,116]. One evident example of PG elasticity is that this macromolecule can withstand the internal turgor pressure of the cell, that presses the cytoplasmic membrane against the PG, stretching the later[117]. In fact, when the cytoplasmic membrane of *E. coli* cells is disrupted by a detergent, causing loss of the internal turgor pressure, the cell surface area suffers a decrease of around 45%, due to relaxation of PG mesh[95,117]. Deformations of PG shape are more pronounced along the long axis of the cell, an observation that corroborates the predicted PG structure with the more flexible stem peptides aligned with the long axis and the more rigid glycan stands perpendicular to it, as already discussed[95,111,118].

In addition to the elastic properties, another structural feature of PG is the presence of pores in the mesh, with similar sizes (around 2 nm radius) in Gram-positive and Gram-negative bacteria[119]. According to estimates, these pores should allow the passage of proteins up to 50 kDa, in normal growth conditions[119]. This porosity has been recently confirmed by AFM in *B. subtilis* and *S. aureus* with the external PG surface presenting large (up to 30 nm radius) and deep (up to 23 nm) pores, while the internal surface is smoother and with smaller pores, to prevent membrane plasmolysis, due to internal turgor pressure[112].

Peptidoglycan biosynthesis

The biosynthesis of PG is an enzymatic pathway, conserved in both Gram-negative and Gram-positive bacteria, involving several steps, spatially distributed in three different stages (Figure 9)[36]. The pathway starts in the cytoplasm leading to the formation of the nucleotide sugar-linked precursors UDP-*N*-acetylmuramyl-pentapeptide (UDP-Mur*N*Ac-pentapeptide) and UDP-*N*-acetylglucosamine (UDP-Glc*N*Ac)[36,120]. The second stage takes place in the inner leaflet of the cytoplasmic membrane and leads to the synthesis of lipid-linked PG precursors that are then flipped to the outer leaflet[36,120]. The last stage takes place in the outer layer of the cytoplasmic membrane and involves the incorporation of the PG precursor into the nascent PG and into the mesh structure that take place in the cytoplasm[36].

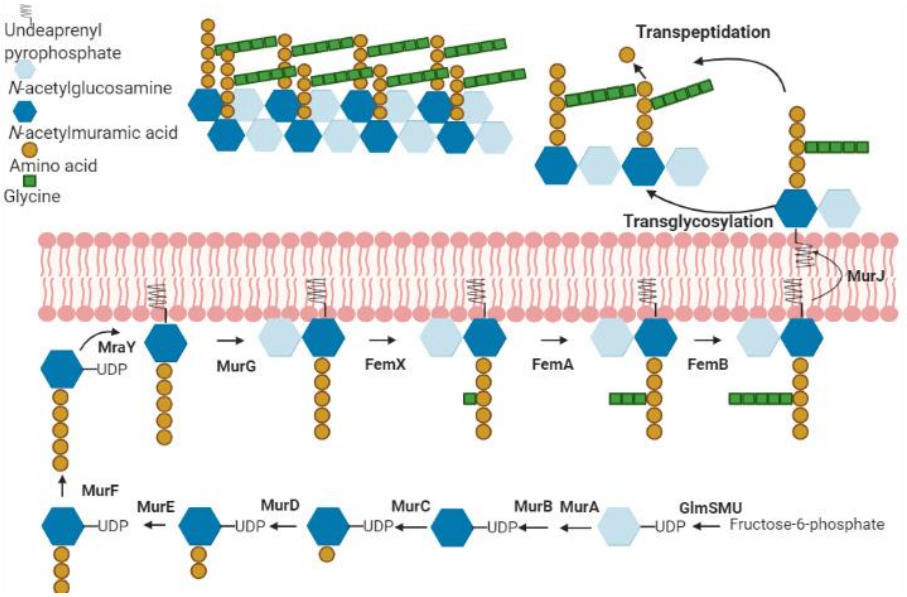

Figure 9. Peptidoglycan biosynthesis in *S. aureus*. The biosynthesis of PG occurs in three different stages (i) synthesis of PG precursor into the cytoplasm, (ii) synthesis of lipid-linked precursors at the inner leaflet of membrane followed by flipping to the outer leaflet and (iii) polymerization of PG in the CW. The cytoplasmic PG precursor is formed by UDP-MurNAc linked to the stem peptide and subsequently attached to bactoprenol, forming lipid I. GlcNAc is then added to lipid I, yielding lipid II, which is modified by the addition of a glycine pentapeptide bridge and translocated across the membrane. Finally, the PG precursor is incorporated into the CW by transglycosylation and transpeptidation reactions.

Cytoplasmic reactions of peptidoglycan biosynthesis

The first step of PG synthesis leads to the formation of uridine 5'-pyrophosphate-*N*-acetylglucosamine (UDP-Glc*N*Ac) from fructose-6-phosphate, catalysed by the GlmSMU enzymes[120,121]. Uridine 5'-pyrophosphate-*N*-acetylmuramic acid (UDP-Mur*N*Ac) is then formed from UDP-Glc*N*Ac through a two-step process, in which MurA catalyses the transfer of enolpyruvate from phosphoenolpyruvate to the Glc*N*Ac residue, generating UDP-Glc*N*Ac-enolpyruvate[120]. The second step involves the reductase MurB, catalysing the reduction of

the enolpyruvyl moiety to D-lactoyl, yielding UDP-Mur*N*Ac[120]. The next reactions involve addition of a stem peptide to the lactoyl group of UDP-Mur*N*Ac, in a stepwise fashion, generally, L-Ala, D-Glu and a diamino acid either L-Lys or *meso*-diaminopimelic acid (mDAP), by MurCDE enzymes[120,122]. Subsequently, the D-Ala-D-Ala dipeptide is added to the UDP-Mur*N*Ac-tripeptide by MurF, yielding UDP-Mur*N*Ac-pentapeptide, also known as Park's nucleotide[120,122,123].

Lipid-linked reactions of peptidoglycan biosynthesis

The membrane steps of PG biosynthesis start with the transfer of UDP-Mur*N*Ac-pentapeptide to the membrane acceptor undecaprenyl phosphate (C55P) or bactoprenol, by MraY enzyme, resulting in Mur*N*Ac-pentapeptide-pyrophosphoryl undecaprenol, known as lipid I[120,123]. MurG transferase then adds *N*-acetylglucosamine to lipid I, yielding Glc*N*Ac-Mur*N*Ac-pentapeptide-pyrophosphoryl-undecaprenol or lipid II[120,124].

In *S. aureus*, a pentaglycine interpeptide bridge is formed by the activity of FemXAB non-ribosomal peptidyltransferases[125]. The first reaction is performed by FemX, which adds the first glycine to the amine group of L-Lysine of the lipid II stem peptide, generating lipid II-Gly_1[126]. Then, using lipid II-Gly_1 as substrate, FemA adds the second and third glycines, forming lipid II-Gly_3 and finally FemB adds the fourth and fifth glycines to lipid II-Gly_3, generating lipidII-Gly_5[125,127,128].

Lipid II-Gly_5 is then flipped to the outer leaflet of the cytoplasmic membrane by an enzyme whose identity was controversial for years[129]. While FtsW is the only enzyme shown to transport lipid II *in vitro*, using *E. coli* membrane vesicles, MurJ was presented as a lipid II translocase *in vivo*[130,131]. Blocking MurJ lipid II flipping activity revealed not only to block lipid II translocation, but also to be

incompatible with cell viability, while depleting FtsW had no major impact on flipped lipid II, *in vivo*, in *E. coli*[131]. On the other hand, FtsW was recently shown to be a PG synthase, capable of synthesizing glycan strands[131,132].

Incorporation of peptidoglycan precursors into the cell wall

PG precursors are incorporated into the CW mesh structure through two reactions: transglycosylation (TG) and transpeptidation (TP). TG activity allows the elongation of glycan strands, by making a β-1,4 linkage between Glc*N*Ac of lipid II-Gly_5 and Mur*N*Ac of the nascent PG[133]. Once lipid II-Gly_5 is added to the growing PG strand, the lipid carrier bactoprenol is recycled back to the inner side of the membrane to pick another cytoplasmic PG precursor[134]. TP, the other biosynthetic activity present on the outer leaflet of the membrane, is responsible for the formation of peptide crosslinks between stem peptides of adjacent glycan strands, concomitant with the release of the terminal D-Ala residue[135,136].

In *S. aureus* TG activity is performed by monofunctional transglycosylases (TGases), namely Mgt and SgtA, and by the bifunctional enzyme PBP2 (possessing both transglycosylase and transpeptidase activities)[137,138,139]. More recently, the SEDS proteins FtsW and RodA were also reported as having TGase activity[140]. The TP activity is performed by the transpeptidase (TPase) domains of pencillin binding proteins (PBPs)[141].

PBPs can be divided in two main groups, high molecular mass (HMM) PBPs and low molecular mass (LMM) PBPs[141]. HMM PBPs can be further divided into class A and class B, based on the structure and function of the N-terminal domains. Both classes have a C-terminal TPase domain, but while class A PBPs have an N-terminal

TGase domain, class B PBPs have an N-terminal domain that can have other roles, such as in cell morphogenesis through interaction with other proteins[141,142]. LMM PBPs can perform different reactions, including D-Ala-D-Ala carboxypeptidation, D-Ala-D-Ala transpeptidation and endopeptidation[141]. Endopeptidation and transpeptidation are reverse activities, while carboxypeptidation cleaves the terminal D-Ala, without performing cross-linkage, as a water molecule is used as an acceptor, instead of a stem peptide[141,143].

Antibiotic resistance in *Staphylococcus aureus*

The transpeptidase activity of PBPs is the target of β-lactam antibiotics, that act as substrate analogs of the D-Ala-D-Ala dipeptide of the PG and bind to the active site of these enzymes, forming a very stable complex. This blocks the access of PBPs to their natural substrate, causing disruption of PG biogenesis[144,145]. According to Cho and colleagues, β-lactams do more than just blocking PG synthesis, they trigger a futile cycle of PG synthesis and degradation that ultimately exhausts cellular resources, leading to cell death[146].

Penicillin, discovered in 1929 by Alexender Fleming, is a β-lactam. The first mechanism used by *S. aureus* to tackle penicillin treatment was through the acquisition of a gene that codes for a β-lactamase, an enzyme that deactivates these antibiotics by cleaving their characteristic β-lactam rings[147]. With the introduction of β-lactamase insensitive antibiotics, like methicillin and oxacillin, the resistance mechanism in *S. aureus* evolved through the acquisition of an extra PBP with low affinity to β-lactams, called PBP2A[148,149]. *S. aureus* has four native PBPs (PBP1-4) and the fifth PBP, PBP2A, is only present in Methicillin Resistant *Staphylococcus aureus* (MRSA) strains,

encoded by the gene *mecA*, which was acquired from a non -*S. aureus* origin[148]. In the presence of β-lactams, PBP2A continues its TPase activity, while the other TPases are deactivated[148]. In these conditions, the TP domain of PBP2A can cooperate with the β-lactam insensitive TG domain of PBP2, which remains functional, to perform CW synthesis, allowing the cells to grow[150].

S. aureus is a versatile pathogen with the ability to cause several diseases ranging from skin infections to pneumonia or life-threatening endocarditis[151]. Although MRSA started as a major concern in nosocomial environments, it is no longer limited to hospitalized patients, since several outbreaks have been reported worldwide in the community[152,153,154]. Nowadays, MRSA continues to represent a burden to healthcare systems worldwide, being included in the World Health Organization list of high priority pathogens to tackle[155,156].

Bacterial two-component systems

Besides specific resistance mechanisms to antibiotics, bacteria employ other wider responses, dependent on Two-component systems (TCS) to cope with the presence of antibiotics. TCS have a widespread distribution amongst bacteria and archaea and their main biological role is to perceive and transduce environmental cues and initiate the appropriate cellular response, involving biological processes like cell division, metabolism, pathogenicity, antibiotic resistance or chemotaxis[157,158]. TCS are able to respond to several chemical and physical stimuli, from small molecules, ions, pH, temperature, osmotic pressure, redox state, amongst others[158]. Sensing of the environmental stimulus can take place in the

extracellular space, the periplasm, within the membrane or even in the cytoplasm[159].

As the name suggests, a TCS is typically formed by two proteins, a sensor histidine kinase (HK) and a cognate response regulator (RR)[157,158]. It is through the coordination of these two protein partners that the stimulus is perceived and processed into a cellular response. Communication between the two proteins is based on three phosphotransfer reactions: (i) autophosphorylation of a conserved histidine residue in the sensor HK, (ii) phosphotransfer to a conserved aspartate residue in the RR and (iii) dephosphorylation of the RR to reset the system to the pre-stimulus state[157,158,159,160].

The sensor histidine kinase

The typical structure of a sensor HK consists of a homodimeric integral membrane protein with each protomer possessing two transmembrane (TM) domains with the N-terminal part in the cytoplasm and the sensor domain lying between the two TM domains, in the extracellular environment (Figure 10)[161]. After the second TM domain (TM2), there is a HAMP domain (domain present in histidine kinases, adenylyl cyclases, methyl-accepting proteins and phosphatases) linking the TM2 to the dimerization and histidine phosphorylation domain (DHp)[161,162]. This way, conformational changes in the TM domains arrive to the HAMP domain and are transmitted towards the C-terminus, through a mechanism that is not fully elucidated. Nevertheless, all models agree that HAMP exists in two alternative conformational states and that the transition between those states is critical for kinase activation[157,163,164]. At the C-terminus, there is a catalytic and adenosine triphosphate (ATP) binding domain (CA) which, together with the DHp, form the HK catalytic core[157]. The

HAMP, DHp and CA domains are usually conserved among bacteria, specially the histidine residue in the DHp that is phosphorylated by the γ-phosphoryl group of ATP and transferred to the RR[157,161]. This autophosphorylation mechanism, in which ATP and the histidine residue are within phosphotransfer distance, can be performed both in cis and in trans, which means that each monomer in the HK dimer is capable of phosphorylating itself or the other, but that varies with each HK[165,166].

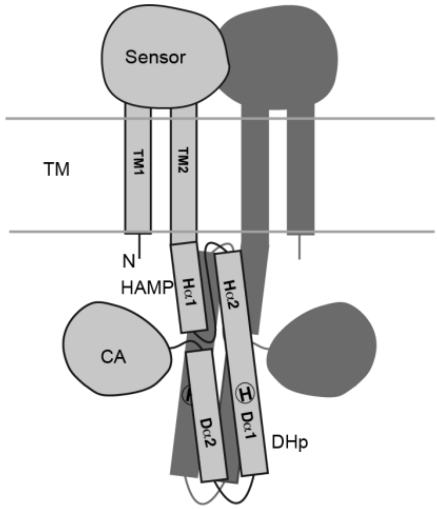

Figure 10. Schematic representation of the modular structure of a typical sensor histidine kinase. The sensor domain is located between the two transmembrane regions (TM1 and TM2).The HAMP domain (see text) is located in the cytoplasm, after TM2 with its second helix (Hα2) connected to the helix Dα1 of the DHp domain, where the phosphorylation site Histidine (H) is present. At the C-terminal region, the catalytic and ATP-binding domain (CA) form, with DHp, the HK catalytic core. The dark shadow represents the other protomer of the homodimer. Adapted from[161].

The N-terminal sensor domains of HK display a great diversity in genetic sequences, membrane topology, composition, and architecture, likely reflecting the different stimuli that HK are able to perceive[157,159]. Taking into consideration this variability, sensor

domains can be grouped according to their architecture, a classification that functionally relates to the sensing mechanism, but does not consider phylogenetic data[159]. Accordingly, HKs can be classified in: (i) extracytosolic/periplasmic sensing HK, (ii) HK with TM-linked sensing mechanisms and (iii) cytoplasmic-sensing HK (Figure 11)[157,159,161].

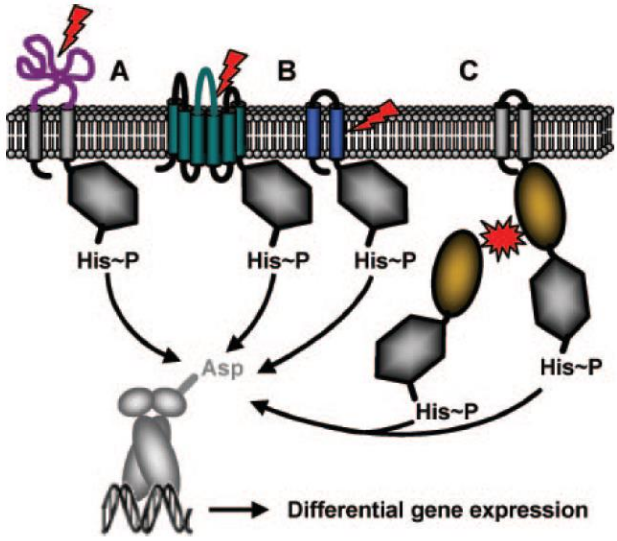

Figure 11. Schematic representation of the three different mechanisms used by HKs to perceive environmental stimuli. (A) Extracytosolic/periplasmic stimulus perception, with the sensor placed outside the cell, between the two TM domains. **(B)** HKs with stimulus perception linked to two or more TM domains. **(C)** Cytoplasmic sensing HKs, either located in the cytoplasm or membrane-anchored. Stimuli are depicted as red thunder or red star. Sensor domains are highlighted in color. Adapted from[159].

Extracytosolic/periplasmic HK represent the largest group of HK with a typical extracellular sensory domain, flanked by two TM domains and with the kinase catalytic core spatially separated from the sensory domain by the cytoplasmic membrane, requiring TM signal transduction[159]. This topological group is typical for HK that sense nutrients or solutes[159].

HK from the group containing TM-linked sensory domains have one key feature in common, which is the presence of 2-20 TM regions connected by short intra or extracellular linkers, lacking an evident extracellular sensory domain[159]. For these HK, stimuli are perceived inside the membrane or are membrane associated, which include mechanical properties of the cell envelope, such as turgor pressure, or stimuli originated from membrane integral components[159]. This functional group can be further divided into several subgroups, taking into consideration the number of TM domains, including the intramembrane-sensing HK (IMHK) subgroup, characterized by a small sensor domain, comprised of two TM domains, linked by a short extracytoplasmic linker[159,167]. These IMHK are then subdivided into two families: (i) BceS-like IMHK, functionally linked to ABC transporters and (ii) LiaS-like IMHK, which are part of a three-component system, only found in Firmicutes[167].

The last group corresponds to cytoplasmic-sensing HK, soluble or membrane-anchored, in which the sensory domain lies inside the cytoplasm and typically detects cytoplasmic solutes or metabolism related activities[159].

The response regulator

The RR is the element of the TCS responsible for the execution of the cellular response to the HK detected stimulus[157,168]. The typical structure of the RR comprises two domains, the conserved N-terminal receiver domain (REC), also called regulatory domain, and a variable C-terminal effector domain[157,168]. In the REC domain, there is a well conserved aspartate residue that accepts the phosphoryl group from the cognate HK, which triggers conformational changes in REC

domain that are required for the effector domain to perform the desired output[157,161,168].

The structure of REC domain consists of a five-stranded parallel β-sheet surrounded by five amphipathic α-helices[168]. The aspartate residue, required for phosphorylation, is located at the end of the third β-strand and two additional acidic residues are placed at the loop that links the β_1 and α_1 strands, which are necessary for the binding of a divalent cation Mg^{2+} or Mn^{2+}, essential or the phosphorylation reaction [157,161,168] (Figure 12).

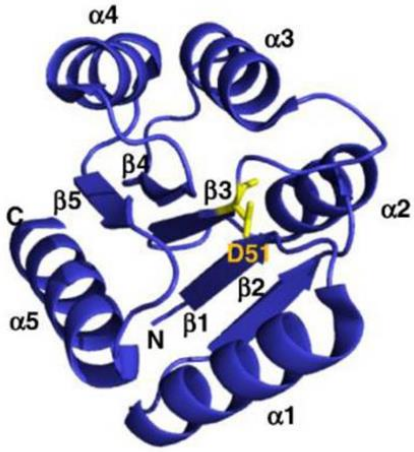

Figure 12. Histidine Kinase Receiver domain (REC) secondary structure. Receiver domain of PhoP depicts the typical structure of a REC, showing the α and β folds in blue. The conserved site of phosphorylation (D51) is shown in yellow. Adapted from[157].

The activation of the RR by phosphorylation promotes structural modifications in the α_4-β_5-α_5 face (Figure 12), not at the secondary structure level, but rather mild displacements and small perturbations at the molecular level[157,161,168]. Phosphorylation of the REC domain promotes, in many cases, RR dimerization or multimerization,

typically required for the output response[157]. The dimerization process usually occurs through the α_4-β_5-α_5 face of the REC[157,161,168].

Contrary to REC domains, effector domains are quite variable, due to the diversity of outputs required for cells to cope with different environmental stimuli[161]. Response regulators are classified according to the response of their effector domains in: (i) DNA-binding, (ii) RNA-binding, (iii) enzymatically active, (iv) protein-binding and (v) single-domain RR. The majority of RR (between 60% and 70%) fall into the DNA-binding category, serving as transcription factors[157,168].

In DNA-binding RRs, phosphorylation of REC domain usually results in dimerization, increasing the affinity in the RR towards specific DNA sequences, commonly direct or inverted repeats[157]. RNA-binding RRs are quite rare (~1% of all RRs) and usually regulate transcription by inhibition of termination by Rho-independent terminators[169]. Response regulators with enzymatic activity represent around 8% of RRs and are characterized for combining a REC domain with different enzymatic domains involved in signal transduction[157]. Lastly, protein-binding RR and single-domain RR exert their function through protein-protein interactions[157].

To terminate the response and allow for adaptation to an environmental context, RRs are subjected to dephosphorylation of the REC domain, that results from a nucleophilic attack of a water molecule to the phosphoryl group in the active centre of the RR[157]. Dephosphorylation rates vary with each RR and can be enhanced by dedicated phosphatases[157,170]

Histidine kinase - response regulator interaction

Communication between the HK and its cognate RR relies on the phosphorylation reaction, during which the RR binds to the DHp domain of the HK, allowing aspartyl phosphorylation, using the phospho-histidine as substrate[157,161].

In general, HK have a kinetic selectivity towards their cognate RR. However the existence of cross-talk between different TCS, meaning a HK phosphorylating a non-cognate RR, has been widely documented, *in vitro*[171,172,173]. Such cross-talk between different signal transduction pathways has to be minimized, to ensure an adequate response to a specific stimulus[172]. Yet, in some conditions, cross-talk can be used as a way to integrate multiple input signals or a way to diversify the response towards a specific stimulus. This is usually referred as cross-regulation, to distinguish it from the biologically detrimental cross-talk[174]. Cross-talk is also documented at the level of RR, since they can be phosphorylated by phospho-donor acetyl-phosphate, a molecule whose levels fluctuate with the cellular metabolic state[175].

One mechanism used by bacteria to exert a tight control over the possible cross-talk is through bifunctional HKs, that can also perform phosphatase activity[157,158,172]. In these bifunctional HKs, the kinase and phosphatase states are mutually exclusive and present different dynamics[158]. A comparative analysis between bifunctional and monofunctional HKs revealed that the bifunctional enzymes are more effective in supressing cross-talk than their monofunctional counterparts[172,176,177]. Under these assumptions, it is suggested that monofunctional HKs are likely present in TCS which have a single RR integrating information from multiple HKs[172,176].

Two-component systems in *Staphylococcus aureus*

The *S. aureus* genome encodes 16 TCS, only one of which is essential WalKR, a TCS common to other low GC Gram-positive bacteria[178,179]. Some of these TCS, including WalKR, VraTSR, GraXSR or BraSR, have roles in maintenance of CW homeostasis[179,180,181,182].

VraTSR regulatory system

VraTSR is a Three Component System in *S. aureus* responsible for triggering a cellular response to the presence of CW damage, by modulating the expression of certain genes involved in CW synthesis, but also genes involved in carbohydrate transport, lipid metabolism, DNA repair, amongst others[180,183,184,185,]. Genes involved in the coordinated response of cells to CW active antibiotics, constitute the so-called CW stress stimulon (CWSS)[183]. The transcriptional profile of cells treated with different CW targeting antibiotics differs but includes a common set of genes under the control of VraTSR system[183,184]. This response aims to mitigate the damage inflicted to the CW, by producing more CW synthetic enzymes, such as PBP2, Mgt (monofunctional TGase) and MurZ (redundant MurA isozyme)[183,186]. At the same time, genes encoding stress-response proteins, like osmoprotectant transporters *proP* and *opuD* are also upregulated, a response thought to prevent cell lysis, due to the high osmolarity of the cytoplasm, in the presence of CW damage[184]. However, the role of some of the VraTSR-regulated genes remains poorly characterized, such as the case of *copA* encoding a copper-transporting ATPase or unknown predicted ORFs[184]. The *vraSR* genes were first described in 2000, in the Vancomycin-Resistant *S. aureus* (VRSA) strain Mu50 and heterogeneously vancomycin

resistant *S. aureus* strain Mu3, as vancomycin-resistant associated genes, whose transcription was up-regulated compared with a vancomycin-susceptible strain[187]. While it was named as a vancomycin resistance associated system, it responds to several CW targeting antibiotics, from glycopeptides, like vancomycin, to β-lactams, such as oxacillin, but also antibiotics blocking the early steps of CW synthesis, like fosfomycin[185]. Accordingly, resistance to most CW active antibiotics is affected when *vraSR* genes are deleted[184].

These genes are encoded in an operon comprised of four co-transcribed open reading frames (ORFs), *orf1*, *yvqF*, *vraS* and *vraR*, under the control of one promoter with one major transcription start point (tsp) 132 bp upstream of *orf1* and one minor tsp 48 bp upstream of *orf1*[180]. *vraS* encodes the HK VraS and *vraR* the cognate RR VraR[180].

VraS is a typical HK with a N-terminal region composed of two TM domains connected by a periplasmic linker and a C-terminal kinase core formed by the dimerization and histidine phosphorylation domain DHp and the ATP binding CA domain[188]. With no clear extracellular sensing domain, VraS likely belongs to the IMHK subgroup[188,189]. Studies performed *in vitro* suggest that 50% of VraS autophosphorylation can occur within 10 min of incubation with [γ-^{32P}] ATP and that 70% of VraR molecules are phosphorylated by radiolabelled VraS in 30 s, which implies that bacteria can trigger a response to CW stress in less than a complete cell cycle (around 20 min), increasing their chances of survival[188,190]. These fast phosphotransfer kinetics between VraS and VraR suggest that these two proteins constitute, in fact, a cognate HK-RR pair[188]. VraS is also described as having phosphatase activity, a typical feature of bifunctional HKs, controlling the levels of phosphorylated VraR[188].

VraR is a typical RR with the receiver or regulatory domain (REC) in the N-terminal region and an effector domain at the C-terminal part[188]. The N-terminal region comprises residues 1-117, with the phosphorylation site corresponding to aspartate (Asp-55) and the C-terminal effector domain comprises residues 141-209, displaying DNA-binding affinity, through a helix-turn-helix motif[188]. Phosphorylation of VraR triggers its dimerization, a process that is required for DNA-binding activity[188]. VraR consensus binding sequence is described as 5'-ACT(X)nAGT-3' and 5'-TGA(X)nTCA-3', where X represents any nucleotide and n varies from 1 to 3[191,192,193]. VraR binding sequences were shown to be present in the promoters of several genes coding enzymes associated with CW synthesis, like *pbpB*, *mgt*, *murZ*, *fmtA* and even *vraSR* own promoter[191,192,193]. Inside *vraTSR* promoter there are two regions with VraR binding sites, called R1 and R2[191,192]. Binding of VraR to these regions is hierarchical, as VraR first binds to R1, in a phosphorylation-independent fashion, in normal growth conditions, providing basal expression levels[191,192]. This phosphorylation independence of R1 site is due to the proximity between two VraR binding sequences, which mediates VraR dimerization[191,192]. In the presence of CW stress, the phosphorylated and dimerized VraR can bind to the less conserved R2 site and enhance *vraSR* expression levels[191,192]. The distance of VraR binding sequences in R2 site ensures that VraR can only bind to this region in a phosphorylation-dependent manner, *i.e*. under CW stress, with the assistance of VraR molecules already bound to R1[191,192].

Amongst the four genes present in the *orf1-yvqf-vraS-vraR* operon, later renamed *vraU-vraT-vraS-vraR*, only *vraU* presents no apparent role in CWSS induction, as well as no observable affect in resistance profiles for CW targeting antibiotics[189,194]. On the other hand, deletion

of *vraT* increases susceptibility towards CW targeting antibiotics, like oxacillin, and results in attenuation of CWSS induction in the presence of CW damage, similar to what is observed for *vraS* or *vraR* deletion mutants[189,194]. Since VraT and VraS can interact *in vivo*, a new role was suggested for VraT as a third player in the TCS, similar to what is observed in other *S. aureus* TCS like GraXSR, or LiaFSR in *B. subtilis*[189,195,196]. VraT is a putative membrane protein, with a possible role of cooperating with VraS in sensing a still unknown stimulus, during CW stress conditions, particularly because VraS belongs to the IMHK family of HKs and lacks an extracellular sensor domain[167,189]. A new model was proposed by Boyle-Vavra and colleagues in which CW damage triggers a structural modification in VraT, influencing the autophosphorylation of VraS, which then phosphorylates VraR, ultimately modulating expression of the CWSS (Figure 13)[189]. The role of VraT, however, remains elusive[189,197].

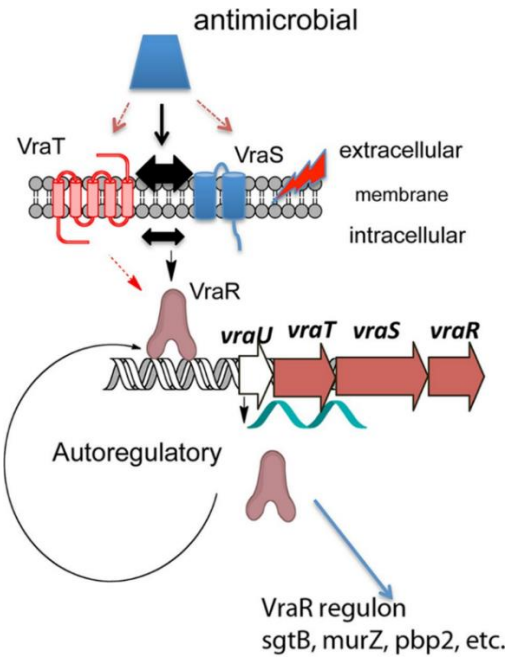

Figure 13. Proposed model for VraTSR regulatory system. The current model for the mechanism of VraTSR activation proposes that damage inflicted on the CW triggers conformational changes in VraT. These conformational changes influence VraS HK autophosphorylation, which then transfers the phosphate group to the RR VraR. VraR will then activate or repress the expression of several genes, known as CWSS, including its own promoter, in a coordinated fashion. The signal detected by VraT (depicted with a lightning bolt) remains elusive. Brown arrows in *vra* operon correspond to genes required for methicillin resistance; white arrow indicates *vraU* which is not required for methicillin resistance; black double-headed arrows in membrane and cytoplasm indicate a possible interaction between VraT and the HK VraS; dotted red and pink arrows, represent hypothetical interactions between the antimicrobial compound and VraS and VraT and between VraT and VraR; blue wavy line represents polycistronic mRNA expression. Adapted from[189].

Concluding remarks

In this thesis, we explore the cell cycle of *S. aureus*, using Super-Resolution microscopy to unveil morphological changes and to study proteins with a relevant role, during this process. Considering that *S. aureus* is an important pathogen worldwide, this information is crucial to tackle this microorganism. On this subject, we also explored a relevant signal transduction mechanism used by *S. aureus* to protect itself against antibiotics, trying to understand its sensing mechanism and activation pattern.

Taken together, the results presented in this thesis provide relevant information regarding the biology of this pathogen.

References

1. Kara R, Robert JK. bacteria | Cell, Evolution, & Classification | Britannica.com. *Encycl Br inc*. 2018.
2. Clark DP, Pazdernik NJ. Bacterial Genetics. In: Molecular Biology. 2013; e641-e646. doi:10.1016/b978-0-12-378594-7.00060-3
3. Donachie WD. Co-ordinate regulation of the *Escherichia coli* cell cycle or The cloud of unknowing. *Mol Microbiol*. 2001; 40(4):779-85. doi:10.1046/j.1365-2958.2001.02439.x
4. Flemming HC, Wuertz S. Bacteria and archaea on Earth and their abundance in biofilms. *Nat Rev Microbiol*. 2019; 17:247–260. doi:10.1038/s41579-019-0158-9
5. Martos A, Jiménez M, Rivas G, Schwille P. Towards a bottom-up reconstitution of bacterial cell division. *Trends Cell Biol*. 2012; 22(12):634-43. doi:10.1016/j.tcb.2012.09.003
6. Vicente M, Rico AI. The order of the ring: Assembly of *Escherichia coli* cell division components. *Mol Microbiol*. 2006; 61(1):5-8. doi:10.1111/j.1365-2958.2006.05233.x
7. Mingorance J, Rivas G, Vélez M, Gómez-Puertas P, Vicente M. Strong FtsZ is with the force: Mechanisms to constrict bacteria. *Trends Microbiol*. 2010; 18(8):348-56. doi:10.1016/j.tim.2010.06.001
8. Rowlett VW, Margolin W. The Min system and other nucleoid-independent regulators of Z ring positioning. *Front Microbiol*. 2015; 6: 478. doi:10.3389/fmicb.2015.00478
9. Wu LJ, Errington J. Nucleoid occlusion and bacterial cell division. *Nat Rev Microbiol*. 2012; 10(1):8-12. doi:10.1038/nrmicro2671
10. Reyes-Lamothe R, Sherratt DJ. The bacterial cell cycle, chromosome inheritance and cell growth. *Nat Rev Microbiol*. 2019; 17:467–478. doi:10.1038/s41579-019-0212-7
11. Wang JD, Levin PA. Metabolism, cell growth and the bacterial cell cycle. *Nat Rev Microbiol*. 2009; 7(11):822-827 doi:10.1038/nrmicro2202
12. Amir A. Cell size regulation in bacteria. *Phys Rev Lett*. 2014;112(20): 208102. doi:10.1103/PhysRevLett.112.208102
13. Donachie WD. Relationship between cell size and time of initiation of DNA replication. *Nature*. 1968; 219(5158):1077-1079. doi:10.1038/2191077a0
14. Jun S, Si F, Pugatch R, Scott M. Fundamental principles in bacterial physiology-history, recent progress, and the future with focus on cell size control: A review. *Reports Prog Phys*.

2018;81(5): e641-e646. doi:10.1088/1361-6633/aaa628
15. Diekmann O, Lauwerier HA, Aldenberg T, Metz JAJ. Growth, fission and the stable size distribution. *J Math Biol.* 1983;18(2):135-148. doi:10.1007/BF00280662
16. Weart RB, Lee AH, Chien AC, Haeusser DP, Hill NS, Levin PA. A metabolic sensor governing cell size in bacteria. *Cell*. 2007;130(2): 335-347. doi:10.1016/j.cell.2007.05.043
17. Lotka AJ. The Stability of the Normal Age Distribution. *Proc Natl Acad Sci*. 1922;8(11):339-345. doi:10.1073/pnas.8.11.339
18. Gyllenberg M. Nonlinear age-dependent population dynamics in continuously propagated bacterial cultures. *Math Biosci*. 1982;62(1):45-74. doi:10.1016/0025-5564(82)90062-1
19. Taheri-Araghi S, Bradde S, Sauls JT, et al. Cell-size control and homeostasis in bacteria. *Curr Biol*. 2015;25(3):385-391. doi:10.1016/j.cub.2014.12.009
20. Lam H, Matroule JY, Jacobs-Wagner C. The asymmetric spatial distribution of bacterial signal transduction proteins coordinates cell cycle events. *Dev Cell*. 2003;5(1):149-159. doi:10.1016/S1534-5807(03)00191-6
21. Hallez R, Bellefontaine AF, Letesson JJ, De Bolle X. Morphological and functional asymmetry in α-proteobacteria. *Trends Microbiol*. 2004; 12(8):361-365. doi:10.1016/j.tim.2004.06.002
22. Donachie WD, Begg KJ, Vicente M. Cell length, cell growth and cell division. *Nature*. 1976;264(5584):328-333. doi:10.1038/264328a0
23. Bergmiller T, Ackermann M. Pole age affects cell size and the timing of cell division in *Methylobacterium extorquens* AM1. *J Bacteriol*. 2011; 193(19): 5216–5221. doi:10.1128/JB.00329-11
24. Jun S, Taheri-Araghi S. Cell-size maintenance: Universal strategy revealed. *Trends Microbiol*. 2015;23(1):4-6. doi:10.1016/j.tim.2014.12.001
25. Si F, Le Treut G, Sauls JT, Vadia S, Levin PA, Jun S. Mechanistic origin of cell-size control and homeostasis in bacteria. *Curr Biol*. 2019;29(11): 1760-1770. doi:10.1016/j.cub.2019.04.062
26. Fantes PA, Grant WD, Pritchard RH, Sudbery PE, Wheals AE. The regulation of cell size and the control of mitosis. *J Theor Biol*. 1975;50(1): 213-244. doi:10.1016/0022-5193(75)90034-X
27. Amir A. Is cell size a spandrel? *Elife*. 2017;6: e22186. doi:10.7554/eLife.22186
28. Campos M, Surovtsev I V., Kato S, et al. A constant size extension drives bacterial cell size homeostasis. *Cell*. 2014; 159(6): 1433–1446. doi:10.1016/j.cell.2014.11.022

29. Harris LK, Theriot JA. Relative rates of surface and volume synthesis set bacterial cell size. *Cell*. 2016; 165(6):1479-1492. doi:10.1016/j.cell.2016.05.045
30. Young KD. Bacterial morphology: why have different shapes? *Curr Opin Microbiol*. 2007; 10(6): 596–600. doi:10.1016/j.mib.2007.09.009
31. Tzagoloff H, Novick R. Geometry of cell division in *Staphylococcus aureus*. *J Bacteriol*. 1977; 129(1): 343–350. doi:10.1128/jb.129.1.343-350.1977
32. Turner RD, Ratcliffe EC, Wheeler R, Golestanian R, Hobbs JK, Foster SJ. Peptidoglycan architecture can specify division planes in *Staphylococcus aureus*. *Nat Commun*. 2010; 1:26. doi:10.1038/ncomms1025
33. Saraiva BM, Sorg M, Pereira AR, et al. Reassessment of the distinctive geometry of *Staphylococcus aureus* cell division. *Nat Commun*. 2020;11(1):1-7. doi:10.1038/s41467-020-17940-9
34. Pinho MG, Kjos M, Veening JW. How to get (a)round: Mechanisms controlling growth and division of coccoid bacteria. *Nat Rev Microbiol*. 2013; 11(9):601-614. doi:10.1038/nrmicro3088
35. Veiga H, Jorge AM, Pinho MG. Absence of nucleoid occlusion effector Noc impairs formation of orthogonal FtsZ rings during *Staphylococcus aureus* cell division. *Mol Microbiol*. 2011; 80(5):1366-80. doi:10.1111/j.1365-2958.2011.07651.x
36. Scheffers D-J, Pinho MG. Bacterial cell wall synthesis: new insights from localization studies. *Microbiol Mol Biol Rev*. 2005;69(4):585-607. doi:10.1128/mmbr.69.4.585-607.2005
37. Foster T. *Staphylococcus*. In: Baron S, editor. Medical Microbiology. 4th edition. Galveston (TX): University of Texas Medical Branch at Galveston; 1996. Chapter 12. Available from: https://www.ncbi.nlm.nih.gov/books/NBK8448/
38. Zhou X, Halladin DK, Rojas ER, et al. Mechanical crack propagation drives millisecond daughter cell separation in *Staphylococcus aureus. Science*. 2015; 348(6234): 574–578. doi:10.1126/science.aaa1511
39. Matias VRF, Beveridge TJ. Cryo-electron microscopy of cell division in *Staphylococcus aureus* reveals a mid-zone between nascent cross walls. *Mol Microbiol*. 2007; 64(1):195-206. doi:10.1111/j.1365-2958.2007.05634.x
40. Matias VRF, Beveridge TJ. Native cell wall organization shown by cryo-electron microscopy confirms the existence of a periplasmic space in *Staphylococcus aureus*. *J Bacteriol*. 2006; 188(3): 1011–1021. doi:10.1128/JB.188.3.1011-1021.2006

41. Lund VA, Wacnik K, Turner RD, et al. Molecular coordination of *Staphylococcus aureus* cell division. *Elife*. 2018;7:e32057. doi:10.7554/eLife.32057
42. Osipovitch DC, Therrien S, Griswold KE. Discovery of novel *S. aureus* autolysins and molecular engineering to enhance bacteriolytic activity. *Appl Microbiol Biotechnol*. 2015;99(15):6315-6326. doi:10.1007/s00253-015-6443-2
43. Kajimura J, Fujiwara T, Yamada S, et al. Identification and molecular characterization of an N-acetylmuramyl-L- alanine amidase Sle1 involved in cell separation of *Staphylococcus aureus*. *Mol Microbiol*. 2005;58(4):1087-1101. doi:10.1111/j.1365-2958.2005.04881.x
44. Yamada S, Sugai M, Komatsuzawa H, et al. An autolysin ring associated with cell separation of *Staphylococcus aureus*. *J Bacteriol*. 1996; 178(6):1565-1571. doi:10.1128/jb.178.6.1565-1571.1996
45. Raser JM, O'Shea EK. Molecular biology - Noise in gene expression: Origins, consequences, and control. *Science*. 2005; 309(5743): 2010–2013. doi:10.1126/science.1105891
46. Couturier E, Rocha EPC. Replication-associated gene dosage effects shape the genomes of fast-growing bacteria but only for transcription and translation genes. *Mol Microbiol*. 2006;59(5):1506-1518. doi:10.1111/j.1365-2958.2006.05046.x
47. Den Blaauwen T, Luirink J. Checks and balances in bacterial cell division. *MBio*. 2019; 10(1):e00149-19. doi:10.1128/mBio.00149-19
48. Oakley AJ. A structural view of bacterial DNA replication. *Protein Sci*. 2019; 28(6): 990–1004. doi:10.1002/pro.3615
49. Mohapatra SS, Fioravanti A, Biondi EG. DNA methylation in *Caulobacter* and other *Alphaproteobacteria* during cell cycle progression. *Trends Microbiol*. 2014;22(9): 528-535. doi:10.1016/j.tim.2014.05.003
50. Marczynski GT, Shapiro L. Control of Chromosome Replication in *Caulobacter crescentus* . *Annu Rev Microbiol*. 2002; 56:625-56. doi:10.1146/annurev.micro.56.012302.161103
51. Sánchez-Romero MA, Casadesús J. The bacterial epigenome. *Nat Rev Microbiol*. 2020; 18:7-20. doi:10.1038/s41579-019-0286-2
52. Low DA, Casadesús J. Clocks and switches: bacterial gene regulation by DNA adenine methylation. *Curr Opin Microbiol*. 2008; 11(2):106-112. doi:10.1016/j.mib.2008.02.012
53. Collier J, McAdams HH, Shapiro L. A DNA methylation ratchet governs progression through a bacterial cell cycle. *Proc Natl*

Acad Sci U S A. 2007; 104(43):17111-17116. doi:10.1073/pnas.0708112104
54. Collier J, Murray SR, Shapiro L. DnaA couples DNA replication and the expression of two cell cycle master regulators. *EMBO J*. 2006; 25(2): 346–356. doi:10.1038/sj.emboj.7600927
55. Quon KC, Yang B, Domian IJ, Shapiro L, Marczynski GT. Negative control of bacterial DNA replication by a cell cycle regulatory protein that binds at the chromosome origin. *Proc Natl Acad Sci U S A*. 1998; 95(1):120-125. doi:10.1073/pnas.95.1.120
56. Domian IJ, Quon KC, Shapiro L. Cell type-specific phosphorylation and proteolysis of a transcriptional regulator controls the G1-to-S transition in a bacterial cell cycle. *Cell*. 1997; 90(3):415-424. doi:10.1016/S0092-8674(00)80502-4
57. Bergé M, Pezzatti J, González-Ruiz V, et al. Bacterial cell cycle control by citrate synthase independent of enzymatic activity. *Elife*. 2020;9:e52272. doi:10.7554/eLife.52272
58. Narayanan S, Janakiraman B, Kumar L, Radhakrishnan SK. A cell cycle-controlled redox switch regulates the topoisomerase IV activity. *Genes Dev*. 2015; 29(11):1175-1187. doi:10.1101/gad.257030.114
59. Radhakrishnan SK, Pritchard S, Viollier PH. Coupling prokaryotic cell fate and division control with a bifunctional and oscillating oxidoreductase homolog. *Dev Cell*. 2010; 18(1):90-101. doi:10.1016/j.devcel.2009.10.024
60. Beaufay F, Coppine J, Mayard A, Laloux G, De Bolle X, Hallez R. A NAD -dependent glutamate dehydrogenase coordinates metabolism with cell division in *Caulobacter crescentus*. *EMBO J*. 2015; 34(13):1786-1800. doi:10.15252/embj.201490730
61. Huberts DHEW, van der Klei IJ. Moonlighting proteins: An intriguing mode of multitasking. *Biochim Biophys Acta - Mol Cell Res*. 2010; 1803(4):520-5. doi:10.1016/j.bbamcr.2010.01.022
62. Hill NS, Buske PJ, Shi Y, Levin PA. A moonlighting enzyme links *Escherichia coli* cell size with central metabolism. *PLoS Genet*. 2013; 9(7): e1003663. doi:10.1371/journal.pgen.1003663
63. Dewachter L, Verstraeten N, Fauvart M, Michiels J. An integrative view of cell cycle control in *Escherichia coli*. *FEMS Microbiol Rev*. 2018;42(2):116-136. doi:10.1093/femsre/fuy005
64. Kampen VNG. *Stochastic Processes in Physics and Chemistry*. 2007. doi:10.1016/B978-0-444-52965-7.X5000-4
65. Elowitz MB, Levine AJ, Siggia ED, Swain PS. Stochastic gene expression in a single cell. *Science*. 2002; 297(5584):1183-

1186. doi:10.1126/science.1070919
66. Mcadams HH, Arkin A. Stochastic mechanisms in gene expression. *Proc Natl Acad Sci U S A*. 1997; 94(3):814-819. doi:10.1073/pnas.94.3.814
67. Raser JM, O'Shea EK. Control of stochasticity in eukaryotic gene expression. *Science*. 2004;304(5678):1811-1814. doi:10.1126/science.1098641
68. Pedraza JH, Van Oudenaarden A. Noise propagations in gene networks. *Science*. 2005; 307(5717):1965-1969. doi:10.1126/science.1109090
69. Rosenfeld N, Young JW, Alon U, Swain PS, Elowitz MB. Gene regulation at the single-cell level. *Science*. 2005;307(5717):1962-1965. doi:10.1126/science.1106914
70. Kar S, Baumann WT, Paul MR, Tyson JJ. Exploring the roles of noise in the eukaryotic cell cycle. *Proc Natl Acad Sci U S A*. 2009; 106(16):6471-6476. doi:10.1073/pnas.0810034106
71. Ozbudak EM, Thattai M, Kurtser I, Grossman AD, van Oudenaarden A. Regulation of noise in the expression of a single gene. *Nat Genet*. 2002;31(1):69-73. doi:10.1038/ng869
72. Vázquez-Jiménez A, Santillán M, Rodríguez-González J. How the extrinsic noise in gene expression can be controlled? *IFAC-PapersOnLine*. 2017; 50(1):15092-15096. doi:10.1016/j.ifacol.2017.08.2236
73. Dubnau D, Losick R. Bistability in bacteria. *Mol Microbiol*. 2006; 61(3):564-572. doi:10.1111/j.1365-2958.2006.05249.x
74. Balaban NQ, Merrin J, Chait R, Kowalik L, Leibler S. Bacterial persistence as a phenotypic switch. *Science*. 2004; 305(5690):1622-1625. doi:10.1126/science.1099390
75. Jung SH, Ryu CM, Kim JS. Bacterial persistence: Fundamentals and clinical importance. *J Microbiol*. 2019; 57(10):829-835. doi:10.1007/s12275-019-9218-0
76. Silhavy TJ, Kahne D, Walker S. The bacterial cell envelope. *Cold Spring Harb Perspect Biol*. 2010; 2(5):a000414. doi:10.1101/cshperspect.a000414
77. Coico R. Gram staining tutorial. *Curr Protoc Microbiol*. 2005. doi:10.1002/9780471729259.mca03cs00
78. Beveridge TJ. Structures of gram-negative cell walls and their derived membrane vesicles. *J Bacteriol*. 1999; 181(16):4725-4733. doi:10.1128/jb.181.16.4725-4733.1999
79. Henderson JC, Zimmerman SM, Crofts AA, et al. The power of asymmetry: architecture and assembly of the Gram-negative outer membrane lipid bilayer. *Annu Rev Microbiol*. 2016; 70:255-278. doi:10.1146/annurev-micro-102215-095308
80. Fortin D, Ferris FG, Beveridge TJ. Surface-mediated mineral

development by bacteria. *Geomicrobiology: Interactions Between Microbes and Minerals*. 2019; 35 (1): 161–180. doi:10.1515/9781501509247
81. Auer GK, Weibel DB. Bacterial Cell Mechanics. *Biochemistry*. 2017; 56(29): 3710–3724. doi:10.1021/acs.biochem.7b00346
82. Vollmer W, Seligman SJ. Architecture of peptidoglycan: more data and more models. *Trends Microbiol*. 2010;18(2): 59-66. doi:10.1016/j.tim.2009.12.004
83. Braun V. Covalent lipoprotein from the outer membrane of *Escherichia coli*. *BBA - Rev Biomembr*. 1975; 415(3):335-377. doi:10.1016/0304-4157(75)90013-1
84. Mullineaux CW, Nenninger A, Ray N, Robinson C. Diffusion of green fluorescent protein in three cell environments in *Escherichia coli*. *J Bacteriol*. 2006;188(10):3442-3448. doi:10.1128/JB.188.10.3442-3448.2006
85. Ehrmann M.*The Periplasm*. 2007. doi:10.1128/9781555815806
86. Matias VRF, Beveridge TJ. Cryo-electron microscopy reveals native polymeric cell wall structure in *Bacillus subtilis* 168 and the existence of a periplasmic space. *Mol Microbiol*. 2005; 56(1):240-251. doi:10.1111/j.1365-2958.2005.04535.x
87. Neuhaus FC, Baddiley J. A Continuum of anionic charge: structures and functions of d-alanyl-teichoic acids in Gram-positive bacteria. *Microbiol Mol Biol Rev*. 2003; 67(4):686-723. doi:10.1128/mmbr.67.4.686-723.2003
88. Mai-Prochnow A, Clauson M, Hong J, Murphy AB. Gram positive and Gram negative bacteria differ in their sensitivity to cold plasma. *Sci Rep*. 2016;6(1):38610. doi:10.1038/srep38610
89. Nakano R, Hara M, Ishiguro H, et al. Broad spectrum microbicidal activity of photocatalysis by TiO_2. *Catalysts*. 2013; 3(1):310-323. doi:10.3390/catal3010310
90. Malanovic N, Lohner K. Gram-positive bacterial cell envelopes: The impact on the activity of antimicrobial peptides. *Biochim Biophys Acta - Biomembr*. 2016; 1858(5):936-946. doi:10.1016/j.bbamem.2015.11.004
91. Beeby M, Gumbart JC, Roux B, Jensen GJ. Architecture and assembly of the Gram-positive cell wall. *Mol Microbiol*. 2013; 88(4):664-672. doi:10.1111/mmi.12203
92. Brown S, Santa Maria JP, Walker S. Wall Teichoic Acids of Gram-Positive Bacteria. *Annu Rev Microbiol*. 2013;67(2013):313-336. doi:10.1146/annurev-micro-092412-155620
93. Wickham JR, Halye JL, Kashtanov S, Khandogin J, Rice C V. Revisiting magnesium chelation by teichoic acid with

phosphorus solid-state nmr and theoretical calculations. *J Phys Chem B*. 2009; 113(7):2177–2183. doi:10.1021/jp809313j

94. Biswas R, Martinez RE, Göhring N, *et al*. Proton-binding capacity of *Staphylococcus aureus* wall teichoic acid and its role in controlling autolysin activity. *PLoS One*. 2012; 7(7): e41415. doi:10.1371/journal.pone.0041415
95. Vollmer W, Blanot D, De Pedro MA. Peptidoglycan structure and architecture. *FEMS Microbiol Rev*. 2008;32(2):149-167. doi:10.1111/j.1574-6976.2007.00094.x
96. Irazoki O, Hernandez SB, Cava F. Peptidoglycan muropeptides: Release, perception, and functions as signaling molecules. *Front Microbiol*. 2019;10:500. doi:10.3389/fmicb.2019.00500
97. Dramsi S, Magnet S, Davison S, Arthur M. Covalent attachment of proteins to peptidoglycan. *FEMS Microbiol Rev*. 2008;32(2):307-320. doi:10.1111/j.1574-6976.2008.00102.x
98. Rogers HJ, Perkins HR, Ward JB. *Microbial Cell Walls and Membranes*.; 1980. doi:10.1007/978-94-011-6014-8
99. Schleifer KH, Kandler O. Peptidoglycan types of bacterial cell walls and their taxonomic implications. *Bacteriol Rev*. 1972; 36(4):407-477. doi:10.1128/mmbr.36.4.407-477.1972
100. Shaikh MS, Kale MA, Sharuk K. Discovery of heterocyclic analogs of diaminopimelic acid as promising antibacterial agents through enzyme targeted inhibition of lysine biosynthesis. *Curr Enzym Inhib*. 2017;14(2):120-130. doi:10.2174/1573408014666171218150219
101. Cava F, de Pedro MA. Peptidoglycan plasticity in bacteria: Emerging variability of the murein sacculus and their associated biological functions. *Curr Opin Microbiol*. 2014; 18:46-53. doi:10.1016/j.mib.2014.01.004
102. Vollmer W. Structural variation in the glycan strands of bacterial peptidoglycan. *FEMS Microbiol Rev*. 2008;32(2):287-306. doi:10.1111/j.1574-6976.2007.00088.x
103. Snowden MA, Perkins HR, Wyke AW, Hayes M V., Ward JB. Cross-linking and O-acetylation of newly synthesized peptidoglycan in *Staphylococcus aureus* H. *J Gen Microbiol*. 1989; 135(11):3015-3022. doi:10.1099/00221287-135-11-3015
104. Azuma I, Thomas DW, Adam A, *et al*. Occurrence of N-glycolylmuramic acid in bacterial cell walls. A preliminary survey. *BBA - Gen Subj*. 1970;208(3): 444-451. doi:10.1016/0304-4165(70)90217-5
105. Amano K, Hayashi H, Araki Y, Ito E. The action of lysozyme on peptidoglycan with N-unsubstituted glucosamine residues. Isolation of glycan fragments and their susceptibility to

lysozyme. *Eur J Biochem*. 1977; 76(1):299-307. doi:10.1111/j.1432-1033.1977.tb11596.x
106. Brumfitt W, Wardlaw AC, Park JT. Development of lysozyme-resistance in *Micrococcus lysodiekticus* and its association with an increased O-acetyl content of the cell wall. *Nature*. 1958;181(4626):1783–1784. doi:10.1038/1811783a0
107. Atrih A, Bacher G, Allmaier G, Williamson MP, Foster SJ. Analysis of peptidoglycan structure from vegetative cells of *Bacillus subtilis* 168 and role of PBP 5 in peptidoglycan maturation. *J Bacteriol*. 1999; 181(13):3956-3966. doi:10.1128/jb.181.13.3956-3966.1999
108. Glauner B, Holtje J V. Growth pattern of the murein sacculus of *Escherichia coli*. *J Biol Chem*. 1990; 265(31):18988-18996.
109. Glauner B, Holtje J V., Schwarz U. The composition of the murein of *Escherichia coli*. *J Biol Chem*. 1988; 263(21):10088-10095.
110. Carlstrom D. The crystal structure of alpha-chitin (poly-N-acetyl-D-glucosamine). *J Biophys Biochem Cytol*. 1957; 3(5):669-683. doi:10.1083/jcb.3.5.669
111. Gan L, Chen S, Jensen GJ. Molecular organization of Gram-negative peptidoglycan. *Proc Natl Acad Sci U S A*. 2008; 105(48):18953-18957. doi:10.1073/pnas.0808035105
112. Pasquina-Lemonche L, Burns J, Turner RD, *et al*. The architecture of the Gram-positive bacterial cell wall. *Nature*. 2020; 582: 294–297. doi:10.1038/s41586-020-2236-6
113. Boneca IG, Huang ZH, Gage DA, Tomasz A. Characterization of *Staphylococcus aureus* cell wall glycan strands, evidence for a new β-N-acetylglucosaminidase activity. *J Biol Chem*. 2000; 275(14):9910-9918. doi:10.1074/jbc.275.14.9910
114. Snowden MA, Perkins HR. Peptidoglycan cross-linking in *Staphylococcus aureus.* An apparent random polymerisation process. *Eur J Biochem*. 1990; 191(2):373-377. doi:10.1111/j.1432-1033.1990.tb19132.x
115. Wietzerbin J, Wietzerbin J, Lederer E, Das BC, Lederer E, Leyh-Bouille M. Occurrence of d-alanyl-(d)-meso-diaminopimelic acid and meso-diaminopimelyl-meso-diaminopimelic acid interpeptide linkages in the peptidoglycan of *Mycobacteria*. *Biochemistry*. 1974; 13(17):3471-3476. doi:10.1021/bi00714a008
116. Koch AL, Woeste S. Elasticity of the sacculus of *Escherichia coli*. *J Bacteriol*. 1992; 174(14): 4811–4819. doi:10.1128/jb.174.14.4811-4819.1992
117. Koch AL, Lane SL, Miller JA, Nickens DG. Contraction of filaments of *Escherichia coli* after disruption of cell membrane

by detergent. *J Bacteriol*. 1987; 169(5):1979–1984. doi:10.1128/jb.169.5.1979-1984.1987
118. Yao X, Jericho M, Pink D, Beveridge T. Thickness and elasticity of gram-negative murein sacculi measured by atomic force microscopy. *J Bacteriol*. 1999; 181(22):6865-6875. doi:10.1128/jb.181.22.6865-6875.1999
119. Demchick P, Koch AL. The permeability of the wall fabric of *Escherichia coli* and *Bacillus subtilis*. *J Bacteriol*. 1996; 178(3):768-773. doi:10.1128/jb.178.3.768-773.1996
120. van Heijenoort J. Assembly of the monomer unit of bacterial peptidoglycan. *Cell Mol Life Sci C*. 1998;54(4):300-304. doi:10.1007/s000180050155
121. Ruiz N. Bioinformatics identification of MurJ (MviN) as the peptidoglycan lipid II flippase in *Escherichia coli*. *Proc Natl Acad Sci U S A*. 2008; 105(40):15553-15557. doi:10.1073/pnas.0808352105
122. Kouidmi I, Levesque RC, Paradis-Bleau C. The biology of Mur ligases as an antibacterial target. *Mol Microbiol*. 2014; 94(2):242-253. doi:10.1111/mmi.12758
123. Chen KT, Chen PT, Lin CK, *et al*. Structural investigation of Park's nucleotide on bacterial translocase MraY: Discovery of unexpected MraY inhibitors. *Sci Rep*. 2016;6(1):31579. doi:10.1038/srep31579
124. van Heijenoort J. Lipid Intermediates in the biosynthesis of bacterial peptidoglycan. *Microbiol Mol Biol Rev*. 2007; 71(4):620-635. doi:10.1128/mmbr.00016-07
125. Schneider T, Senn MM, Berger-Bächi B, Tossi A, Sahl HG, Wiedemann I. In vitro assembly of a complete, pentaglycine interpeptide bridge containing cell wall precursor (lipid II-Gly5) of *Staphylococcus aureus*. *Mol Microbiol*. 2004; 53(2):675-685. doi:10.1111/j.1365-2958.2004.04149.x
126. Rohrer S, Ehlert K, Tschierske M, Labischinski H, Berger-Bachi B. The essential *Staphylococcus aureus* gene *fmhB* is involved in the first step of peptidoglycan pentaglycine interpeptide formation. *Proc Natl Acad Sci U S A*. 1999; 96(16):9351-9356. doi:10.1073/pnas.96.16.9351
127. Strandén AM, Ehlert K, Labischinski H, Berger-Bachi B. Cell wall monoglycine cross-bridges and methicillin hypersusceptibility in a *femAB* null mutant of methicillin-resistant *Staphylococcus aureus*. *J Bacteriol*. 1997; 179(1):9-16. doi:10.1128/jb.179.1.9-16.1997
128. Henze U, Sidow T, Wecke J, Labischinski H, Berger-Bachi B. Influence of *femB* on methicillin resistance and peptidoglycan metabolism in *Staphylococcus aureus*. *J Bacteriol*. 1993;

175(6): 1612–1620. doi:10.1128/jb.175.6.1612-1620.1993
129. Egan AJF, Errington J, Vollmer W. Regulation of peptidoglycan synthesis and remodelling. *Nat Rev Microbiol*. 2020;18(8): 446-460. doi:10.1038/s41579-020-0366-3
130. Mohammadi T, Van Dam V, Sijbrandi R, *et al*. Identification of FtsW as a transporter of lipid-linked cell wall precursors across the membrane. *EMBO J*. 2011; 30(8):1425-1432. doi:10.1038/emboj.2011.61
131. Sham LT, Butler EK, Lebar MD, Kahne D, Bernhardt TG, Ruiz N. MurJ is the flippase of lipid-linked precursors for peptidoglycan biogenesis. *Science*. 2014; 345(6193):220-222. doi:10.1126/science.1254522
132. Taguchi A, Welsh MA, Marmont LS, et al. FtsW is a peptidoglycan polymerase that is functional only in complex with its cognate penicillin-binding protein. *Nat Microbiol*. 2019;4(4):587-594. doi:10.1038/s41564-018-0345-x
133. Anderson JS, Meadow PM, Haskin MA, Strominger JL. Biosynthesis of the peptidoglycan of bacterial cell walls. Utilization of uridine diphosphate acetylmuramyl pentapeptide and uridine diphosphate acetylglucosamine for peptidoglycan synthesis by particulate enzymes from *Staphylococcus aureus* and *Micrococcus lysodeikticus*. *Arch Biochem Biophys*. 1966; 116(1):487-515. doi:10.1016/0003-9861(66)90056-7
134. Bouhss A, Trunkfield AE, Bugg TDH, Mengin-Lecreulx D. The biosynthesis of peptidoglycan lipid-linked intermediates. *FEMS Microbiol Rev*. 2008;32(2): 208–233. doi:10.1111/j.1574-6976.2007.00089.x
135. Di Guilmi AM, Mouz N, Andrieu JP, et al. Identification, purification, and characterization of transpeptidase and glycosyltransferase domains of *Streptococcus pneumoniae* penicillin-binding protein 1a. *J Bacteriol*. 1998; 180(21):5652-5659. doi:10.1128/jb.180.21.5652-5659.1998
136. Lupoli TJ, Tsukamoto H, Doud EH, Wang TSA, Walker S, Kahne D. Transpeptidase-mediated incorporation of d-amino acids into bacterial peptidoglycan. *J Am Chem Soc*. 2011; 133(28):10748-10751. doi:10.1021/ja2040656
137. Wang QM, Peery RB, Johnson RB, Alborn WE, Yeh WK, Skatrud PL. Identification and characterization of a monofunctional glycosyltransferase from *Staphylococcus aureus*. *J Bacteriol*. 2001; 183(16):4779-4785. doi:10.1128/JB.183.16.4779-4785.2001
138. Reed P, Veiga H, Jorge AM, Terrak M, Pinho MG. Monofunctional transglycosylases are not essential for *Staphylococcus aureus* cell wall synthesis. *J Bacteriol*.

2011;193(10):2549-2556. doi:10.1128/JB.01474-10
139. Łęski TA, Tomasz A. Role of penicillin-binding protein 2 (PBP2) in the antibiotic susceptibility and cell wall cross-linking of *Staphylococcus aureus*: Evidence for the cooperative functioning of PBP2, PBP4, and PBP2A. *J Bacteriol*. 2005; 187(5):1815–1824. doi:10.1128/JB.187.5.1815-1824.2005
140. Reichmann NT, Tavares AC, Saraiva BM, *et al*. SEDS–bPBP pairs direct lateral and septal peptidoglycan synthesis in *Staphylococcus aureus*. *Nat Microbiol*. 2019;4(8):1368-1377. doi:10.1038/s41564-019-0437-2
141. Sauvage E, Kerff F, Terrak M, Ayala JA, Charlier P. The penicillin-binding proteins: Structure and role in peptidoglycan biosynthesis. *FEMS Microbiol Rev*. 2008; 32(2):234-258. doi:10.1111/j.1574-6976.2008.00105.x
142. Den Blaauwen T, De Pedro MA, Nguyen-Distèche M, Ayala JA. Morphogenesis of rod-shaped sacculi. *FEMS Microbiol Rev*. 2008; 32(2):321-344. doi:10.1111/j.1574-6976.2007.00090.x
143. Navratna V, Nadig S, Sood V, Prasad K, Arakere G, Gopal B. Molecular basis for the role of *Staphylococcus aureus* penicillin binding protein 4 in antimicrobial resistance. *J Bacteriol*. 2010; 192(1):134-144. doi:10.1128/JB.00822-09
144. Zapun A, Contreras-Martel C, Vernet T. Penicillin-binding proteins and β-lactam resistance. *FEMS Microbiol Rev*. 2008; 32(2):361-385. doi:10.1111/j.1574-6976.2007.00095.x
145. Tipper DJ, Strominger JL. Mechanism of action of penicillins: a proposal based on their structural similarity to acyl-D-alanyl-D-alanine. *Proc Natl Acad Sci U S A*. 1965; 54(4):1133–1141. doi:10.1073/pnas.54.4.1133
146. Cho H, Uehara T, Bernhardt TG. Beta-lactam antibiotics induce a lethal malfunctioning of the bacterial cell wall synthesis machinery. *Cell*. 2014; 159(6):1300-1311. doi:10.1016/j.cell.2014.11.017
147. Öztürk H, Ozkirimli E, Özgür A. Classification of beta-lactamases and Penicillin Binding Proteins using ligand-centric network models. *PLoS One*. 2015;10(2):e0117874. doi:10.1371/journal.pone.0117874
148. Fishovitz J, Hermoso JA, Chang M, Mobashery S. Penicillin-binding protein 2a of methicillin-resistant *Staphylococcus aureus*. *IUBMB Life*. 2014; 66(8): 572–577. doi:10.1002/iub.1289
149. Lim D, Strynadka NCJ. Structural basis for the β-lactam resistance of PBP2a from methicillin-resistant *Staphylococcus aureus*. *Nat Struct Biol*. 2002;9(11):870–876.

doi:10.1038/nsb858
150. Pinho MG, De Lencastre H, Tomasz A. An acquired and a native penicillin-binding protein cooperate in building the cell wall of drug-resistant *staphylococci*. *Proc Natl Acad Sci U S A*. 2001;98(19):10886-10891. doi:10.1073/pnas.191260798
151. Boucher H, Miller LG, Razonable RR. Serious infections caused by methicillin-resistant *Staphylococcus aureus*. *Clin Infect Dis*. 2010;15(51):S183-197. doi:10.1086/653519
152. Gorak EJ, Yamada SM, Brown JD. Community-acquired methicillin-resistant *Staphylococcus aureus* in hospitalized adults and children without known risk factors. *Clin Infect Dis*. 1999;29(4):797-800. doi:10.1086/520437
153. Kluytmans-VandenBergh MFQ, Kluytmans JAJW. Community-acquired methicillin-resistant *Staphylococcus aureus*: Current perspectives. *Clin Microbiol Infect*. 2006;12(Suppl1):9-15. doi:10.1111/j.1469-0691.2006.01341.x
154. Bukharie H. A review of community-acquired methicillin-resistant *Staphylococcus aureus* for primary care physicians. *J Fam Community Med*. 2010;17(3):117. doi:10.4103/1319-1683.74320
155. Lena P, Ishak A, Karageorgos SA, Tsioutis C. Presence of Methicillin-Resistant *Staphylococcus aureus* (MRSA) on healthcare workers' attire: A systematic review. *Trop Med Infect Dis*. 2021;6(2):42. doi:10.3390/tropicalmed6020042
156. De Oliveira DMP, Forde BM, Kidd TJ, *et al*. Antimicrobial resistance in ESKAPE pathogens. *Clin Microbiol Rev*. 2020;33(3):e00181-19. doi:10.1128/CMR.00181-19
157. Zschiedrich CP, Keidel V, Szurmant H. Molecular mechanisms of two-component signal transduction. *J Mol Biol*. 2016; 428(19):3752-3775. doi:10.1016/j.jmb.2016.08.003
158. Jacob-Dubuisson F, Mechaly A, Betton JM, Antoine R. Structural insights into the signalling mechanisms of two-component systems. *Nat Rev Microbiol*. 2018;16(10): 585–593. doi:10.1038/s41579-018-0055-7
159. Mascher T, Helmann JD, Unden G. Stimulus perception in bacterial signal-transducing histidine kinases. *Microbiol Mol Biol Rev*. 2006; 70(4): 910–938. doi:10.1128/mmbr.00020-06
160. Parkinson JS. Signal transduction schemes of bacteria. *Cell*. 1993; 73(5):857-871. doi:10.1016/0092-8674(93)90267-T
161. Wang S. Bacterial two-component systems: Structures and signaling mechanisms. In: *Protein Phosphorylation in Human Health*. 2012. doi:10.5772/48277
162. Aravind L, Ponting CP. The cytoplasmic helical linker domain of receptor histidine kinase and methyl-accepting proteins is

common to many prokaryotic signalling proteins. *FEMS Microbiol Lett*. 1999; 176(1):111-116. doi:10.1016/S0378-1097(99)00197-4

163. Hulko M, Berndt F, Gruber M, *et al*. The HAMP domain structure implies helix rotation in transmembrane signaling. *Cell*. 2006;126(5):929-940. doi:10.1016/j.cell.2006.06.058
164. Airola M V., Watts KJ, Bilwes AM, Crane BR. Structure of concatenated HAMP domains provides a mechanism for signal transduction. *Structure*. 2010;18(4): 436–448. doi:10.1016/j.str.2010.01.013
165. Ninfa EG, Atkinson MR, Kamberov ES, Ninfa AJ. Mechanism of autophosphorylation of *Escherichia coli* nitrogen regulator II (NR(II) or NtrB): trans-phosphorylation between subunits. *J Bacteriol*. 1993;175(21): 7024–7032. doi:10.1128/jb.175.21.7024-7032.1993
166. Casino P, Rubio V, Marina A. Structural insight into partner specificity and phosphoryl transfer in two-component signal transduction. *Cell*. 2009;139(2):325-336. doi:10.1016/j.cell.2009.08.032
167. Mascher T. Intramembrane-sensing histidine kinases: A new family of cell envelope stress sensors in Firmicutes bacteria. *FEMS Microbiol Lett*. 2006; 264(2):133-144. doi:10.1111/j.1574-6968.2006.00444.x
168. Gao R, Mack TR, Stock AM. Bacterial response regulators: versatile regulatory strategies from common domains. *Trends Biochem Sci*. 2007; 32(5):225-234. doi:10.1016/j.tibs.2007.03.002
169. O'Hara BP, Norman RA, Wan PTC, *et al*. Crystal structure and induction mechanism of AmiC-AmiR: A ligand-regulated transcription antitermination complex. *EMBO J*. 1999;18(19): 5175–5186. doi:10.1093/emboj/18.19.5175
170. Silversmith RE. Auxiliary phosphatases in two-component signal transduction. *Curr Opin Microbiol*. 2010; 13(2):177-183. doi:10.1016/j.mib.2010.01.004
171. Skerker JM, Prasol MS, Perchuk BS, Biondi EG, Laub MT. Two-component signal transduction pathways regulating growth and cell cycle progression in a bacterium: A system-level analysis. *PLoS Biol*. 2005;3(10):e334. doi:10.1371/journal.pbio.0030334
172. Laub MT, Goulian M. Specificity in two-component signal transduction pathways. *Annu Rev Genet*. 2007;41:121-145. doi:10.1146/annurev.genet.41.042007.170548
173. Siryaporn A, Goulian M. Characterizing cross-talk *in vivo* avoiding pitfalls and overinterpretation. *Methods Enzymol*.

2010; 471:1-16. doi:10.1016/S0076-6879(10)71001-6
174. Wanner BL. Is cross regulation by phosphorylation of two-component response regulator proteins important in bacteria? *J Bacteriol*. 1992; 174(7): 2053–2058. doi:10.1128/jb.174.7.2053-2058.1992
175. Wolfe AJ. The acetate switch. *Microbiol Mol Biol Rev*. 2005; 69(1):12-50. doi:10.1128/mmbr.69.1.12-50.2005
176. Alves R, Savageau MA. Comparative analysis of prototype two-component systems with either bifunctional or monofunctional sensors: Differences in molecular structure and physiological function. *Mol Microbiol*. 2003; 48(1):25-51. doi:10.1046/j.1365-2958.2003.03344.x
177. Verhamme DT, Arents JC, Postma PW, Crielaard W, Hellingwerf KJ. Investigation of *in vivo* cross-talk between key two-component systems of *Escherichia coli*. *Microbiology*. 2002; 148(1):69-78. doi:10.1099/00221287-148-1-69
178. Villanueva M, García B, Valle J, et al. Sensory deprivation in *Staphylococcus aureus*. *Nat Commun*. 2018;9(1):523. doi:10.1038/s41467-018-02949-y
179. Ji Q, Chen PJ, Qin G, *et al*. Structure and mechanism of the essential two-component signal-transduction system WalKR in *Staphylococcus aureus*. *Nat Commun*. 2016;7(1):11000. doi:10.1038/ncomms11000
180. Yin S, Daum RS, Boyle-Vavra S. VraSR two-component regulatory system and its role in induction of *pbp2* and *vraSR* expression by cell wall antimicrobials in *Staphylococcus aureus*. *Antimicrob Agents Chemother*. 2006;50(1):336–343. doi:10.1128/AAC.50.1.336-343.2006
181. Falord M, Mäder U, Hiron A, Dbarbouillé M, Msadek T. Investigation of the *Staphylococcus aureus* GraSR regulon reveals novel links to virulence, stress response and cell wall signal transduction pathways. *PLoS One*. 2011;6(7):e21323. doi:10.1371/journal.pone.0021323
182. Hiron A, Falord M, Valle J, Débarbouillé M, Msadek T. Bacitracin and nisin resistance in *Staphylococcus aureus*: A novel pathway involving the BraS/BraR two-component system (SA2417/SA2418) and both the BraD/BraE and VraD/VraE ABC transporters. *Mol Microbiol*. 2011; 81(3):602-622. doi:10.1111/j.1365-2958.2011.07735.x
183. Utaida S, Dunman PM, Macapagal D, *et al*. Genome-wide transcriptional profiling of the response of *Staphylococcus aureus* to cell-wall-active antibiotics reveals a cell-wall-stress stimulon. *Microbiology*. 2003;149(10):2719-2732. doi:10.1099/mic.0.26426-0

184. Kuroda M, Kuroda H, Oshima T, Takeuchi F, Mori H, Hiramatsu K. Two-component system VraSR positively modulates the regulation of cell-wall biosynthesis pathway in *Staphylococcus aureus*. *Mol Microbiol*. 2003;49(3):807-821. doi:10.1046/j.1365-2958.2003.03599.x
185. Dengler V, Meier PS, Heusser R, Berger-Bächi B, McCallum N. Induction kinetics of the *Staphylococcus aureus* cell wall stress stimulon in response to different cell wall active antibiotics. *BMC Microbiol*. 2011;11:16. doi:10.1186/1471-2180-11-16
186. Blake KL, O'Neill AJ, Mengin-Lecreulx D, *et al*. The nature of *Staphylococcus aureus* MurA and MurZ and approaches for detection of peptidoglycan biosynthesis inhibitors. *Mol Microbiol*. 2009; 72(2):335-343. doi:10.1111/j.1365-2958.2009.06648.x
187. Kuroda M, Kuwahara-Arai K, Hiramatsu K. Identification of the up- and down-regulated genes in vancomycin-resistant *Staphylococcus aureus* strains Mu3 and Mu50 by cDNA differential hybridization method. *Biochem Biophys Res Commun*. 2000; 269(2):485-490. doi:10.1006/bbrc.2000.2277
188. Belcheva A, Golemi-Kotra D. A close-up view of the VraSR two-component system: A mediator of *Staphylococcus aureus* response to cell wall damage. *J Biol Chem*. 2008;283(18):12354-12364. doi:10.1074/jbc.M710010200
189. Boyle-Vavra S, Yin S, Jo DS, Montgomery CP, Daum RS. VraT/YvqF is required for methicillin resistance and activation of the VraSR regulon in *Staphylococcus aureus*. *Antimicrob Agents Chemother*. 2013;57(1):83-95. doi:10.1128/AAC.01651-12
190. Domingue G, Costerton JW, Brown MRW. Bacterial doubling time modulates the effects of opsonisation and available iron upon interactions between *Staphylococcus aureus* and human neutrophils. *FEMS Immunol Med Microbiol*. 1996;16(3): 223-228. doi:10.1016/S0928-8244(96)00086-7
191. Belcheva A, Verma V, Golemi-Kotra D. DNA-binding activity of the vancomycin resistance associated regulator protein VraR and the role of phosphorylation in transcriptional regulation of the *vraSR* operon. *Biochemistry*. 2009; 48(24):5592-5601. doi:10.1021/bi900478b
192. Belcheva A, Verma V, Korenevsky A, Fridman M, Kumar K, Golemi-Kotra D. Roles of DNA sequence and sigma A factor in transcription of the *vraSR* operon. *J Bacteriol*. 2012;194(1):61-71. doi:10.1128/JB.06143-11
193. Sengupta M, Jain V, Wilkinson BJ, Jayaswal RK. Chromatin immunoprecipitation identifies genes under direct VraSR

regulation in *Staphylococcus aureus*. *Can J Microbiol*. 2012;58(6):703-708. doi:10.1139/W2012-043

194. McCallum N, Stutzmann Meier P, Heusser R, Berger-Bächi B. Mutational analyses of open reading frames within the *vraSR* operon and their roles in the cell wall stress response of *Staphylococcus aureus*. *Antimicrob Agents Chemother*. 2011;55(4):1391–1402. doi:10.1128/AAC.01213-10
195. Jordan S, Junker A, Helmann JD, Mascher T. Regulation of LiaRS-dependent gene expression in *Bacillus subtilis*: Identification of inhibitor proteins, regulator binding sites, and target genes of a conserved cell envelope stress-sensing two-component system. *J Bacteriol*. 2006;188(14):5153-5166. doi:10.1128/JB.00310-06
196. Falord M, Karimova G, Hiron A, Msadeka T. GraXSR proteins interact with the VraFG ABC transporter to form a five-component system required for cationic antimicrobial peptide sensing and resistance in *Staphylococcus aureus*. *Antimicrob Agents Chemother*. 2012; 56(2):1047-1058. doi:10.1128/AAC.05054-11
197. Hu Q, Peng H, Rao X. Molecular events for promotion of vancomycin resistance in vancomycin intermediate *Staphylococcus aureus*. *Front Microbiol*. 2016;7:1601. doi:10.3389/fmicb.2016.01601

Chapter II

Cell shape dynamics during the staphylococcal cell cycle

Chapter contents

Abstract 74
Introduction 75
Experimental Procedures 77
Bacterial growth conditions 77
Construction of *S. aureus* mutants 80
Scanning electron microscopy 85
Super-resolution Structured Illumination Microscopy (SIM) 86
Fast time-lapse imaging of *S. aureus* 86
Labelling and imaging of *S. aureus* 87
Labelling and imaging of *Sporosarcina ureae* 88
Photoactivated Localisation Microscopy (PALM) 89
Hyperosmotic shock 90
Calculation of cell dimensions 90
Calculation of fluorescence ratio in NADA labelled cells 91
Statistical analysis 91
Results 92
S. aureus cells elongate during the cell cycle 92
The septum gives less than one hemisphere of each daughter cell 97
S. aureus grows by remodelling the entire cell surface 102
S. aureus enlarges via peptidoglycan synthesis and autolysis 104
Discussion 114
References 121

Author contributions

J. M. Monteiro and P.B. Fernandes performed all experiments shown, except SEM imaging of *S. aureus,* which was done by A. C. Tavares and PALM imaging of PBP4-PAmcherry, which was done by A. R. Pereira. Strains COLΔ*atl*, COLΔ*sle1* and NCTCΔ*lytM* were constructed by F. Vaz; strains COLΔ*sle1*pBCBover and COLΔ*sle1*pSle1 were constructed by H. Veiga; strains BCBPM120 and BCBPM138 were constructed by P. M. Pereira.

Acknowledgments

We thank Suckjoon Jun (UCSD), Adriano Henriques (ITQB) and Nathalie Reichmann (ITQB) for critically reading the manuscript. We thank T. Meylheuc from the Microscopy and Imaging Platform MIMA2 (INRA, France) for SEM observations, Rut Carballido-López and Arnaud Chastanet (Micalis Institute, INRA Jouy-en-Josas) for support for SEM observations and assistance with the preparation of the SEM samples, Luis Morgado (ITQB) for schematics in Fig. 5.

This chapter contains data published in:

Monteiro JM*, **Fernandes PB***, Vaz F, Pereira AR, Tavares AC, Ferreira MT, Pereira PM, Veiga H., Kuru E, VanNieuwenhze MS, Brun YV, Filipe SR and Pinho MG. Cell shape dynamics during the staphylococcal cell cycle. *Nature Communications* **6**, 8055, doi:10.1038/ncomms9055 (2015)

*J.M.M. and P.B.F. contributed equally to this work

Abstract

Staphylococcus aureus is an aggressive pathogen and a model organism to study cell division in sequential orthogonal planes in spherical bacteria. However, the small size of staphylococcal cells has impaired analysis of changes in morphology during the cell cycle. Here we use super-resolution microscopy and determine that *S. aureus* cells are not spherical throughout the cell cycle, but elongate during specific time windows, through peptidoglycan synthesis and remodelling. Both peptidoglycan hydrolysis and turgor pressure are required during division for reshaping the flat division septum into a curved surface. In this process, the septum generates less than one hemisphere of each daughter cell, a trait we show is common to other cocci. Therefore, cell surface scars of previous divisions do not divide the cells in quadrants, generating asymmetry in the daughter cells. Our results introduce a need to reassess the models for division plane selection in cocci.

Introduction

Staphylococci are spherical organisms that divide sequentially in three orthogonal planes over three consecutive division cycles[1,2]. This mode of division is less common in bacterial cells than equatorial division, observed in many genera. Division in three planes implies that cells retain information about the positioning of the two preceding divisions in order to divide with precision. Given that this spatial information varies with each division, it cannot be encoded by DNA[3]. Peptidoglycan, the major component of the bacterial cell wall, has been proposed to encode epigenetic information in the form of protuberant, ring-like structures that mark previous division planes and are used by *Staphylococcus aureus* to divide accurately in sequential perpendicular planes[3].

Orientation of division planes is merely one of the distinctive features of the staphylococcal cell cycle. *S. aureus* has been proposed to have only one cell wall synthesis machine, which incorporates peptidoglycan mostly at the division septum[4,5] , while rod-shaped bacteria such as *Escherichia coli* or *Bacillus subtilis* have two major cell wall synthesis machines, one for incorporation of new peptidoglycan at the division septum and another for elongation of the lateral wall[4]. Accordingly, *S. aureus* has only four native Penicillin-Binding Proteins (PBPs 1-4), described to localize at the septum, while *E. coli* and *B. subtilis* have 12 and 16 PBPs, respectively, which localize at the septum or at the lateral wall[4]. PBPs are enzymes involved in the last steps of peptidoglycan biosynthesis, which catalyse the polymerization of the glycan strands, as well as their crosslinking via peptide stems. Given that an elongation-specific machinery seems to be absent in *S. aureus,* increase of the cell

surface area required for growth has been attributed to a process of reshaping the flat septum into curved hemispheres of the two daughter cells, which occurs immediately after splitting of the mother cell during division[2]. Reshaping of the flat septum, resulting in doubling of the external surface area of peptidoglycan, could theoretically occur in the absence of synthesis, if accompanied by changes in the angle of the glycan chains with respect to the peptide chains[6]. Alternatively, increase of the surface area could be driven by hydrolysis of peptidoglycan bonds catalysed by specific autolysins. At least 13 genes of the *S. aureus* genome encode known or putative peptidoglycan hydrolases, although the products of only three of these genes (*atl*, *sle1* and *lytM*) have been characterized. Of these genes, *atl* encodes the major autolysin in *S. aureus,* which is involved in the separation of the daughter cells after division[7,8]. Interestingly, orthogonal rings of Atl can be observed by immunoelectron microscopy at the surface of *S. aureus* cells, similar to scars of previous divisions[9], confirming that information regarding the localisation of previous, orthogonal, division planes can be present at the cell surface.

S. aureus is an aggressive pathogen and one of the most important nosocomial bacteria causing antibiotic-resistant infections. Despite its clinical relevance, the small size of staphylococcal cells (with a ~1 µm diameter, only four times larger than the diffraction limit of resolution of conventional light microscopy) has impaired a detailed analysis of its cell cycle and of the morphological changes that occur as *S. aureus* grows and divides. This lack of knowledge extends to the cell cycle of other cocci as well. Therefore, detailed characterization of the mode of growth and division of *S. aureus* has implications for the global understanding of the cell cycle of cocci. Here, we have used

super-resolution microscopy to analyse the dynamics of cell shape and size during the cell cycle of *S. aureus*. We found that, contrary to current thinking, *S. aureus* cells elongate before dividing. Furthermore, we show that the division septum generates less than one hemisphere of each daughter cell and therefore scars of previous divisions do not mark quadrants of the cell. Our results suggest that the models for division plane selection in cocci should be re-examined.

Experimental Procedures

Bacterial growth conditions

Strains and plasmids used in this study are listed in Table 1. *S. aureus* strains were grown in tryptic soy broth (TSB, Difco) with aeration at 37 °C or on tryptic soy agar (TSA, Difco) at 30 °C or 37 °C. For microscopy experiments, overnight cultures of *S. aureus* strains were diluted 1:200 in fresh TSB medium and allowed to grow at 37 °C until an OD_{600nm} of approximately 0.5. Cells were then harvested and resuspended in the same medium. *Escherichia coli* and *Sporosarcina ureae* strains were grown in Luria-Bertani broth (LB, Difco) with aeration, or LB agar (LA, Difco) at 37 °C or 30 °C, respectively. Antibiotics ampicillin (Amp) and erythromycin (Ery) were added to the media at a final concentration of 100 μg ml^{-1} and 10 μg ml^{-1}, respectively, when necessary. 5-Bromo-4-chloro-3-indolyl β-D-galactopyranoside (X-gal) was used at 100 μg ml^{-1}. Expression of PBP4 from plasmid pBCBPM115 was induced with cadmium chloride (1 μM). Expression of Sle1 from plasmid pSle1 was induced with IPTG (1 mM) in the presence of 10 μg ml^{-1} of chloramphenicol.

Table 1. Bacterial strains and plasmids used in this study

Strains	Description	Source or reference
Escherichia coli		
DC10B	Δ*dcm* in the DH10B background; Dam methylation only	[10]
Staphylococcus aureus		
COL	HA-MRSA	[11]
NCTC8325-4	MSSA strain	R. Novick
RN4220	Restriction-deficient derivative of NCTC8325-4	R. Novick
COLΔ*pbpD*	*pbp4* in-frame deletion mutant of parental strain COL	[12]
COLpPBP4-YFP	COL encoding a C-terminal YFP fusion to PBP4 at the native locus	[13]
COLΔ*atl*	Δ*atl* in-frame deletion mutant of parental strain COL	This study
COLΔ*sle1*	Δ*sle1* in-frame deletion mutant of parental strain COL	This study
COLΔ*sle1*pBCBover	COLΔ*sle1* with pBCBover	This study
COLΔ*sle1*pSle1	COLΔ*sle1* complemented with pSle1	This study
COL*walKR*i	COL strain with WalKR operon under the control of the IPTG inducible P_{spac} promoter; Ery^r	This study
NCTCΔ*lytM*	Δ*lytM* in-frame deletion mutant of parental strain NCTC8325-4	This study
NCTCΔ*sle1*	Δ*sle1* in-frame deletion mutant of parental strain NCTC8325-4	This study
NCTCΔ*pbpD::pbpDPAmCherry*	NCTC strain with the *pbpD* gene substituted by the *pbpD-PAmCherry* photoactivable derivative	This study
BCBPM120	COLΔ*pbpD* with pCNX	This study

BCBPM138	COLΔ*pbpD* with pBCBPM115, encoding PBP4 under the control of P_{Cad}	This study
Sporosarcina ureae SL6708	Derivative of *S. ureae* ATCC 1388	[14]

Table 1. Bacterial strains and plasmids used in this study (cont.)

Plasmids	Description	Source or reference
pMAD	*E. coli-S. aureus* shuttle vector with a thermosensitive origin of replication for Gram-positive bacteria; Amp^rEry^r *lacZ*	[15]
pMUTIN4	Integrative vector for *S. aureus* encoding IPTG inducible P_{spac} promoter; Amp^r, Ery^r	[16]
pCN34	Vector containing the aphA-3 kanamycin resistance cassette	[17]
pCN51	Shuttle vector containing a cadmium inducible P_{cad} promoter; Amp^R Ery^R	[17]
pCNX	Shuttle vector containing a cadmium inducible P_{cad} promoter; Amp^R Kan^R	This study
pGC2	*E. coli/S. aureus* shuttle vector, Amp^r Cm^r	[18]
pDH88	*B. subtilis* with P_{spac} promoter and *lacI*	[19]
pBAD/HisBPAmCherry1	Plasmid encoding the sequence of the photoactivable PAmCherry1 protein	[20]
pΔ*atl*	pMAD derivative with the up- and downstream regions of *atl*	[21]
pΔ*lytM*	pMAD derivative with the up- and downstream regions of *lytM*	This study

p∆*sle1*	pMAD derivative with the up- and downstream regions of *sle1*	This study
pBCBover	pGC2 derivative containg P_{spac} promoter and *lacI*	This study
pSle1	pBCBover encoding Sle1 under the control of P_{spac} promoter	This study
p*walKR*	pMUTIN4 derivative containing the ribosome binding site and 5' end of *walKR*	This study
pBCBRP007	pCNX derivative containing P_{cad}-RBS-*pbpD*-7aaLinker-*PAmCherry*; Amp^R Kan^R	This study
pBCBRP008	pMAD derivative containing truncated *pbpD*-7aa-*PAmCherry*-Downstream region; Amp^R Ery^R	This study
pBCBPM115	pCNX encoding PBP4 under the control of P_{cad}	This study

Construction of *S. aureus* mutants

The full sequences of each primer used to construct mutants are in Table 2.

Table 2. Oligonucleotides used in this study

Primer name	Sequence (5'-3')
P1_Sle1	CATGCCATGGGCAGTAGATGCACAACAAACTG
P2_Sle1	CATTATATATTTATATACGTAAGACTTTATTTAAAAT CCTCCTC TTGCTTAAC
P3_Sle1	GTTAAGCAAGAGGAGGATTTTAAATAAAGTCTTAC GTATATA AATATATAATG
P4_Sle1	TGGAGATCTCAGCGCGTGTACTTGTGATTC
P1_lytM	CATGCCATGGGCAATGAAGCAGGTACATTTG
P2_lytM	GCAACTTGGGATTTTCTGTATTAGTATAAAACATCC TCCATTA AAG
P3_lytM	CTTTAATGGAGGATGTTTTATACTAATACAGAAAAT CCCAAGT

	TGC
P4_lytM	TGGAGATCT GGAGCGTAACTGATGATAG
yycF fw EcoRI	GCGCGCGAATTCTATTAATGATTTAAGAAAAGAGG
yycF stop rv BamHI	CGCGCGCGGATCCCTAGCCACGTTTTTTAATAGAA TATGCG
P1pbp4pCNX	GGATCCAGGAGGTACCTTATGAAAAATTTAATATC
P2pbp4pCNX	CACCATGCTAGCGGCGCGCCGGGTACCTTTTCTTT TTCTAAAT AAACGATTGATTA
P3pbp4pCNX	AGGTACCCGGCGCGCCGCTAGCATGGTGAGCAAG GGCGAGG A
P4pbp4pCNX	GCCTAAGAATTCTTACTTGTACAGCTCGTCCATGC
P1pMADpbp4PAmCherry	GATATCGGATCCACAGTCACAATGACGAACAAAG
P2pMADpbp4PAmCherry	GTCCGTTTTTAGTATGTTTTACTTGTACAGCTCGTC CATGCCG
P3pMADpbp4PAmCherry	TGGACGAGCTGTACAAGTAAAACATACTAAAAACG GACAAG TTGC
P4pMADpbp4PAmCherry	ATGGTACCCGGGACAAGTAACGATGAAGATTTTAA TAG
Pspac_pDH88_P9_XhoI_ SalI	GCTGCGCTGTCGACGTTCACCTCGAGTTCTACACA GCCCAGTC CAGAC
Pspac_pDH88_SpeI_P10	GTTAACAAAGACTAGTATGCTCTAGAAACCCGGGA AAAGC
Pspac_pDH88_SpeI_P11	CTAGAGCATACTAGTCTTTGTTAACTTAGATCTTTA TCG
Pspac_pDH88_P12_XhoI_ EcoRI	GCTGAATTCGATGCCCTCGAGCTGATCCTAACTCA CATTAATT GCG
Sle1_FW_XmaI	TACTCCCCGGGGCAAGAGGAGGATTTTAAAGTGC
Sle1_RV_XbaI	GCTGCTCTAGATTAGTGAATATATCTATAATTATTTA C
PBP4pCadP1BamFW	CGCAGGATCCAGGAGGTACCTTATGAAAAATTTAA TATCTATT ATC
pCADPBP4wt_EcoREV	GCGTGAATTCTTAGGTACCTTATTTTCTTTTTCTAAA TAAAC

Underlined sequences correspond to restriction sites

The COLΔ*atl*, COLΔ*sle1* and NCTCΔ*lytM* null mutants were constructed using the pMAD vector[15] containing the upstream and downstream regions of each gene of interest, to allow recombination and integration of the plasmids into the chromosome, followed by their excision with the genes to be deleted. Briefly, upstream and downstream regions of *sle1* and *lytM* were amplified by PCR, using primers P1_Sle1/P2_Sle1 and P3_Sle1/P4_Sle1, P1_lytM/P2_lytM and P3_lytM/P4_lytM, respectively. The PCR fragments encoding the upstream and downstream regions of each gene were joined by overlap PCR using the pairs of primers P1_Sle1/P4_Sle1 and P1_lytM and P4_lytM. The resulting fragments were digested with *Nco*I and *Bgl*II (Fermentas) and cloned into the pMAD vector, giving plasmids pΔ*sle1* and pΔ*lytM,* which were propagated in *E. coli* DC10B and the inserts were sequenced. The plasmids, as well as pΔ*atl*[21], were then electroporated into *S. aureus* RN4220 strain at 30 °C, using Ery and Xgal selection, and transduced into COL or NCTC8325-4 using phage 80α. The integration of the plasmids into the chromosome and their excision was done as previously described[22]. Gene deletions were confirmed by PCR and sequencing of the amplified fragment.

For complementation of COLΔ*sle1*, plasmid pBCBover was constructed by introducing a DNA fragment containing the P_{spac} promoter, a multiple cloning site and the *lacI* gene into the *S. aureus* replicative vector pGC2[18]. For that, two DNA fragments, one containing the P_{spac} coding sequence and HindIII, SmaI, and XbaI restriction sites and a second one encompassing a BglII restriction site upstream of the *lacI* gene, were amplified from pDH88 plasmid[19] by using respectively the pair of primers Pspac_pDH88_P9_XhoI_SalI / Pspac_pDH88_SpeI_P10 and

Pspac_pDH88_SpeI_P11 / PspacpDH88-P12-XhoI-EcoRI. These two PCR products were then joined in a second PCR, using primers Pspac-pDH88_P9_XhoI_SalI and PspacpDH88-P12-XhoI-EcoRI, to originate a 1743 bp fragment in which a SpeI restriction site was introduced between XbaI and BglII restriction sites. The resulting fragment was restricted with SalI and EcoRI, cloned into the pGC2 vector and sequenced. The pSle1 plasmid was constructed by cloning the entire sle1 coding sequence downstream of P_{spac} promoter in pBCBover. For that, a 1024 bp DNA fragment containing *sle1* gene and its upstream RBS site was amplified from NCTC8325-4 genome using primers Sle1_FW_XmaI and Sle1_RV_XbaI, digested with SmaI and XbaI and cloned into pBCBover. The insert was then sequenced. Both pBCBover and pSle1 plasmids were electroporated into RN4220 (selection with 10 μg ml^{-1} chloramphenicol) and subsequently transduced, using phage 80α, to strain COLΔ*sle1*, generating strains COLΔ*sle1*pBCBover and COLΔ*sle1*pSle1 respectively.

Construction of an *S. aureus* COL mutant with *yycFG* (also known as *walKR*) under the control of the IPTG-inducible P_{spac} promoter was done using the pMUTIN4 plasmid[16]. A 518 bp fragment containing the ribosome binding site and 5' end of *yycF* (*walR*) was amplified using primers yycF_fw_EcoRI and yycF_stop_rv_BamHI. The DNA fragment was then digested with EcoRI and BamHI, cloned into pMUTIN4 giving plasmid p*walKR*, which was propagated in *E. coli* DC10B and the insert was sequenced. Plasmid p*walKR* was then electroporated into *S. aureus* RN4220 at 37°C, using erythromycin selection, and transduced into COL using phage 80α. Integration of the plasmid occurred through a single crossover event, placing the *walKR* operon under the control of the P_{spac} promoter.

To study PBP4 localisation in *S. aureus* NCTC8325-4 by PALM, we replaced the *pbpD* gene, encoding PBP4, for a gene encoding a photoactivatable derivative (*pbpD-PAmCherry*). For that purpose, *pbpD* was cloned fused to *PAmCherry1*[20] in the backbone of pCNX. The pCNX plasmid was constructed by substituting the *erm* erythromycin resistance cassette of the pCN51 plasmid[17] by the *aphA*-3 kanamycin cassette from pCN34[17], using ApaI and XhoI restriction sites. To clone *pbpD-PAmCherry* into pCNX, a fragment encompassing a ribosomal binding site, the *pbpD* gene lacking the stop codon and seven codons encoding an amino acid linker was amplified using NCTC8325-4 genomic DNA as template and primers P1pbp4pCNX and P2pbp4pCNX. A fragment encompassing *PAmCherry1* was amplified from the pBAD/HisB-PAmCherry1 plasmid[20] using P3pbp4pCNX and P4pbp4pCNX primers. The two fragments were joined by overlap PCR, digested with BamHI and EcoRI, ligated into the pCNX plasmid generating plasmid pBCBRP007, and the insert was sequenced. We then replaced the *pbpD* gene from its native locus in the *S. aureus* genome by the *pbpD-PAmCherry* fusion. For this purpose two DNA fragments were amplified, one encompassing a truncated *pbpD* (last 999 bp), a sequence encoding a 7 amino acid linker and *PAmCherry1* amplified from the pBCBRP007 plasmid using primers P1pMADpbp4PAmCherry and P2pMADpbp4PAmCherry and a second DNA fragment of 1,000 bp corresponding to the region downstream of *pbpD* amplified from the NCTC8325-4 genome, using primers P3pMADpbp4PAmCherry and P4pMADpbp4PAmCherry. The two fragments were joined by overlap PCR using primers P1pMADpbp4PAmCherry and P4pMADpbp4PAmCherry, digested with BamHI and XmaI restriction enzymes and cloned into pMAD, generating pBCBRP008. Correct sequence of the insert was

confirmed and the pBCBRP008 plasmid was electroporated into RN4220 and subsequently transduced to NCTC8325-4 strain using phage 80*α*. Integration and excision of pBCBRP008 from the genome was performed as previously described[22]; colonies in which *pbpD* had been replaced by the *pbpD-PAmCherry* were identified by PCR and the strain was named NCTCΔ*pbpD*::*pbpD-PAmCherry*.

To complement COLΔ*pbpD* with a plasmid encoding PBP4, the 1.3 kb pbp4 gene was PCR amplified from NCTC8325-4 genomic DNA using primers PBP4pCadP1BamFW and pCADPBP4wt_EcoREV and cloned into the pCNX replicative plasmid, under the control of a cadmium inducible promoter, using BamHI and EcoRI sites, generating plasmid pBCBPM115. Plasmids pCNX and pBCBPM115 were electroporated into RN4220 and then transduced into COLΔ*pbpD*, giving rise to strains BCBPM120 (COLΔ*pbpD*pCNX) and BCBPM138 (COLΔ*pbpD*pPBP4).

Scanning electron microscopy

Exponentially growing *S. aureus* COL cells[11] were harvested by centrifugation, resuspended in fixative solution (2.5% glutaraldehyde in 0.2 M sodium cacodylate buffer, pH 7.4), deposited on glass discs (Marienfeld) and kept for 1 week at 4 °C. The fixative solution was subsequently removed and the cells were washed three times with sodium cacodylate. The sample was progressively dehydrated by immersion in a graded series of ethanol (50% - 100%) and then mounted on aluminum stubs with carbon adhesive discs (Agarscientific). The sample was critical-point dried under CO_2 and sputter coated with gold-palladium (Polaron SC7640) for 200 s at 10 mA. SEM observations were performed using secondary electron images (2 kV) with a Hitachi S4500 instrument at the Microscopy and

Imaging Platform (Micalis, B2HM, Massy, France) of the INRA research center of Jouy-en-Josas (France).

Super-resolution Structured Illumination Microscopy (SIM)

SIM imaging was performed using a Plan-Apochromat 63x/1.4 oil DIC M27 objective, in an Elyra PS.1 microscope (Zeiss). Images were acquired using either 3 or 5 grid rotations, with 34 µm grating period for the 561 nm laser (100 mW), 28 µm period for 488 nm laser (100 mW) and 23 µm period for 405 nm laser (50 mW). Images were acquired using a Pco.edge 5.5 camera and reconstructed using ZEN software (black edition, 2012, version 8.1.0.484) based on a structured illumination algorithm[23], using synthetic, channel specific Optical Transfer Functions (OTFs) and noise filter settings ranging from -6 to -8.

Fast time-lapse imaging of *S. aureus*

A 2 µl aliquot of an exponentially growing culture of *S. aureus* was placed on an agarose pad in TSB. Cells were imaged at 2 ms intervals for a total time of 10 s, using a Pco.edge 5.5 camera and a Plan-Apochromat 100x /1.46 NA Oil DIC ELYRA objective in an Elyra PS.1 microscope (Zeiss).

Labelling and imaging of *S. aureus*

For time-lapse experiments *S. aureus* cells were incubated with the membrane dye Nile Red (Invitrogen) at a final concentration of 10 µg ml^{-1}, for 5 min at 37 °C, with agitation (550 rpm). Subsequently, the cells were placed on an agarose pad containing 50% TSB in Phosphate Buffer Saline (PBS) and imaged during growth by SIM. Image sets were acquired every 3 min, for a total period of 1 h, using 2% of 561 nm laser power and 50 ms exposure times. Measurements were performed on reconstructed super-resolution images using ZEN software.

To determine the fraction of old/new cell wall in *S. aureus*, cells were stained with either a wheat germ agglutinin Alexa Fluor 488 conjugate (WGA-488, Invitrogen) or fluorescent D-amino acid HADA[24,25] at a final concentration of 2 µg ml^{-1} and 250 µM, respectively. The cells were incubated at 37°C with agitation for 5 min or 30 min for WGA-488 or HADA, respectively. Unbound dye was removed from the media by washing cells with TSB and cells were then incubated with Nile Red (10 µg ml^{-1}) for 5 min at room temperature and placed on an agarose pad containing 50% TSB in PBS. Cells showing uniform WGA-488 or HADA staining were imaged by SIM at 0, 3, 6, 30 and 60 min, using 2% 561 nm laser with 50 ms exposure for Nile Red, 3% 488 nm laser with 50 ms exposure for WGA-488 and 20% 405 nm laser with 100 ms exposure for HADA.

To evaluate localisation of peptidoglycan synthesis activity, *S. aureus* cells grown to an OD_{600nm} of approximately 0.5 were labelled with fluorescent D-amino acid NADA (250 µM) for 20 min at 37°C, 550 rpm. Cells were then washed with PBS, placed on an agarose pad and visualized by SIM, using 10% 488 nm laser, 100 ms

exposure. For pulse labeling experiments, *S. aureus* cells were incubated with either HADA or its L-enantiomer HALA[24] for 5 min at 37°C, 550 rpm and then imaged as described above.

S. aureus cell wall labelling with vancomycin was performed by incubating the cells for 2 min at room temperature with a mixture containing equal amounts of vancomycin (Sigma) and a BODIPY FL conjugate of vancomycin (Van-FL, Molecular Probes) to a final concentration of 0.8 μg ml^{-1}. Cells were visualized by SIM, using 2% 488 nm laser, 100 ms exposure.

Labelling and imaging of *Sporosarcina ureae*

To determine the fraction of old/new cell wall in *S. ureae* by time lapse microscopy, cells from cultures at OD_{600nm}~0.5 were stained with WGA-488 at a final concentration of 6 μg ml^{-1}. The cells were incubated at 30°C with agitation for 10 min. Unbound dye was removed from the medium by washing cells with LB. Cells were then incubated with Nile Red (10 μg ml^{-1}) for 5 min at room temperature and placed on an agarose pad containing 50% LB in PBS. Cells showing uniform WGA-488 labeling were imaged by SIM at 0, 15, 30, 45 and 60 min, using 2% 561 nm laser with 50 ms exposure for Nile Red, 3% 488 nm laser with 50 ms exposure for WGA-488.

Photoactivated Localisation Microscopy (PALM)

To observe PBP4-PAmCherry single molecules by PALM, an overnight culture of NCTCΔ*pbpD::pbpD-mCherryPA* was diluted 1/200 in TSB and incubated at 37 °C. At mid-exponential phase (OD_{600nm} 0.6), 1 ml of culture was harvested by centrifugation and washed with 1 ml of PBS. Cells were re-suspended in 20 µl of PBS and 1 µl was placed on a thin layer of 1.2% agarose in PBS mounted on a gene frame. Image sequences for PALM analysis were obtained using a Zeiss Elyra PS.1 microscope with a 100x 1.46NA objective, additional magnification of 1.6X, equipped with an EMCCD camera (Andor - iXon DU897) using Zeiss ZEN software. For an initial bleach of auto-fluorescent molecules and unwanted pre-activated fluorophores, the sample was first imaged with a 561 nm laser at ~0.76 kW cm^{-2} and 33 ms exposure for 2,000 frames. After bleaching, the continuous activation and imaging of PAmCherry molecules was performed for 8,000 frames by simultaneously irradiating the sample with a 405 nm laser at ~1.9 W cm^{-2} and a 561 nm laser at ~ 0.76 kW cm^{-2}, using 33 ms of exposure time. To maintain a stable density of fluorophores photo activating in each frame and compensate the depletion of PAmCherry molecules during the course of the experiment, the intensity of the 405 nm laser was increased until ~ 38W cm^{-2}. Post-processing of the last 8,000 frames was performed using the ZEN software where an *xy* 2D-Gaussian fit was applied to the individually resolvable sub-diffraction molecules present in each frame (mask of 9 pixels with a minimum signal to noise ratio of 6).

Hyperosmotic shock

Cells were grown in TSB until an OD_{600nm} of approximately 0.5 and then incubated for 30 min at 37 °C with agitation (700 rpm) in the presence of NADA (250 µM). The cells were harvested, washed once with 50 mM Tris-HCl buffer pH=7.5 containing a saturating concentration of NaCl (4.96 M) and incubated for 15 min at 37 °C. Cells were pelleted and placed on an agarose pad containing the same medium used to perform the hyperosmotic shock and imaged by SIM.

Calculation of cell dimensions

To calculate the volume of each cell, an ellipse was fitted to the border limits of the cellular membrane of Nile Red labelled cells, overlaying the membrane dye signal. Subsequently, the shorter and longer axes were measured, coinciding with the septum and the axis perpendicular to it, respectively. The volume of the cell was obtained by an approximation to the volume of a prolate spheroid (equation 1) where a and b correspond to the longer and shorter semi-axes, respectively.

$$(1) V = \frac{4}{3}\,\pi\, ab^2$$

Cell surface area was calculated using the Knud Thomsen approximation[26] (equation 2) to calculate the surface area of ellipsoids, where a corresponds to the longer semi-axis and *b* and *c* correspond to shorter semi-axes, which are identical in the case of *S. aureus* cells.

$$(2) S \approx 4\pi\left[\frac{1}{3}\left(ab^{1.6}ac^{1.6}bc^{1.6}\right)\right]^{1/1.6}$$

To evaluate cellular symmetry and identify “D” shaped cells, cells in Phase 1 of the cell cycle were selected and an ellipse was fit to the cell borders corresponding to the old cell wall. The ellipse centre was defined as the middle point of the longer axis and the distances from this point (along a perpendicular axis) to new peripheral cell wall and old peripheral cell wall were calculated (see Fig. 8d). Symmetry was assessed by the ratio between the distance from the centre to the old cell wall and the distance from the centre to the new cell wall. A cell was considered as asymmetric when this ratio was more than 1.33, *i.e.* when the distance from the cell centre to the new cell wall was less than 75% of the distance to the old cell wall.

Calculation of fluorescence ratio in NADA labelled cells

NADA labelled *S. aureus* cells were observed using a Zeiss Axio Observer microscope equipped with a Photometrics CoolSNAP HQ2 camera (Roper Scientific) and Metamorph 7.5 software (Molecular Devices). To quantitatively assess D-amino acid incorporation, the fluorescence signal at the septum and at the peripheral cell wall was determined for 50 cells with fully formed septa. A fluorescence ratio (FR) for septal *versus* peripheral cell wall signals was determined as previously described[27].

Statistical analysis

Statistical analyses were done using GraphPad Prism 6 (GraphPad Software). Unpaired student’s t-tests were used to evaluate the differences in cellular volume and shape between cell cycle stages

and between the initial and final stages of each phase, as well as to compare fluorescence ratios between peripheral and septal wall signal intensity. One-way ANOVA was used to compare old/new cell wall fraction at different time points. *P*-values ≤ 0.05 were considered as significant for all analysis performed and were indicated with asterisks: *P ≤ 0.05, **P ≤ 0.01 and ***P ≤ 0.001.

Results

S. aureus cells elongate during the cell cycle

To follow morphology dynamics during the cell cycle of *S. aureus,* cells of wild-type strain COL were labelled with the membrane dye Nile Red, placed on an agarose pad containing growth medium and imaged during growth at room temperature by Super-Resolution Structured Illumination Microscopy (SIM) (Fig. 1a). During the initial phase of the cell cycle (here referred to as Phase 1), prior to initiation of division septum formation, cells were approximately spherical in shape, as determined by calculating the ratio between the longer axis of the cell (perpendicular to the division septum) and the shorter axis (coincident with the septum) and then became slightly elongated (Fig. 1c, Fig. 2 and Table 3). In a second stage (Phase 2), cells initiated and completed the synthesis of the division septum and did not significantly elongate. Finally, during the last stage of the cell cycle (Phase 3), cells with a complete septum elongated further, before splitting into two daughter cells. Splitting was accompanied by fast reshaping of the flat septum to become approximately one hemisphere of each daughter cell.

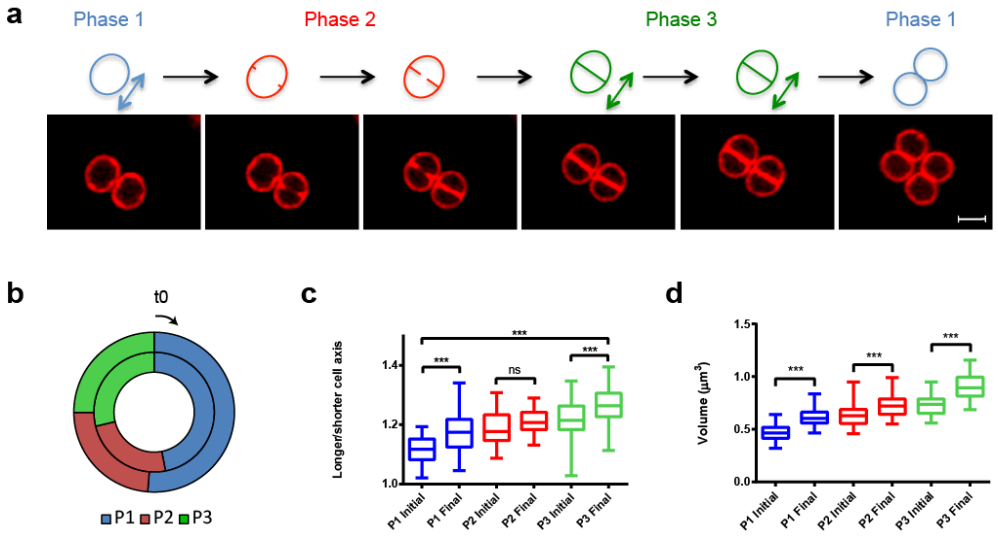

Figure 1. Morphological changes during the cell cycle of *Staphylococcus aureus* (**a**) *S. aureus* COL cells were stained with membrane dye Nile Red and imaged by SIM for 60 min, at 3 min intervals. Phase 1 (P1) cells have recently divided and have not initiated synthesis of the septum. Phase 2 (P2) cells are undergoing septum synthesis. Phase 3 (P3) cells have a complete septum and are going to split into two daughter cells. Coloured arrows indicate periods of cell elongation. The time interval between panels was 6 min. Scale bar, 1 μm. (**b**) Duration of each phase of the cell cycle (represented as a fraction of the duplication time) was measured in individual cells imaged by SIM while growing at room temperature on agarose slides containing growth medium (inner circumference); or after growing in liquid culture, at 37 °C, and placed on the microscopy slide just before imaging (outer circumference). (**c**) Elongation of *S. aureus* cells during the cell cycle was evaluated by calculating the ratio of the longer to the shorter axis of each cell. *n*=40 cells for each phase. (**d**) Cell volume was measured at the beginning and at the end of each phase of the cell cycle. Cells increased their volume continuously throughout the cell cycle. *n*=40 for each phase. Data in (**c**,**d**) were collected from two independent experiments and are represented as box-and-whisker plots where boxes correspond to the first to third quartiles, lines inside the boxes indicate the median and ends of whiskers represent the minimum and maximum of all data. Statistical analysis was performed using the unpaired *t* test (***P<0.001; ns, not significant).

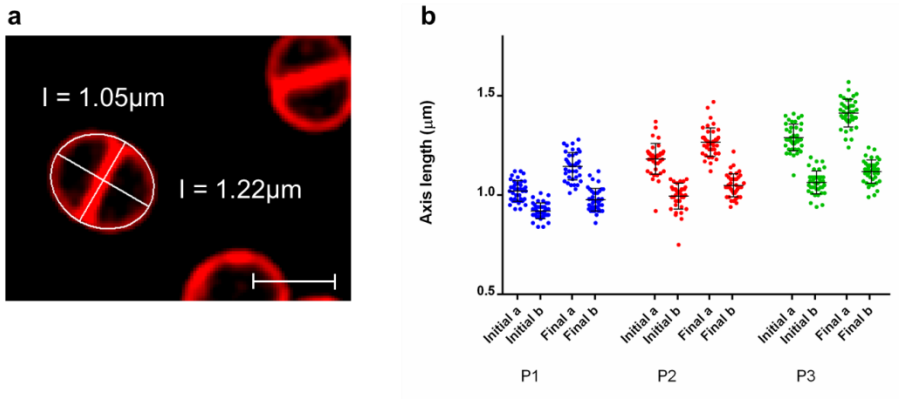

Figure 2. Size measurements of *S. aureus* cells imaged by SIM during the cell cycle. (a) The shape of *S. aureus* cells was approximated to a prolate spheroid and superimposition of an elipse was used to measure the longer and shorter cellular axes during the different phases of growth. Scale bar = 1 µm **(b)** Scatter plot of the measurements of the longer (a) and shorter (b) axes of *S. aureus* cells when starting (Initial) and finishing (Final) each of the three growth phases defined in Fig. 1.

Table 3: Average ratio of longer/shorter axes of *S. aureus* cells upon initiation and completion of the three phases of the cell cycle.

	P1		P2		P3	
Strain	Initial	Final	Initial	Final	Initial	Final
COL	1.11±0.04	1.17±0.06	1.19±0.05	1.21±0.04	1.22±0.06	1.27±0.05
COLΔ*pbpD*	1.13±0.09	1.17±0.07	1.20±0.06	1.23±0.05	1.22±0.04	1.28±0.06
COLΔ*atl*	1.13±0.07	1.14±0.05 (**)	1.15±0.06 (**)	1.17±0.06 (***)	1.17±0.06 (**)	1.23±0.05 (*)
COLΔ*sle1*	1.19±0.08 (***)	1.20±0.08	1.19±0.06	1.19±0.06	1.20±0.07	1.23±0.10

*p ≤ 0.05, ** p ≤ 0.01, *** p ≤ 0.001 mutants vs. parental strain COL (n=40 cells for each strain)

Although we were able to observe cells undergoing complete cell cycles by SIM imaging, we noticed a delay in growth, when compared to cells on the same slide that were not exposed to laser light. Photodamage is cumulative and therefore could cause an increasing bias towards longer duration of growth phases over the course of the experiment. In order to overcome this limitation, all quantitative analyses were only performed on the first complete growth phase of each cell (*i.e.*, in cells observed finishing the previous phase and starting the next phase), and not on the entire cell cycle. Using this approach we measured the duration of each growth phase of the *S. aureus* cell cycle (Fig. 1b). Cells spent approximately half of the cell cycle in Phase 1 (47±9%), with the other half being spent in septum synthesis (Phase 2, 24±7%) and the final elongation step (Phase 3, 29±6%), with a cell cycle duration of 66 ± 9 min. Because the cells analysed by this method were growing at room temperature on growth medium containing agarose pads, on the microscope stage, we independently confirmed the length of each phase by growing *S. aureus* cells in liquid culture with aeration at 37°C, labelling cell membranes and immediately observing them by SIM. The percentage of cells observed in each phase should be proportional to the fraction of the cell cycle spent in that stage. Fig. 1b shows that similar results for the duration of Phases 1-3 were obtained by both methods.

Interestingly, at the timescale of this experiment, we never observed intermediate stages in the process of cell splitting and reshaping of the flat septum into a curved surface, implying that these events are likely to be extremely fast. In order to verify this assumption, we imaged cells growing on an agarose pad, at 2 ms intervals (Fig. 3a). *S. aureus* cells divided into two daughter cells in the interval between two acquisitions, indicating that splitting takes less than 2 ms (n=10).

The spatial and temporal resolution of these images does not allow us to determine if (i) splitting and septum reshaping occur simultaneously, as one could expect if remodelling of the flat septum did not require any enzymatic activity and resulted solely from the increased turgor pressure imposed upon the septum as it splits and becomes exposed to the external milieu, or (ii) splitting and septum reshaping are two consecutive processes. We reasoned that if the latter hypothesis was correct, we should be able to capture intermediates in the division process in which the septum had already split but remained flat. For this purpose, we fixed cells during exponential growth and imaged them using Scanning Electron Microscopy (SEM) (Fig. 3b). In agreement with previous data[9], we observed recently divided cells in which the previous septum was seen as a smooth flat surface, indicating that septum splitting and reshaping are likely to be sequential events.

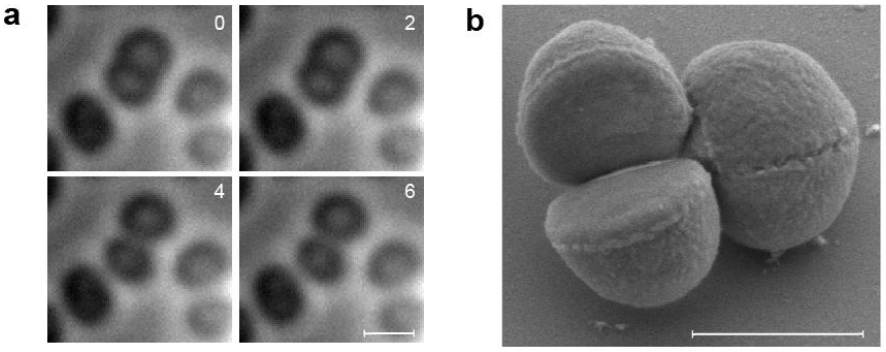

Figure 3. Splitting of *S. aureus* cells occurs on the millisecond timescale. (**a**) Dividing *S. aureus* cells were imaged on an agarose pad, acquiring frames every 2 ms, showing that splitting of the mother cell occurs in <2 ms (between the 2 ms and the 4 ms frame). Time is indicated in milliseconds. Scale bar, 1 µm. (**b**) To capture intermediate stages in the splitting process, *S. aureus* cells were fixed with glutaraldehyde during growth and imaged by SEM. The cell on the left has just divided in two daughter cells. The previous division septum is seen as a smooth flat

surface indicating that septum splitting and reshaping into a curved hemisphere are likely to be sequential events. Note that cells with flat septa were not as rare as could be expected given the speed of the splitting process. It is therefore possible that the cell treatment required for SEM stabilizes this stage. Scale bar, 750 nm.

The septum gives less than one hemisphere of each daughter cell

Previous descriptions of the *S. aureus* cell cycle suggested that cell wall synthesis occurred mainly, if not only, at the division septum[5]. Furthermore, it was assumed that the "new" cell wall material from the septum of the mother cell formed one complete hemisphere of each of the daughter cells, while the other hemisphere was made of "old" cell wall material originating from the peripheral wall of the mother cell. However, we observed that just prior to splitting, at the end of Phase 3, the mother cell has an ellipsoid shape, with a semi-major axis of 0.70±0.04 µm (perpendicular to the septum) and two semi-minor axes of 0.55±0.03 µm (equivalent to the radius of the septum), resulting in a septal surface area of 0.95 μm^2. After splitting, at the beginning of Phase 1, each daughter cell has semimajor and semi-minor axes of 0.52±0.03 µm and 0.46±0.03 µm, respectively. Therefore, the total surface area of each daughter cell is ~2.89 μm^2 (see Experimental Procedures for Knud Thomsen approximation used for calculations), of which 0.95 μm^2, or ~33%, should be composed of new cell wall material, originating from the septum of the mother cell. The remaining ~67% of the cell surface should be composed of "old" cell wall material, originating from one hemisphere of the mother cell, *i.e.*, the distribution of old and new cell wall material should not be 50% of each, as previously assumed[3,5,6] (Fig. 4a). To determine whether the mode of *S. aureus* growth was

consistent with these assumptions, cells were labelled with a green fluorescent derivative of wheat germ agglutinin (WGA-488), a lectin which labels *N*-acetylglucosamine residues present in peptidoglycan and in wall teichoic acids. Importantly, WGA labels the cell wall present at the cell surface (peripheral wall) but does not diffuse into (and therefore does not label) the division septum. Cells were next washed to remove unbound WGA-488, and stained with the membrane dye Nile Red, which diffuses through the septum and therefore labels the entire membrane of the cell. Finally, cells were placed on an agarose pad containing growth medium and imaged by SIM during growth (Fig. 4b). Cells whose surface was completely labelled by WGA-488 were selected for analysis and both the perimeter of each cell, as well as the fraction of the cell surface made of old cell wall (WGA-488 labelled), were measured. In agreement with our model, we found that after splitting of the mother cell, each daughter cell had 61.3±3.3% (n=30) of its surface labelled by WGA-488, *i.e.*, made of old cell wall, clearly showing that the flat septum, even after reshaping, does not contribute to half of the cell surface (Fig. 4c).

These results were confirmed in a second experiment, similar to the one described above, in which cells were labelled with HADA instead of WGA-488. HADA is a blue fluorescent derivative of 3- amino-D-alanine that can be incorporated in the pentapeptide chain of peptidoglycan[24]. Selected cells whose entire surface was labelled with HADA at time zero were followed during growth for 60 min (Fig. 4d). Similar to the results obtained with WGA-488 labelling, upon splitting of the mother cell, 62.5±3.4% of the surface of each daughter cell was labelled with HADA.

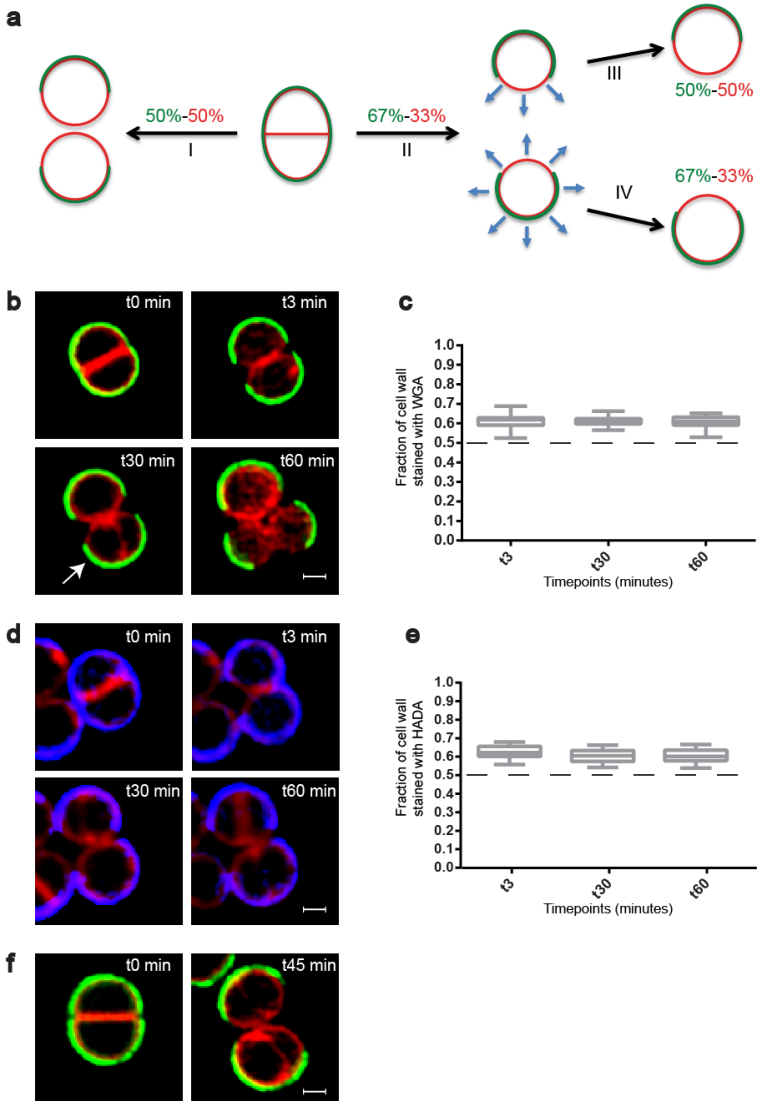

Figure 4. Asymmetrical inheritance of cell wall material during *S. aureus* cell division. (**a**) Schematic representation of the possible modes of division and growth of *S. aureus.* Peripheral cell wall of the mother cell is represented in green and cell membrane is represented in red. Upon division of the mother cell, the new cell wall material, derived from the previous septum, may constitute 50% of the surface of each daughter cell, if the surface area of the flat septum increases as it becomes curved (I), or 33%, if there is no increase in the surface area of septum material (II). In the latter case, the cell can then grow by peptidoglycan synthesis and/or autolysis

either at the site of the new cell wall material only (III) or throughout the entire cell surface (IV). (**b**) *S. aureus* COL cells were labelled for 5 min with peripheral cell wall dye WGA-488 (green), washed and stained with membrane dye Nile Red. Cells were placed on an agarose pad and resumed growth at room temperature. Upon division, the old cell wall preserved the green WGA-488 signal. Cells were imaged by SIM at 3, 30 and 60 min after splitting. The cell indicated by the arrow underwent a second round of division. (**c**) The fraction of WGA-488-labelled cell wall (green) relative to cell perimeter (red) remained above 0.60 during the cell cycle, *n*=30. No statistically significant variation was found (P>0.05). (**d**) An experiment equivalent to that described in panel (**b**) was done using cell wall dye HADA instead of WGA-488. (**e**) The fraction of cell wall labelled with HADA (blue) relative to the cell perimeter (red), decreased slightly during the first 30 min but remained above 0.60 during the cell cycle, *n*=30. (P=0.03). (**f**) The cell wall of *Sporosarcina ureae* was labelled with WGA-488, washed, labelled with Nile Red and imaged by SIM. Panels show the same cell before and after division, indicating that old cell wall material (green) constitutes more than half of the daughter cells surface. Contrast of individual channels was adjusted on merged images. Scale bars, 0.5 µm. Data in (**c**,**e**) are represented as box-and whisker plots where boxes correspond to the first to third quartiles, lines inside the boxes indicate the median and ends of whiskers represent the minimum and maximum of all data. Statistical analysis was performed using one-way analysis of variance.

Careful inspection of SEM images of *S. aureus* cells confirms that the "old" cell wall constitutes more than 50% of the surface of each daughter cell (Fig. 5). Cell wall material which is at least one generation old has been described as having an irregular, rough appearance, while newly synthesized cell wall, resulting directly from the septum of the mother cell, has a smoother appearance with concentric rings[3,28], with a clear border separating the two types of cell surface[29]. These borders, seen in Fig. 5 and denoted in blue in the schematic representation of the cells, are clearly not placed at mid cell, reinforcing the idea that more than half of the surface of *S. aureus* cells is at least one generation old.

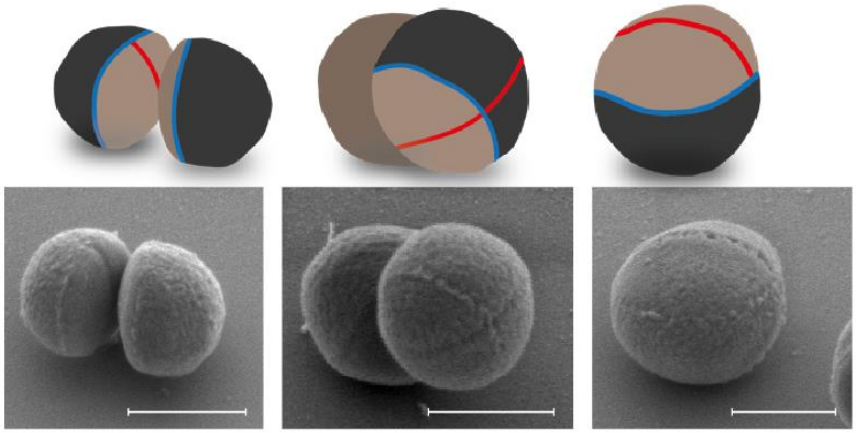

Figure 5. Scars of previous divisions do not mark cell quadrants. SEM images of *S. aureus* COL cells showing an asymmetric scar (blue line in scheme) corresponding to the previous division site and a fissure located in the middle of the cell (red line), presumably corresponding to the next division site. The new cell wall (light brown), resulting from septal material from the mother cell, which has a smooth surface immediately after division (first panel), occupies less than half of the total surface. Scale bars, 600 nm.

We then asked if this mode of division of spherical cells, in which the division septum of the mother cell generates less than one hemisphere of each daughter cells was restricted to *S. aureus* or common to other cocci. Labelling of peripheral cell walls in *Sporosarcina ureae* with WGA-488 showed that division of spherical cells from this organism also results in daughter cells with a fraction of approximately 60% of the surface made of “old” cell wall (Fig. 4f).

S. aureus grows by remodelling the entire cell surface

The fact that cell wall synthesis in staphylococci occurred mainly, if not exclusively, at the division septum[5], led to the suggestion that *S. aureus* does not enlarge during the cell cycle and that the conversion of the flat division septum into one hemisphere of each daughter cell accounted for the doubling in volume required for cell division to take place[3,5,6]. Importantly, the diffraction limit of resolution of conventional light microscopy (~250 nm)[30,31] impaired until now, detection of size variations in the range of those required for the doubling of *S. aureus* cell volume (see discussion). These variations can, however, be observed by SIM, which improves the lateral xy resolution to approximately 110 nm[32]. Using this technique, we observed that staphylococcal cells increased in volume during the entire cell cycle, from a volume of 0.47±0.07 μm^3 at the beginning of Phase 1 to a volume of 0.91±0.12 μm^3 at the end of Phase 3 (Fig. 1d and Table 4). If enlargement of *S. aureus* cells was due mainly to the remodelling of the flat septum into a hemisphere, the volume increase should be essentially restricted to the process of splitting and reshaping of the septum. On the contrary, we have observed that there is no significant increase in volume when staphylococcal cells divide, *i.e.*, that each of the two daughter cells has approximately half of the volume of the Phase 3 mother cell (Fig. 1d). Furthermore, the largest and fastest increase in volume occurs during Phase 3 (Δvolume = 0.16±0.07 μm^3 at a rate of 0.009±0.003 μm^3 min^{-1}, Table 4), during which there is no reshaping of the flat septum, clearly indicating that other mechanisms must be involved with the enlargement of *S. aureus* cells.

Table 4. Average volume (μm^3) of *S. aureus* cells upon initiation and completion of the three phases of the cell cycle.

	P1		P2		P3	
Strain	Initial	Final	Initial	Final	Initial	Final
COL	0.47±0.07	0.62±0.08	0.63±0.10	0.72±0.10	0.73±0.10	0.91±0.12
COLΔ*pbpD*	0.40±0.08 (***)	0.59±0.10	0.61±0.08	0.69±0.09	0.70±0.07	0.86±0.11
COLΔ*atl*	0.46±0.07	0.66±0.10	0.68±0.10(*)	0.79±0.10(**)	0.82±0.13 (***)	0.97±0.16
COLΔ*sle1*	0.48±0.07	0.55±0.06 (***)	0.55±0.07 (***)	0.64±0.09 (***)	0.63±0.09 (***)	0.98±0.17 (*)

* P ≤ 0.05, ** P ≤ 0.01, *** P ≤ 0.001 mutants vs. parental strain COL (n=40 cells for each strain)

Next we wondered if enlargement of cells occurred via remodelling only of the material derived from the previous septum or via remodelling of the entire cell surface (Fig. 4a). In the former case, the percentage of “new” cell wall should increase during the course of the cell cycle, eventually reaching half of the total cell surface, while in the latter case the ratio of new to old cell wall observed immediately after splitting of the mother cell (~39% to ~61%, respectively, Fig. 4b) should be maintained over the cell cycle. Therefore, following the growth of cells in which the “old” cell wall was labelled with WGA-488 should allow us to determine how *S. aureus* cells enlarge. The

perimeter of WGA-488 labelled cells increased from 3.08±0.17 µm to 3.40±0.21 µm after 60 min on the slide, confirming that cells were growing. Under these conditions, the fraction of cell wall labelled by WGA-488 remained at 60.6±3.2%, even in cells that were already initiating the next round of division (Fig. 4b and c). Similar results were obtained with HADA labelled cells, in which the fraction of labelled cell wall remained at 60.5±3.8% after 60 min (Fig. 4d and e), indicating that cell enlargement was due to remodelling of the entire cell surface and not exclusively of the septal material.

S. aureus enlarges via peptidoglycan synthesis and autolysis

Enlargement of bacterial cells can occur via synthesis of new peptidoglycan, autolysis of old peptidoglycan, or a combination of both processes. We have previously observed that peptidoglycan synthesis occurred mostly at the division septum[5]. Given that we have now shown that growth of staphylococcal cells occurs via remodelling of the entire cell surface, we considered the possibility that enlargement was mainly due to autolytic activity. However, autolysis without synthesis would lead to a thinning and/or increase in the porosity of the old peptidoglycan mesh over consecutive generations. Since approximately 60% of old cell wall is transmitted to daughter cells in each cell division, staphylococcal cells would have regions of the surface a few generations old, which were necessarily submitted to the enlargement process multiple times. Thinning of these regions due to peptidoglycan autolysis without synthesis could therefore endanger the integrity of the bacterial cell. Making use of newly available tools to study peptidoglycan synthesis and to image protein localisation, we revisited the question regarding the localisation of

peptidoglycan synthesis in *S. aureus. S. aureus* cells were labelled with HADA, which can be incorporated by PBPs in the pentapeptide chain of peptidoglycan[24]. Cells in growth phases 2 and 3, *i.e.*, cells with partial or complete septa, showed labelling mostly at the septum, in agreement with previous reports showing that the majority of PBP activity takes place at the septum[4,5,33]. However, peripheral signal was also observable (Fig. 6a). Labelling around the entire cell surface was even more noticeable in Phase 1 cells, lacking a division septum (Fig. 6a, arrows).

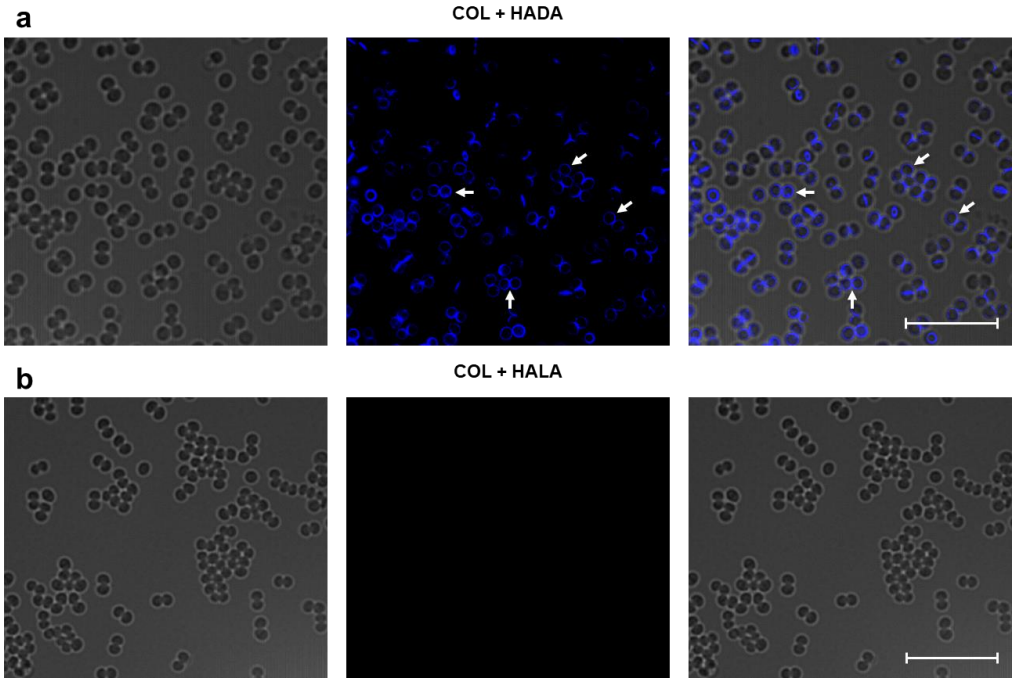

Figure 6. Fluorescent D-amino acid HADA is incorporated at the peripheral wall of *S. aureus* cells. *S. aureus* COL cells were labelled for 5 min with HADA, a fluorescent derivative of 3-amino-D-alanine that can be incorporated in the pentapeptide chain of peptidoglycan (a) or its Lenantiomer HALA that should not be incorporated into the peptidoglycan (b), used as a control for non-specific binding.

Cells were then imaged by SIM, showing that the peripheral walls of cells in Phase 1 (examples indicated by white arrows) were labelled by HADA but not by HALA. Scale bars = 10 µm

We then asked which of the four native *S. aureus* PBPs had peripheral activity. Given that PBP1 and PBP2 are essential proteins in MSSA strains and therefore cannot be depleted[34,35], *S. aureus* mutants lacking PBP3 and PBP4 were initially tested. For this purpose, we used a green fluorescent variant of HADA, NADA. COLΔ*pbpD* cells, lacking PBP4, were virtually devoid of NADA labelling away from the septum (Fig. 7b), when compared to COL (Fig. 7a), showing that this protein is the main enzyme responsible for the peripheral signal. Complementation of COLΔ*pbpD* with a plasmid-encoded PBP4 resulted in recovery of the peripheral signal (Fig. 7c and d). A comparison of the ratio of the septal *versus* peripheral fluorescence signal in the COL parental strain (7.91±0.42) and COLΔ*pbpD* (18.7±0.76) confirmed that incorporation of D-alanine labelled analogues was essentially absent from the peripheral wall of the mutant lacking PBP4 (Fig. 7e). In agreement, localisation of a fluorescent derivative of PBP4 showed that although this protein is mainly localized at the septum, as we have previously reported[36], peripheral fluorescent signal could also be observed (Fig. 7f). Quantification by PhotoActivated Localisation Microscopy (PALM) showed that 26±11% of the total PBP4 molecules (fused to photoactivatable mCherry) in Phase 3 cells are present at the peripheral membrane (Fig. 7g).

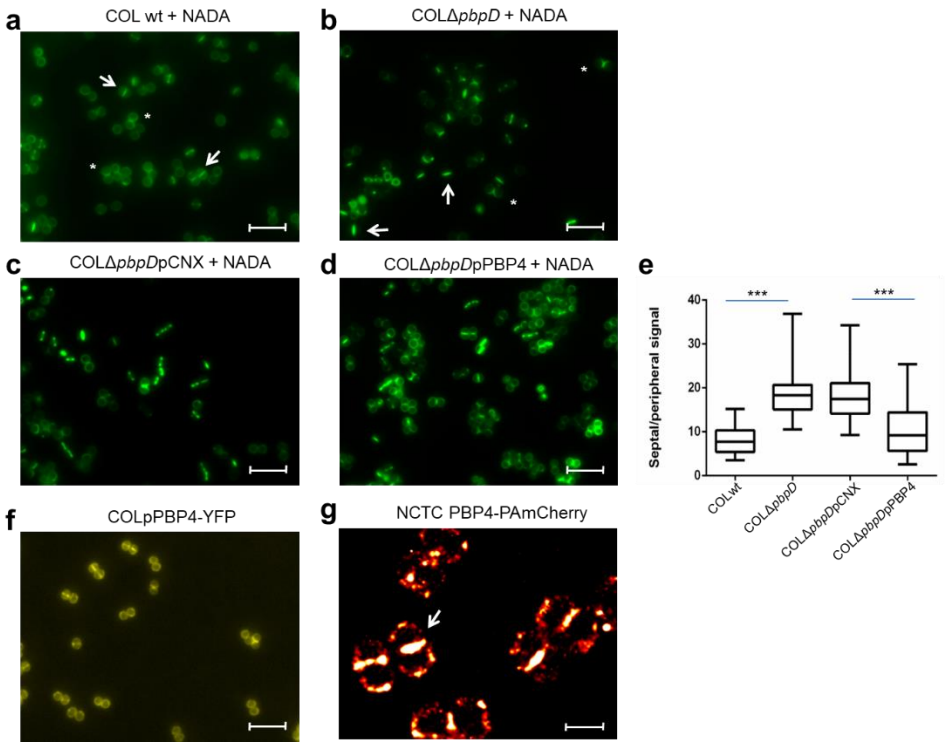

Figure 7. PBP4 is active at the division septum and at the peripheral wall. (a) *S. aureus* COL cells were incubated for 20 min with NADA and imaged by wide-field fluorescence microscopy. Cells with partial (Phase 2) or complete (Phase 3) septa (arrows) showed labelling mostly at the septum, although some fluorescent signal could also be observed at the peripheral cell surface. Cells without septa (Phase 1, asterisks) showed NADA incorporation at the peripheral cell wall. Scale bar = 5 µm. **(b)** COLΔ*pbpD* cells, lacking PBP4 were imaged as described above. NADA incorporation at the peripheral cell surface was virtually absent both in cells undergoing septation (arrows) and in newly split cells (asterisk), indicating that PBP4 is responsible for the majority of peripheral NADA incorporation. Scale bar = 5 µm. **(c,d)** Strain COLΔ*pbpD* was complemented with empty pCNX vector (c) and pCNX encoding PBP4 under the control of P_{cad} (d), in the presence of cadmium chloride (1 µM), and imaged as above. NADA incorporation at the peripheral cell surface was only observed in the strain complemented with PBP4. Scale bar = 5 µm. **(e)** The intensity of the NADA fluorescence signal was measured at the septum and peripheral wall, in cells (n=50) with complete division septa, and the ratio between septal and peripheral signal was calculated for each cell. This ratio was significantly

higher for COLΔ*pbpD* than for COL cells (18.7±5.4 *vs* 7.9±3.0, P<0.001) showing that the mutant lacking PBP4 is deficient in peripheral NADA incorporation. This ratio was also higher in COLΔ*pbpD* containing the empty vector pCNX than in the same strain complemented with plasmid-encoded PBP4 (18.2±5.7 *vs* 10.2±5.4, P<0.001).**(f)** Localisation of a YFP-tagged derivative of PBP4 in COL cells by wide-field fluorescence microscopy showing that a small fraction of PBP4 localizes at the cell periphery. Scale bar = 5 µm. **(g)** PALM image showing PBP4-PAmCherry localisation in *S. aureus* NCTC8325-4 background. Cells (n=50) showing PBP4-PAmCherry in complete septa (white arrow) were used to quantify the number of PBP4 molecules (n=27533) present either at the peripheral membrane (26±11%) or at the septa (74±11%). Images are false coloured showing red to white increasing intensity range. Scale bar, 1 µm.

Furthermore, the duration of Phase 1 is longer in COLΔ*pbpD* than in the parental strain COL (Fig. 8a) and the cell volume is smaller (Table 4), reinforcing the hypothesis that PBP4 is one of the proteins that have a role in peripheral peptidoglycan synthesis during this growth phase. In contrast, cell elongation is unaffected in COLΔ*pbpD* cells (Table 3), suggesting that additional proteins play a role in cell growth. We therefore evaluated the role of two major autolysins, Atl[7] and Sle1[37] in cell enlargement and elongation, as well as in septum remodelling, by deleting chromosomal *atl* or *sle1* genes of strain COL. The lack of Atl amidase and glucosaminidase activities led to larger cells which are less elongated when compared to the parental strain COL (Tables 3 and 4), indicating that Atl autolytic activity is involved not only in cell separation, as previously shown[8,9], but also in cell size homeostasis and shape maintenance. COLΔ*sle1* cells remain elongated throughout the entire cell cycle, which could result from increased stiffness of peptidoglycan in the absence of Sle1 amidase activity, possibly impairing correct reshaping of the cell following division. Furthermore, these cells have a longer Phase 3 than the

parental strain COL (Fig. 8a), suggesting that cell splitting is impaired in this mutant.

Interestingly, we have observed the appearance, albeit at low frequency, of cells with the shape of the letter “D” in cultures of COLΔ*sle1* (Fig. 8b, arrows). These cells seem to be impaired in the process of reshaping of the flat septum, generated immediately after the splitting of the mother cell, into a curved hemisphere. D-shaped cells were never observed in the parental strain COL by SIM. This phenotype seems to be a consequence of defects in specific autolytic enzymes whose activity is required for the reshaping of the flat septum, since asymmetric cells were also identified at higher frequencies than in the parental strains in (i) an *sle1* deletion mutant in the background of a different *S. aureus* strain, namely NCTC8325-4 (Fig. 9b); (ii) an NCTC8325-4 mutant lacking LytM, an autolysin with glycylglycine endopeptidase activity[38] (Fig. 9c); (iii) a COL mutant depleted for the two-component system WalK/WalR (also known as YycG/YycF), which positively controls autolytic activity[39] (Fig. 9e). Interestingly, although WalKR is essential in RN4220[39], strain COL grows in its absence.

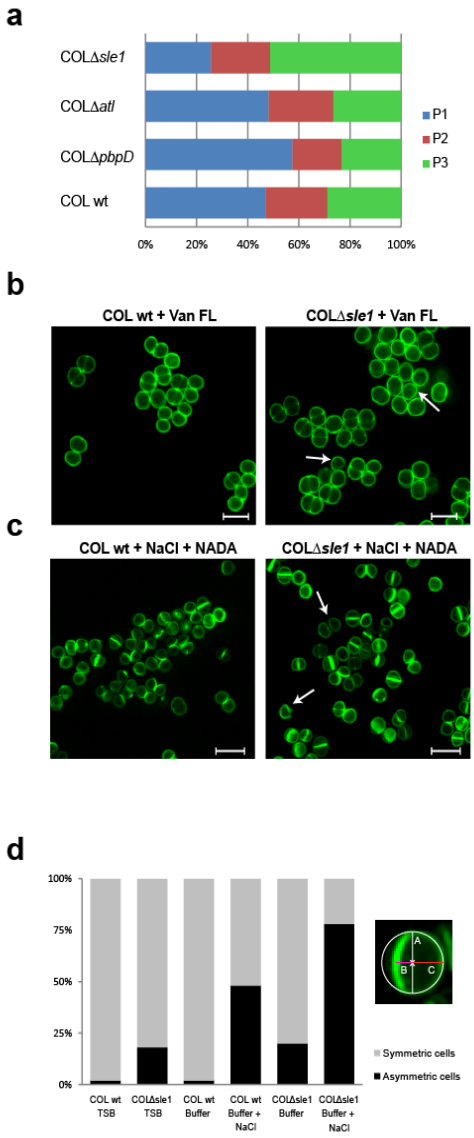

Figure 8. Effect of impaired peptidoglycan synthesis or autolysis on the cell cycle and morphology of *S. aureus*. (**a**) Duration of phases of the cell cycle of *S. aureus* mutants lacking peptidoglycan synthesis enzyme PBP4 (COLΔ*pbpD*, total duration of cell cycle 73±10 min) or autolysins Atl (COLΔ*atl*, 82±8 min) and Sle1 (COLΔ*sle1*, 86±15 min), compared with the parental strain COL (66±9 min). Cells (*n*=40 for each phase) were growing in solid medium and only cells that completed at least one growth phase during the time of the experiment were included in the analysis. Approximately 50% of COLΔ*pbpD* cells that initiated Phase 1 did not complete it (*versus* 20% of COL cells) and were not included in the analysis. (**b**) The

cell wall of COL and COLΔ*sle1* was stained with Van-FL and imaged by SIM. Asymmetric cells with a shape close to a 'D' (white arrows) were observed, indicating that reshaping of the flat septum into a curved hemisphere following division was impaired in this mutant. (**c**) Exponentially growing COL and COLΔ*sle1* cells were stained with NADA, incubated for 15 min in saturating concentration of NaCl, placed on an agarose pad containing the same salt concentration and imaged by SIM. Cells with a shape close to a 'D' (examples indicated by white arrows) were observed at higher frequency in the mutant lacking Sle1 (right) than in the parental strain COL (left). Scale bars, 2 µm. (**d**) Symmetry of cells depicted in panels **b** and **c** was assessed by fitting an ellipse to the cells (*n*=50 for each class) and defining its centre (X) as the middle point of the shorter axis (A). The distances from X to new peripheral cell wall (B) and old peripheral cell wall (C) were calculated. Cells were considered as asymmetric (black bars) if the ratio C/B was more than 1.33 and symmetric (grey bars) when this ratio was ≤1.33. wt, wild type.

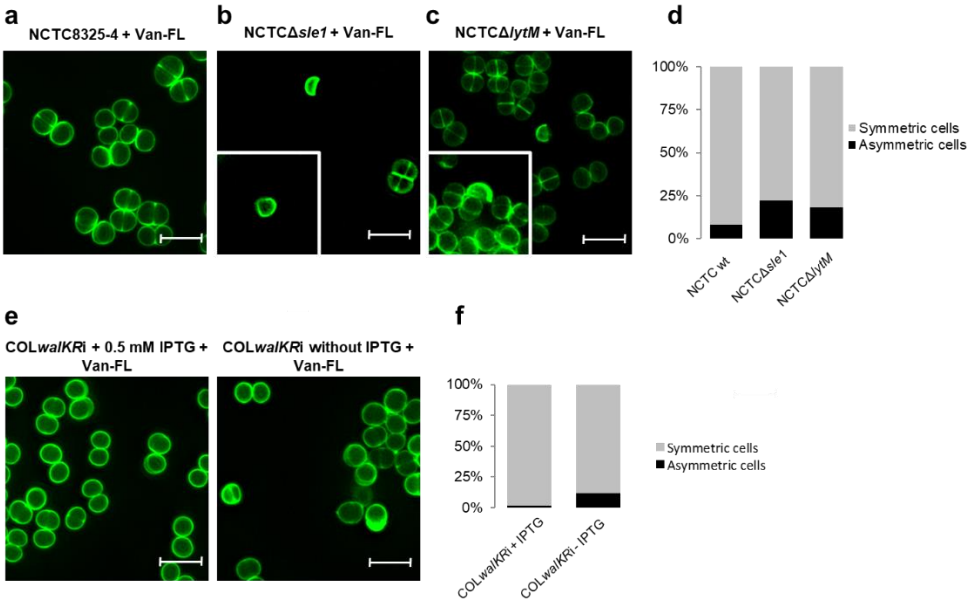

Figure 9. Effect of impaired peptidoglycan autolysis on the morphology of *S. aureus*. Cells of MSSA strain NCTC8325-4 **(a)**, its mutant lacking autolysin Sle1 (NCTCΔ*sle1*, **(b)**), or lacking autolysin LytM (NCTCΔ*lytM,* **(c)**) were labelled with cell wall dye Van-FL and imaged by SIM, confirming the presence of D-shaped cells in the mutants. **(d)** Symmetry of cells depicted in panels "a" to "c" was assessed as described in Fig. 8d, showing an increase in the frequency of asymmetric cells in the

two autolysin mutants. **(e)** Cells of MRSA strain COL with the two-component system *walKR* (positive regulator of autolysins) placed under the control of the IPTG-inducible promoter P_{spac} (COL*walKR*i), were grown in the presence or in the absence of inducer, labelled with Van-FL and imaged by SIM, showing the presence of D-shaped cells. **(f)** Symmetry of cells depicted in panel "e" was assessed as described in Fig. 8d, showing an increase in the frequency of asymmetriccells upon depletion of the WalKR two-component system. Scale bars = 2 µm

In order to determine if turgor pressure also had a role in driving the reshaping of the flat septum, we incubated COL and COLΔ*sle1* in buffer containing saturating NaCl concentration. The decreased turgor pressure led to higher frequency of "D" shaped or asymmetric cells both in COLΔ*sle1* and in parental strain COL, albeit to lower levels in the parental strain (Fig. 8d). Strain COLΔ*sle1* complemented with a plasmid-encoded Sle1 behaved as the parental strain COL (Fig. 10). These results suggest that the division septum requires the action of both autolytic enzymes and turgor pressure to change from a flat to a curved surface, although we cannot exclude the possibility that the effect of NaCl is due to an impact on the activity of autolysins.

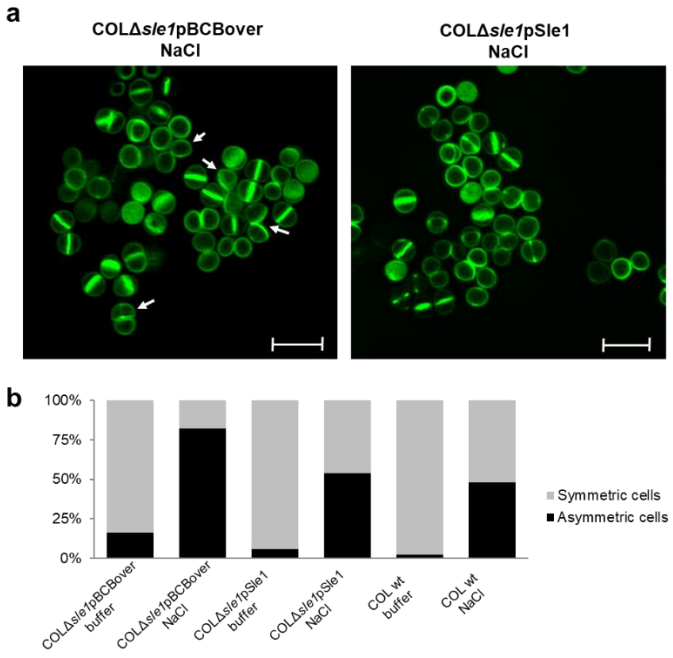

Figure 10. Complementation of COLΔ*sle1* with plasmid-encoded *sle1.* (a) Cells of COLΔ*sle1* strain were transformed with empty vector pBCBover (left) or the same vector encoding *sle1* under the control of IPTG inducible P_{spac} promoter (right) were labelled with NADA, incubated for 15 min in saturating concentration of NaCl, placed on an agarose pad containing the same salt concentration and imaged by SIM. Asymmetric cells with a shape close to a "D" (white arrows) were observed in higher frequency in the strain containing the empty vector. Scale bars = 2 µm. **(b)** Symmetry of cells depicted in panel "a" was assessed as described in Fig 8d, showing that the phenotype of strain COLΔ*sle1* is complemented by the expression of Sle1 from a plasmid.

Discussion

Despite its importance as a clinical pathogen, the small size of *S. aureus* cells has impaired a detailed analysis of the morphological changes occurring during its cell cycle, given that size variations required to double the cell volume are close to the limit of resolution of conventional optical microscopy: *S. aureus* cells are approximately 1 µm in diameter (or 0.52 μm^3 in volume). Approximating the cell shape to a sphere, an increase of the diameter to 1.26 µm is sufficient to double cell volume. However, this 260 nm increase is close to the diffraction limit of resolution of conventional optical microscopy, which is ~250 nm for most biocompatible fluorophores[30,31].

The current model for *S. aureus* cell division postulates that cells do not significantly enlarge during the cell cycle and that the major variation in cell volume occurs upon splitting of the mother cell, when the flat septum is reshaped into a curved surface to generate one hemisphere of each daughter cell. This model was based on the fact that both incorporation of new peptidoglycan material and localisation of the major peptidoglycan synthesis enzymes, the PBPs, occurred mostly at the septum[5,22,33,34,36], two observations that still hold true. However, here, by fast imaging of dividing *S. aureus* cells, we show that reshaping of the division septum is an extremely rapid process, on the timescale of less than two milliseconds, and therefore not compatible with a duplication of cellular volume and the consequent abrupt changes in concentrations of cellular contents. It is therefore more likely that, similar to other bacteria, the volume of *S. aureus* cells gradually increases over the cell cycle, but these size variations are too small to be observable by conventional light microscopy.

Recent advances in fluorescence microscopy, specifically the introduction of super-resolution techniques, now allow an unprecedented level of detail in the analysis of bacterial cell morphology. Making use of SIM, with a lateral resolution of approximately 110 nm[32], we measured variations of the volume of *S. aureus* cells and concluded that (i) cell volume increases gradually over the entire cell cycle and (ii) there is no substantial increase in cell volume due to reshaping of the flat septum, given that upon splitting of a mother cell, each newly generated daughter cell has approximately half of the mother cell´s volume. Furthermore, and contrary to previous assumptions, the cell wall material resulting from the division septum of the mother cell (new cell wall) does not constitute half of the cell surface of each daughter cell, but approximately 33% (Fig. 11). Taken together, these observations suggest that other mechanisms besides septum reshaping are responsible for cell growth in *S. aureus.*

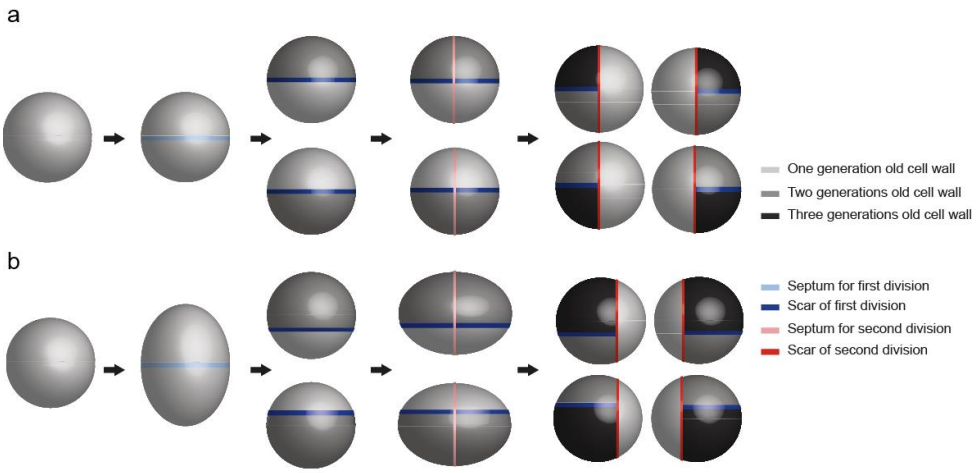

Figure 11. Comparison of two models for *S. aureus* growth and division. (**a**) Previous model which assumed that *S. aureus* cells remained approximately spherical over the cell cycle and that, on division, the cell wall material from the septum of the mother cell increased in cell surface area to constitute half (one hemisphere made of new cell wall) of the cell surface of each daughter cell. As a consequence, scars of previous divisions divided the cell in quadrants and formed T-junctions at the cell poles, which could be used as topological cues to direct cellular processes such as chromosome segregation. These scars were proposed to encode epigenetic information that could be used by *S. aureus* to determine orthogonal placement of division septum. (**b**) In the model proposed based on this work, *S. aureus* cells are approximately spherical at the beginning of the cell cycle and elongate as the cell cycle progresses. On division, there is no increase in the surface area of the previous septum, which becomes ~33% of the surface area of each daughter cell. This asymmetry in the regions composed of new and old cell wall results in scars of previous divisions that do not divide cells in quadrants. Consequently, T-junctions of scars of two previous divisions are not located at the cell poles. Two consecutive divisions in orthogonal planes are depicted in panels (**a**,**b**).

Upon division of the mother cell, *S. aureus* cells could grow by (i) remodelling and enlarging only the new cell wall material or (ii) remodelling the entire cell surface. In the first case, the surface area corresponding to new cell wall material would be expected to expand from 33% and eventually constitute half of the cell surface, while in the second case the 33/67 ratio of new/old cell wall would be maintained during the entire cell cycle. We have labelled peripheral cell wall with a lectin (WGA-488) as well as a fluorescent derivative of D-alanine (HADA) and confirmed that the latter hypothesis is correct.

Cell enlargement can occur by synthesis of new peptidoglycan material, autolysis of old peptidoglycan or a combination of both processes. The fact that the entire cell surface is enlarged during growth, but different sections of the surface vary in age, seems incompatible with the notion that peptidoglycan synthesis or autolysis alone are responsible for the increase in cell surface. If that were the case, then regions with different ages of the cell wall would have different thickness and/or porosity. By transmission electron microscopy, *S. aureus* peripheral cell wall seems homogeneous in thickness[40]. The porosity of new and old cell wall may be different, as the former shows a series of concentric rings while the latter appears as a network of fibers with a large number of empty spaces between them, perhaps resulting from autolytic activity[28,41]. However, if this autolytic activity would occur across the entire cell surface multiple times, *i.e.*, over several generations, in the absence of peptidoglycan synthesis, holes in older regions of the cell surface would presumably become larger, possibly endangering the integrity of the cell.

It therefore seems likely that peptidoglycan synthesis has to occur across the cell surface, concomitantly with autolysis. In fact, we were able to detect peripheral PBP activity through the incorporation of

fluorescent derivatives of 3-amino-D-alanine[24], mediated mostly by PBP4, in agreement with recent data by Gautam *et al*.[42]. It is possible that other PBPs also have a role in peripheral peptidoglycan synthesis, which is not detected in our assay given that PBP4 is the main responsible for incorporation of exogenous peptidoglycan synthesis probes[42,43]. It is important to note that these probes may be incorporated by PBPs in an exchange reaction that occurs outside the cell, and therefore do not necessarily reflect the sites of incorporation of lipid-linked peptidoglycan precursors. It is possible that PBP4 activity is required, not (only) to incorporate new peptidoglycan precursor molecules, therefore increasing the amount of peptidoglycan material in the cell wall, but also to make new bonds in pre-existing material that was subjected to autolytic activity during cell expansion leading to an increased mechanical strength. In fact PBP4 was shown to be responsible for the very high levels of peptidoglycan crosslinking characteristic of *S. aureus*[12,44] and required to increase the stiffness of the cell envelope[13].

Finally, we have also pondered over the question of the extremely fast process of septum reshaping into a curved hemisphere, namely if it was a purely mechanical process or if it required enzymatic activity. Previous reports using atomic force microscopy (AFM) imaging have shown the presence of perforation holes around the bacterial circumference coincident with the outer edge of the division septum. These holes become larger, merge and form longer nicks in the peripheral wall as splitting of the septum proceeds[41]. These holes are most likely the result of activity of autolysins such as Atl, a protein required for cell separation, which localizes in rings at the division site[8,9]. Interestingly, Atl localizes exclusively at the external edge of the septum, not across the entire septal surface[9], suggesting that its

activity is only required at the initial steps of splitting. This would be in agreement with the suggestion by Matias and Beveridge that the septum of *S. aureus* has a middle zone that separates two adjacent septal cross walls[45]. Once the outer edge of the septum is cleaved by autolysins, cell separation could proceed through a merely mechanical process driven by turgor pressure on the two separate halves of the cross-wall, as no additional cleavage of peptidoglycan bonds would be required across the septum. The time required for splitting, which we have now shown to occur in less than two milliseconds, does indeed suggest a mechanical process, probably driven by turgor pressure, in agreement with our data showing that septum reshaping is impaired in high osmolarity conditions and with recent data published while this manuscript was under revision[46]. However, we have also shown that autolysins such as Sle1 and LytM have a role in reshaping of the flat septum, given that mutants lacking one of these proteins, particularly when exposed to medium with high osmolarity, generate daughter cells in which the previous septum remains flatter. Nevertheless, we cannot determine if Sle1 and LytM activities occur before or during splitting. Interestingly, Bailey and colleagues have recently shown that the new cell wall material in the flat septum is stiffer than the rest of the cell wall and becomes softer when fully expanded into a hemisphere[47]. Therefore, these authors suggest that reshaping of the flat septum cannot occur only through stretching (as this would require the flat septum to be thicker but softer than the rest of the cell wall), but instead requires partial degradation of the peptidoglycan by autolytic enzymes[47].

The increase in resolution resulting from advances in superresolution microscopy has allowed us to completely redefine the cell cycle of *S. aureus*, one of the most relevant bacterial pathogens,

with important implications for current models of cell division in cocci. *S. aureus* cells divide in three orthogonal planes over three consecutive division cycles[1,2], raising the question of how do the cells retain "memory" of the two previous planes of division, in order to define a third, perpendicular, division plane. Scars of previous divisions have been proposed to contain epigenetic information regarding the previous planes of division[3]. Junctions of these scars at the cell poles could be used as topological cues to drive chromosome segregation in an axis perpendicular to the next division plane[48]. The process of nucleoid occlusion, which prevents assembly of the divisome over the chromosome, would then restrict the localisation of the next division plane to a plane orthogonal to the two previous ones[48]. However, these models assume that scars of previous division planes are placed precisely at the center of the cell (similar to the equator or meridians of earth, Fig. 11a), and therefore cross each other at poles of the cells. Our observation that lines dividing the *S. aureus* cell surface containing old/new cell wall material do not divide the cell in two equal parts (Fig. 11b), reopens the question of how staphylococci divide in orthogonal planes. Our findings may also be extended to other cocci which divide in orthogonal planes, such as *Sporosarcina*, and thus our observations described for *S. aureus* should have implications for the global understanding of cell division in other coccal bacteria.

References

1. Tzagoloff H, Novick R. Geometry of cell division in *Staphylococcus aureus*. *J Bacteriol*. 1977; 129(1): 343-350. doi:10.1128/jb.129.1.343-350.1977

2. Pinho MG, Kjos M, Veening JW. How to get (a)round: Mechanisms controlling growth and division of coccoid bacteria. *Nat Rev Microbiol*. 2013; 11: 601–614 doi:10.1038/nrmicro3088

3. Turner RD, Ratcliffe EC, Wheeler R, Golestanian R, Hobbs JK, Foster SJ. Peptidoglycan architecture can specify division planes in *Staphylococcus aureus*. *Nat Commun*. 2010; 1, 26. doi:10.1038/ncomms1025

4. Scheffers D-J, Pinho MG. Bacterial cell wall synthesis: New insights from localization studies. *Microbiol Mol Biol Rev*. 2005; 69(4): 585-607. doi:10.1128/mmbr.69.4.585-607.2005

5. Pinho MG, Errington J. Dispersed mode of *Staphylococcus aureus* cell wall synthesis in the absence of the division machinery. *Mol Microbiol*. 2003;50(3):871-881. doi:10.1046/j.1365-2958.2003.03719.x

6. Seligman SJ, Pincus MR. A model for the three-dimensional structure of peptidoglycan in staphylococci. *J Theor Biol*. 1987;124(3):275-292. doi:10.1016/S0022-5193(87)80116-9

7. Oshida T, Sugai M, Komatsuzawa H, Hong YM, Suginaka H, Tomasz A. A *Staphylococcus aureus* autolysin that has an N-acetylmuramoyl-L-alanine amidase domain and an endo-β-N-acetylglucosaminidase domain: Cloning, sequence analysis,

and characterization. *Proc Natl Acad Sci U S A*. 1995;92(1):285-289. doi:10.1073/pnas.92.1.285

8. Sugai M, Komatsuzawa H, Akiyama T, et al. Identification of endo-β-N-acetylglucosaminidase and N-acetylmuramyl-L-alanine amidase as cluster-dispersing enzymes in *Staphylococcus aureus*. *J Bacteriol*. 1995;177(6):1491-1496. doi:10.1128/jb.177.6.1491-1496.1995

9. Yamada S, Sugai M, Komatsuzawa H, et al. An autolysin ring associated with cell separation of *Staphylococcus aureus*. *J Bacteriol*. 1996; 178(6): 1565-1571. doi:10.1128/jb.178.6.1565-1571.1996

10. Monk IR, Shah IM, Xu M, Tan MW, Foster TJ. Transforming the untransformable: Application of direct transformation to manipulate genetically *Staphylococcus aureus* and Staphylococcus epidermidis. *MBio*. 2012;3(2). doi:10.1128/mBio.00277-11

11. Gill SR, Fouts DE, Archer GL, et al. Insights on evolution of virulence and resistance from the complete genome analysis of an early methicillin-resistant *Staphylococcus aureus* strain and a biofilm-producing methicillin-resistant *Staphylococcus epidermidis* strain. *J Bacteriol*. 2005;187(7):2426-2438. doi:10.1128/JB.187.7.2426-2438.2005

12. Memmi G, Filipe SR, Pinho MG, Fu Z, Cheung A. *Staphylococcus aureus* PBP4 is essential for β-lactam resistance in community-acquired methicillin-resistant strains. *Antimicrob Agents Chemother*. 2008;52(11):3955-3966. doi:10.1128/AAC.00049-08

13. Loskill P, Pereira PM, Jung P, et al. Reduction of the peptidoglycan crosslinking causes a decrease in stiffness of the *Staphylococcus aureus* cell envelope. *Biophys J*. 2014;107(5):1082-1089. doi:10.1016/j.bpj.2014.07.029

14. Zhang L, Higgins ML, Piggot PJ. The division during bacterial sporulation is symmetrically located in *Sporosarcina ureae*. *Mol Microbiol*. 1997;25(6):1091-1098. doi:10.1046/j.1365-2958.1997.5341892.x

15. Arnaud M, Chastanet A, Débarbouillé M. New vector for efficient allelic replacement in naturally nontransformable, low-GC-content, gram-positive bacteria. *Appl Environ Microbiol*. 2004;70(11):6887-6891. doi:10.1128/AEM.70.11.6887-6891.2004

16. Vagner V, Dervyn E, Ehrlich SD. A vector for systematic gene inactivation in *Bacillus subtilis*. *Microbiology*. 1998;144(11):3097-3104. doi:10.1099/00221287-144-11-3097

17. Charpentier E, Anton AI, Barry P, Alfonso B, Fang Y, Novick RP. Novel cassette-based shuttle vector system for gram-positive bacteria. *Appl Environ Microbiol*. 2004;70(10):6076-6085. doi:10.1128/AEM.70.10.6076-6085.2004

18. Wu S, De Lencastre H, Sali A, Tomasz A. A phosphoglucomutase-like gene essential for the optimal expression of methicillin resistance in *Staphylococcus aureus*: Molecular cloning and DNA sequencing. *Microb Drug Resist*. 1996;2(2):277-286. doi:10.1089/mdr.1996.2.277

19. Henner DJ. Inducible expression of regulatory genes in *Bacillus subtilis*. *Methods Enzymol*. 1990;185(C):223-228.

doi:10.1016/0076-6879(90)85022-G

20. Subach F V, Patterson GH, Manley S, Gillette JM, Lippincott-Schwartz J, Verkhusha V V. Photoactivatable mCherry for high-resolution two-color fluorescence microscopy. *Nat Methods*. 2009;6(2):153-159. doi:10.1038/nmeth.1298

21. Atilano ML, Pereira PM, Vaz F, et al. Bacterial autolysins trim cell surface peptidoglycan to prevent detection by the drosophila innate immune system. *Elife*. 2014;3:e02277. doi:10.7554/eLife.02277

22. Pereira PM, Veiga H, Jorge AM, Pinho MG. Fluorescent reporters for studies of cellular localization of proteins in *Staphylococcus aureus*. *Appl Environ Microbiol*. 2010;76(13):4346-4353. doi:10.1128/AEM.00359-10

23. Heintzmann R, Cremer CG. Laterally modulated excitation microscopy: Improvement of resolution by using a diffraction grating Super-resolution localisation microscopy of the nuclear architecture and chromatin structure View project Scientific Camera Calibration View project. In: *Optical Biopsies and Microscopic Techniques III*. 1999; 3568:185-196. doi:10.1117/12.336833

24. Kuru E, Hughes HV, Brown PJ, et al. In Situ probing of newly synthesized peptidoglycan in live bacteria with fluorescent D-amino acids. *Angew Chemie Int Ed*. 2012;51(50):12519-12523. doi:10.1002/ANIE.201206749

25. Kuru E, Tekkam S, Hall E, Brun Y V., VanNieuwenhze MS. Synthesis of fluorescent D-amino acids (FDAAs) and their use for probing peptidoglycan synthesis and bacterial growth in

situ. *Nat Protoc*. 2015;10(1):33. doi:10.1038/NPROT.2014.197

26. Xu D, Cui J, Bansal R, et al. The ellipsoidal area ratio: an alternative anisotropy index for diffusion tensor imaging. *Magn Reson Imaging*. 2009;27(3):311-323. doi:10.1016/J.MRI.2008.07.018

27. Pereira PM, Filipe SR, Tomasz A, Pinho MG. Fluorescence ratio imaging microscopy shows decreased access of vancomycin to cell wall synthetic sites in vancomycin-resistant *Staphylococcus aureus*. *Antimicrob Agents Chemother*. 2007;51(10):3627-3633. doi:10.1128/AAC.00431-07

28. Amako K, Umeda A, Murata K. Arrangement of peptidoglycan in the cell wall of *Staphylococcus spp*. *J Bacteriol*. 1982;150(2):844.

29. Amako K, Umeda A. Scanning electron microscopy of *Staphylococcus*. *J Ultrasructure Res*. 1977;58(1):34-40. doi:10.1016/S0022-5320(77)80005-1

30. Abbe E. Beiträge zur Theorie des Mikroskops und der mikroskopischen Wahrnehmung: I. Die Construction von Mikroskopen auf Grund der Theorie. *Arch für mikroskopische Anat*. 1873;9(1):413-418. doi:10.1007/BF02956173

31. Rayleigh, Lord. On the Theory of Optical Images, with special reference to the Microscope. *J R Microsc Soc*. 1903;23(4):474-482. doi:10.1111/j.1365-2818.1903.tb04831.x

32. Schermelleh L, Heintzmann R, Leonhardt H. A guide to super-resolution fluorescence microscopy. *J Cell Biol*. 2010;190(2):165-175. doi:10.1083/jcb.201002018

33. Pinho MG, Errington J. Recruitment of penicillin-binding protein PBP2 to the division site of *Staphylococcus aureus* is dependent on its transpeptidation substrates. *Mol Microbiol*. 2005;55(3):799-807. doi:10.1111/j.1365-2958.2004.04420.x

34. Pereira SFF, Henriques AO, Pinho MG, De Lencastre H, Tomasz A. Role of PBP1 in cell division of *Staphylococcus aureus. J Bacteriol*. 2007;189(9):3525-3531. doi:10.1128/JB.00044-07

35. Pinho MG, Filipe SR, De Lencastre H, Tomasz A. Complementation of the essential peptidoglycan transpeptidase function of penicillin-binding protein 2 (PBP2) by the drug resistance protein PBP2A in *Staphylococcus aureus*. *J Bacteriol*. 2001;183(22):6525-6531. doi:10.1128/JB.183.22.6525-6531.2001

36. Atilano ML, Pereira PM, Yates J, et al. Teichoic acids are temporal and spatial regulators of peptidoglycan cross-linking in *Staphylococcus aureus*. *Proc Natl Acad Sci U S A*. 2010;107(44):18991-18996. doi:10.1073/pnas.1004304107

37. Kajimura J, Fujiwara T, Yamada S, et al. Identification and molecular characterization of an N-acetylmuramyl-L- alanine amidase Sle1 involved in cell separation of *Staphylococcus aureus*. *Mol Microbiol*. 2005;58(4):1087-1101. doi:10.1111/j.1365-2958.2005.04881.x

38. Ramadurai L, Lockwood KJ, Nadakavukaren MJ, Jayaswal RK. Characterization of a chromosomally encoded glycylglycine endopeptidase of *Staphylococcus aureus*. *Microbiology*. 1999;145(4):801-808. doi:10.1099/13500872-145-4-801

39. Dubrac S, Boneca IG, Poupel O, Msadek T. New insights into the WalK/WalR (YycG/YycF) essential signal transduction pathway reveal a major role in controlling cell wall metabolism and biofilm formation in *Staphylococcus aureus*. *J Bacteriol*. 2007;189(22):8257-8269. doi:10.1128/JB.00645-07

40. Giesbrecht P, Kersten T, Maidhof H, Wecke J. Staphylococcal cell wall: Morphogenesis and fatal variations in the presence of penicillin. *Microbiol Mol Biol Rev*. 1998;62(4):1371-1414. doi:10.1128/mmbr.62.4.1371-1414.1998

41. Touhami A, Jericho MH, Beveridge TJ. Atomic force microscopy of cell growth and division in *Staphylococcus aureus*. *J Bacteriol*. 2004;186(11):3286-3295. doi:10.1128/JB.186.11.3286-3295.2004

42. Gautam S, Kim T, Spiegel DA. Chemical Probes Reveal an Extraseptal Mode of Cross-Linking in *Staphylococcus aureus*. *J Am Chem Soc*. 2015;137(23):7441-7447. doi:10.1021/jacs.5b02972

43. Qiao Y, Lebar MD, Schirner K, et al. Detection of lipid-linked peptidoglycan precursors by exploiting an unexpected transpeptidase reaction. *J Am Chem Soc*. 2014;136(42):14678-14681. doi:10.1021/ja508147s

44. Łęski TA, Tomasz A. Role of penicillin-binding protein 2 (PBP2) in the antibiotic susceptibility and cell wall cross-linking of *Staphylococcus aureus*: Evidence for the cooperative functioning of PBP2, PBP4, and PBP2A. *J Bacteriol*. 2005;187(5):1815-1824. doi:10.1128/JB.187.5.1815-1824.2005

45. Matias VRF, Beveridge TJ. Native cell wall organization shown by cryo-electron microscopy confirms the existence of a periplasmic space in *Staphylococcus aureus*. *J Bacteriol*. 2006; 188(3):1011-1021. doi:10.1128/JB.188.3.1011-1021.2006

46. Zhou X, Halladin DK, Rojas ER, et al. Mechanical crack propagation drives millisecond daughter cell separation in *Staphylococcus aureus*. *Science* 2015; 348(6234):574-578. doi:10.1126/science.aaa1511

47. Bailey RG, Turner RD, Mullin N, Clarke N, Foster SJ, Hobbs JK. The interplay between cell wall mechanical properties and the cell cycle in *Staphylococcus aureus*. *Biophys J*. 2014;107(11):2538-2545. doi:10.1016/j.bpj.2014.10.036

48. Veiga H, Jorge AM, Pinho MG. Absence of nucleoid occlusion effector Noc impairs formation of orthogonal FtsZ rings during *Staphylococcus aureus* cell division. *Mol Microbiol*. 2011; 80(5): 1366-1380. doi:10.1111/j.1365-2958.2011.07651.x

Chapter III

Preliminary studies on variability of *vraTSR* expression in *Staphylococcus aureus* cells exposed to cell wall targeting antibiotics

Chapter contents

Abstract 132
Introduction 133
Experimental Procedures 136
Bacterial growth conditions 136
Construction of COL Pvra-sGFP strain 136
Fluorescence microscopy 137
Mechanical compression of *S. aureus* 138
Time-Lapse Microfluidic Microscopy 139
Statistical Analysis 139
Results and Discussion 140
vraTSR expression is heterogeneous 140
VraTSR is triggered in cells growing in microfluidic plates 141
Higher *vraTSR* expression levels do not lead to higher tolerance to CW targeting antibiotics 151
Final Remarks 155
References 156

Author contributions

P.B. Fernandes performed all experiments shown, except statistical analysis, which was performed by V. de Bakker.

Acknowledgments

We thank Professor Sean Sun, from Johns Hopkins University, for providing the mechanical compression device.

Abstract

Staphylococcus aureus is a Gram-positive pathogen known for its antibiotic resistance, especially to antibiotics that target the cell wall. One strategy used by this pathogen to respond to this group of antibiotics is mediated by VraTSR. This three-component regulatory system is activated whenever damage is inflicted onto the cell wall and transduces the signal to the inside of the cell, regulating the expression of several genes, including of the *vraTSR* operon itself. Here we show that, after antibiotic challenge, expression of *vraTSR* is variable within an isogenic population and cells expressing higher *vraTSR* levels appear to be more susceptible to antibiotic treatment.

Introduction

Antibiotic resistance has become a challenge worldwide, with the emergence of several multi-drug resistant bacteria[1,2]. As a result, we may enter a post-antibiotic era, where bacterial infections might no longer be treated successfully[3]. One remarkable example of antibiotic resistant bacteria is the Gram-positive pathogen *Staphylococcus aureus*. This microorganism became one of the most important pathogens responsible for infections in nosocomial environments, having subsequently spread to the community, worldwide[4]. The mechanism underlying antibiotic resistance in *S. aureus* involves the expression of an exogenous transpeptidase called PBP2A, an enzyme that can catalyse cell wall crosslinking in the presence of β-lactam antibiotics[5], which inhibit native transpeptidases. However, the ability to overcome antibiotic treatment is not restricted to acquired genetic determinants[6]. Antibiotic treatment failure can be due to antibiotic resistance, antibiotic tolerance or antibiotic persistence. Antibiotic resistance can be defined as the ability to grow in the presence of an antimicrobial compound, and can be measured by the minimum inhibitory concentration (MIC), that corresponds to the lowest concentration of the antibiotic required to prevent visible bacterial growth[7]. Resistance determinants are typically acquired via horizontal gene transfer of resistance-encoding genes, like *mecA* gene encoding PBP2A in *S. aureus*, or through mutations. Antibiotic tolerance and persistence are both mechanisms where bacteria can transiently survive in the presence of an antibiotic without an increase in the MIC. However, while tolerance refers to the capacity of the overall population to temporarily withstand the

effects of antibiotic treatment, persistence affects only a subpopulation of cells[7]. Tolerance factors, which can be environmental or genetic, increase the minimum time it takes to kill a bacterial population[7,8]. Persistence has the same effect, but only for a subset of the population. In this sense, persistence can be regarded as a particular case of tolerance, where most of the bacterial population is rapidly killed by the antibiotic while a smaller subpopulation is able to survive for a longer time[7,8]. Thus persistence is characterized by a biphasic killing curve[7]. Persistent cells represent a subset of the population that enters a dormant, non-dividing state[9]. When a population is treated with an antibiotic, normally dividing cells die, while persisters are able to survive[9]. These dormant variants are able to grow once the antibiotic is removed, being responsible for recalcitrance in chronic infections[9]. The concept of persistence is based on the heterogeneity of the response to antibiotics in a population. This heterogeneous behaviour in an isogenic bacterial population is referred to as phenotypic variability[10] and may provide fitness advantages in fluctuating environments, such as during an antibiotic treatment, when compared to an homogenous population[11]. The source of such behaviour has been attributed to several factors, including cell cycle stage, cell ageing, stochasticity in genetic expression and the metabolic state of the cells[12,13,14,15]. In *Escherichia coli*, a positive correlation was observed between the frequency of persisters in a population and the likelihood to evolve resistance against different antibiotic classes[16,17].

Antibiotics have a large spectrum of targets including blocking DNA replication and repair, protein synthesis, membrane integrity or cell wall (CW) biosynthesis[18,19]. To overcome antibiotic action,

bacterial cells trigger specific responses, often coordinated by protein complexes known as Two-component (TCS) or Three-component systems. In *S. aureus*, when CW biosynthesis is impaired, cells trigger a response that results in the coordinated modulation of expression of the so-called CW stress stimulon (CWSS), a group of more than one hundred genes from different functional categories[20,21,22]. Several genes from the CWSS are directly activated by a TCS (currently described as three-component system), VraTSR[23]. VraTSR is encoded in an operon comprised of four non-essential genes *vraU*, *vraT*, *vraS* and *vraR*[23]. Despite being non-essential for cell viability, these genes were shown to be important for resistance against CW targeting antibiotics[23,24,25]. The function of *vraU* remains unknown, while *vraT* encodes the membrane protein VraT, the hypothetical sensor of VraTSR, that upon detecting a still elusive CW damage signal, is proposed to undergo a conformational change which would promote the autophosphorylation of the histidine kinase VraS[23]. VraS then transfers the phosphoryl group to its cognate response regulator VraR[23], which subsequently activates the expression of several genes, including genes encoding proteins involved in CW synthesis, like *pbpB* or *mgt*, as well as its own promoter[21,23].

In this chapter, we describe that the expression of *vraTSR* varies from cell to cell, within an isogenic population and that, surprisingly, cells that highly express *vraTSR*, seem to be more susceptible to antibiotic treatment than the cells that maintain lower expression levels.

Experimental Procedures

Bacterial growth conditions

Strains and plasmids used in this study are listed in Table 1. *S. aureus* strains were grown in tryptic soy broth (TSB, Difco) with aeration at 37 °C or on tryptic soy agar (TSA, Difco) at 37 °C. For microscopy experiments, overnight cultures of *S. aureus* strains were diluted 1:200 in fresh TSB medium and allowed to grow at 37 °C until an $OD_{600\ nm}$ of approximately 0.5. Cells were then harvested and resuspended in the same medium. *E. coli* strains were grown in Luria-Bertani broth (LB, Difco) with aeration, or LB agar (LA, Difco) at 30 °C. Culture medium was supplemented with appropriate antibiotics (100 μg mL^{-1} ampicillin, 10 μg mL^{-1} erythromycin).

Construction of COL Pvra-sGFP strain

To construct the *vraTSR* promoter fusion, an 814 bp DNA fragment containing the *vraTSR* promoter region was amplified from COL genomic DNA using the primers PvraSR_P1_KpnI (gctgcggtacccggtgctatttctgcgcc) and PvraSR_P2_New_XhoI (cgcgctcgagttataataagttttaaaataccaaatgcgc), digested with KpnI and XhoI, and cloned into KpnI/XhoI digested pFAST3, upstream of sfgfp-p7, resulting in plasmid pPvra-pFAST3, confirmed by DNA sequencing. pPvrap-FAST3 was electroporated into the *S. aureus* RN4220 strain and integrated into the chromosome at the *vraTSR* promoter site by homologous recombination, as confirmed by PCR and sequencing; the resulting strain was named RN Pvra-sGFP. Strain COL Pvra-sGFP was constructed by transducing the

integrated plasmid pPvra-pFAST3 from RN Pvra-sGFP into COL using phage 80α, as previously described[26].

Table 1. Plasmids and strains used in this study

Plasmids and Strains	Description	Source or reference
Plasmids		
pFAST3-Pvra	*S. aureus* integrative vector with *vraTSR* promoter upstream of sfgfp-p7	This work
Strains		
DC10B	*Δdcm* in DH10B background; Dam methylation only; for cloning	[27]
RN4220	Restriction-negative derivative of NCTC8325-4	[28]
COL	HA-MRSA strain	[29]
COL Pvra-sGFP	COL with pFAST3-Pvra; Ery^R	This work

Fluorescence microscopy

Overnight cultures of COL Pvra-sGFP were re-inoculated 1:200 in TSB and grown until $OD_{600\ nm}$ ~0.4. The *vraTSR* promoter was induced by incubating the cells with sub-MIC concentrations of oxacillin (200 µg mL^{-1}) for 120 min or with sub-MIC concentrations of the MurJ inhibitor 2-(2-Chlorophenyl)-3-[1-(2,3-dimethylbenzyl)piperidin-4-yl]-5-fluoro-1H-indole CDFI (0.5 µg mL^{-1})[30]. For the timelapse experiments, cells were then placed on a 1.2% agarose pad containing phosphate-buffered saline (NaCl 137 mM, KCl 2.7 mM, Na_2HPO_4 10 mM, KH_2PO_4 1.8 mM) and SSM9PR minimal media[31] containing 1 x M9 salts (Na_2HPO_4 12.8 g L^{-1}, KH_2PO_4 3 g L^{-1}, NaCl 5 g L^{-1}, NH_4Cl 1 g L^{-1}), $MgSO_4$ 2 mM, $CaCl_2$ 0.1 mM, glucose 1%, casaminoacids 1%, Thiamine-HCl 1 mM and nicotinamide 0.05 mM. The agarose pads were supplemented with

2 mg mL^{-1} (4x MIC of oxacillin) and propidium iodide (2 µg mL^{-1}). To measure cytoplasm fluorescence in two different strains on the same microscopy slide, one strain was labelled with DNA dye Hoechst 33342, both cultures were washed with TSB, and then the two cultures were mixed prior to visualization by epifluorescence microscopy. Fluorescence imaging was performed with a Zeiss Axio Observer Z1 microscope, HXP 120 V Illuminator (Zeiss) and Photometrics CoolSNAP HQ camera (Roper Scientific, Inc.), using a Plan-Apochromat 100x/1.40 oil immersion M27 objective, Numerical aperture 0.55 and ZEN 2 (blue edition) software was employed. Phase-contrast images were acquired with 100 ms exposure time; GFP was imaged using the eGFP filter (excitation/emission wavelengths 488/509 nm) with 1500 ms exposure time; PI was imaged using the Texas Red filter (excitation/emission wavelengths 592/614 nm) with 100 ms exposure time. Images were acquired every 15 min, for a total of 255 min.

Mechanical compression of *S. aureus*

Overnight TSB cultures of *S. aureus* strains to be tested were diluted 1:200 with fresh TSB and grown at 37 °C to exponential growth phase ($OD_{600\ nm}$ of 0.5-0.7). 200 µL of cell culture were transferred to a 3D printed well, whose bottom was opened to the glass microscopy slide. The PDMS compression device was placed on top of the well and mechanical compression was achieved by pressing the top part of the PDMS device with a hexagonal metal nut placed between the device and the microscope condenser.

Time-Lapse Microfluidic Microscopy

Microfluidic experiments were performed using the CellASIC® ONIX Microfluidic Platform and B04A microfluidic plates for bacterial cells (Merck-Millipore). Prior to each experiment, wells, channels, and chambers of microfluidic plates were washed with TSB, using 8 psi for 10 min. Exponential growing cultures ($OD_{600\ nm}$ ~0.4) were loaded into the microfluidic chamber according to manufacturer's instructions. Microscope objective was kept at 37 ºC during the timelapse. Epifluorescence microscopy images were acquired every 20 min for 180 min. Phase-contrast images were acquired with 100 ms exposure time; GFP was imaged using the eGFP filter (excitation/emission wavelengths 488/509 nm) with 1500 ms exposure time.

Statistical Analysis

Survival analyses were done using the R (version 4.1.2) package survival (version 3.2.13). A Cox Proportional Hazards model was used to analyse survival of individual bacterial cells, allowing for the use of a continuous explanatory variable, here median fluorescence, and can account for slide-specific effects using the cluster argument of the coxph() R function. The assumption of proportional hazards was tested with the cox.zph() function, and met.

Results and Discussion

vraTSR expression is heterogeneous

To monitor the expression of *vraTSR,* we used a strain where *gfp* was placed under the control of *vraTSR* promoter (COL Pvra-sGFP). In the presence of CW targeting antibiotics, *vraTSR* expression is upregulated[22]. Interestingly, when we incubated COL Pvra-sGFP cells with sub-MIC concentrations (0.5 µg mL^{-1}) of the MurJ inhibitor CDFI[30], *vraTSR* expression levels displayed variability at the single cell level, in an isogenic population (Fig. 1), although we never observed two different subpopulations corresponding to a bistable phenotype. Phenotypic heterogeneity has been previously described[10] and may be advantageous for population fitness in fluctuating environments[32]. It is therefore possible that cells expressing higher levels of *vraTSR* could be better adapted for an antibiotic challenge, since these genes revealed to be crucial for CWSS activation and antibiotic resistance[23,25].

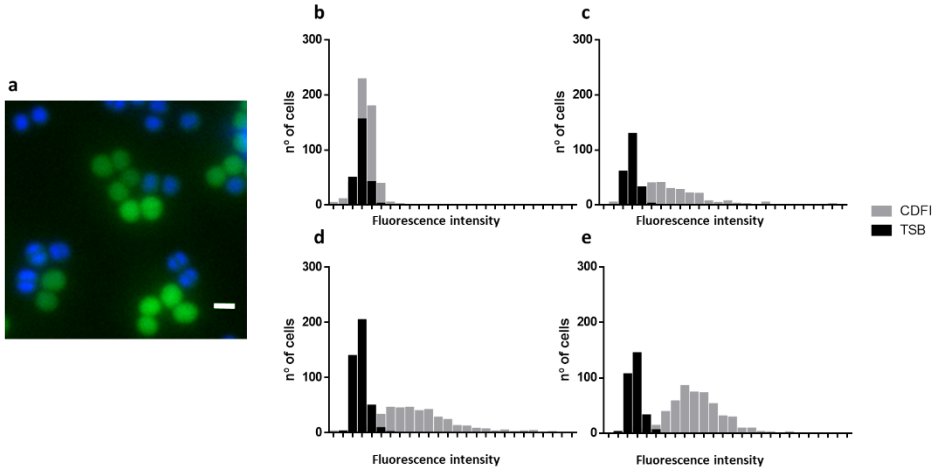

Figure 1. *vraTSR* expression is variable in *S. aureus*. COL Pvra-sGFP cells were incubated with or without 0.5x MIC of CW targeting antibiotic CDFI. **(a)** Cells incubated without antibiotic were then stained with DNA dye Hoechst 33342, to differentiate the two populations, which were mixed prior to imaging on the same slide. In the presence of CDFI, the range of fluorescence levels increases, compared with the control. Scale bar = 1 µm. Different timepoints were acquired **(b)** = t_{0h}, **(c)** = t_{1h}, **(d)** = t_{2h}, **(e)** = t_{3h}. N > 223 cells for each condition.

VraTSR is triggered in cells growing in microfluidic plates

To study the potential relationship between *vraTSR* expression levels and bacterial survival under antibiotic inhibitory conditions, at the single cell level, we used the CellASIC® ONIX Microfluidic Platform (Figure 2). This device allows cell immobilization, while controlling media flow and growth temperature, as well as enabling rapid switching of the growth medium (*e.g.* addition of antibiotics).

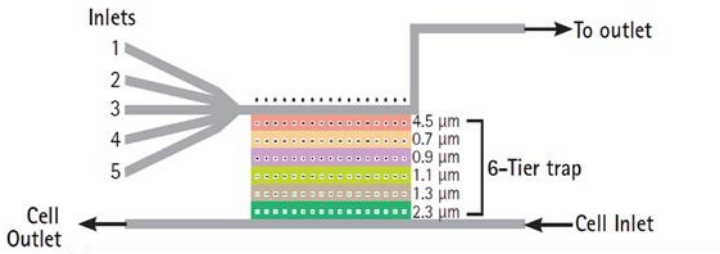

Figure 2. Schematic diagram of the CellASIC® ONIX Microfluidic Platform. The chamber is connected to the inlet channels, where media are injected and to the outlet channel where media are discarded. The chamber presents several sections with varying ceiling heights, where cells are trapped, according to their size. Typically, *S. aureus* cells are immobilized in the 0.9 µm section (adapted from [33])

Surprisingly, when cells were immobilized inside the device chamber, VraTSR system was triggered, albeit to low levels when compared with antibiotic-driven activation, with only TSB flowing through the chamber (Figure 3).

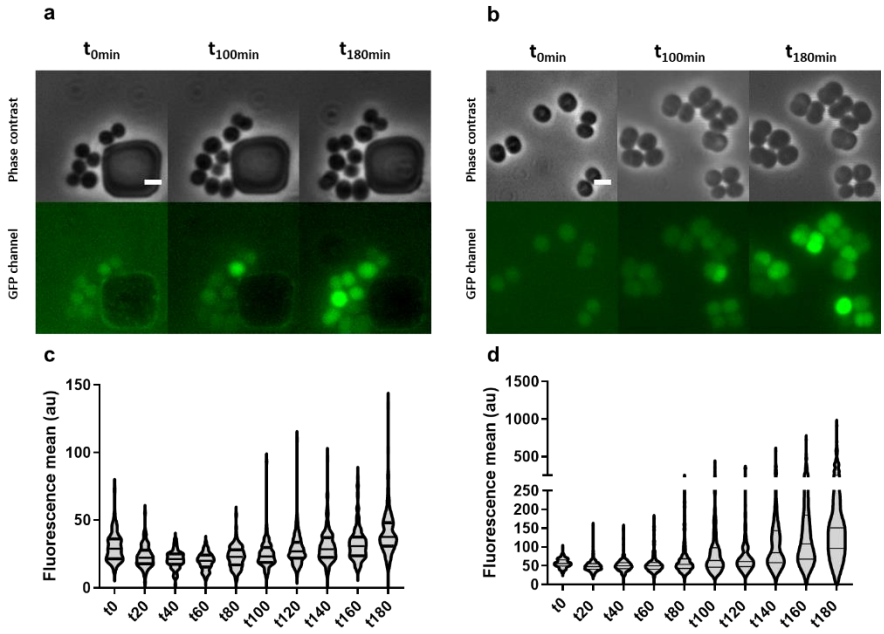

Figure 3. VraTSR is triggered in cells grown in the microfluidic platform. COL Pvra-sGFP cells were imaged by epifluorescence time-lapse microscopy, after being immobilized inside the microfluidic plates. TSB flow was maintained applying a constant pressure of 8 psi. Images were captured at 20 min intervals during 180 min. Images display the same fluorescence range. The images depicted correspond to the condition where no antibiotic was supplemented to the media **(a)** or in the presence of 200 µg mL^{-1} oxacillin **(b)**. Scale bar = 1 µm. **(c)** GFP fluorescence increases during the time-lapse experiment, showing that *vraTSR* levels increase over time, although no CW targeting compound was added to the growth media. N > 86 cells for each timepoint. **(d)** COL Pvra-sGFP cells immobilized inside the microfluidic plates and incubated with 200 µg mL^{-1} of oxacillin show *vraTSR* expression levels increase over time with a greater magnitude compared with the condition in which no antibiotic was added. N>196 cells for each timepoint.

Given that no CW targeting compound was added to the growth media, we wondered what was inducing stress to the CW, namely if it could be fluid shear stress exerted by the moving fluid. Fluid circulation inside microfluidics systems was already described to cause shear stress[34]. The resulting mechanical stress has numerous biological responses, like change of bacterial cell morphology[35]. Moreover, above a certain threshold value, shear stress can decrease bacterial viability[36]. To address whether shear stress could be playing a role in triggering VraTSR, we imaged positions inside the 0.9 µm section, where the cells are usually trapped inside microfluidics chamber, in which cells were either behind the platform structural columns or directly facing the flow (Fig. 4).

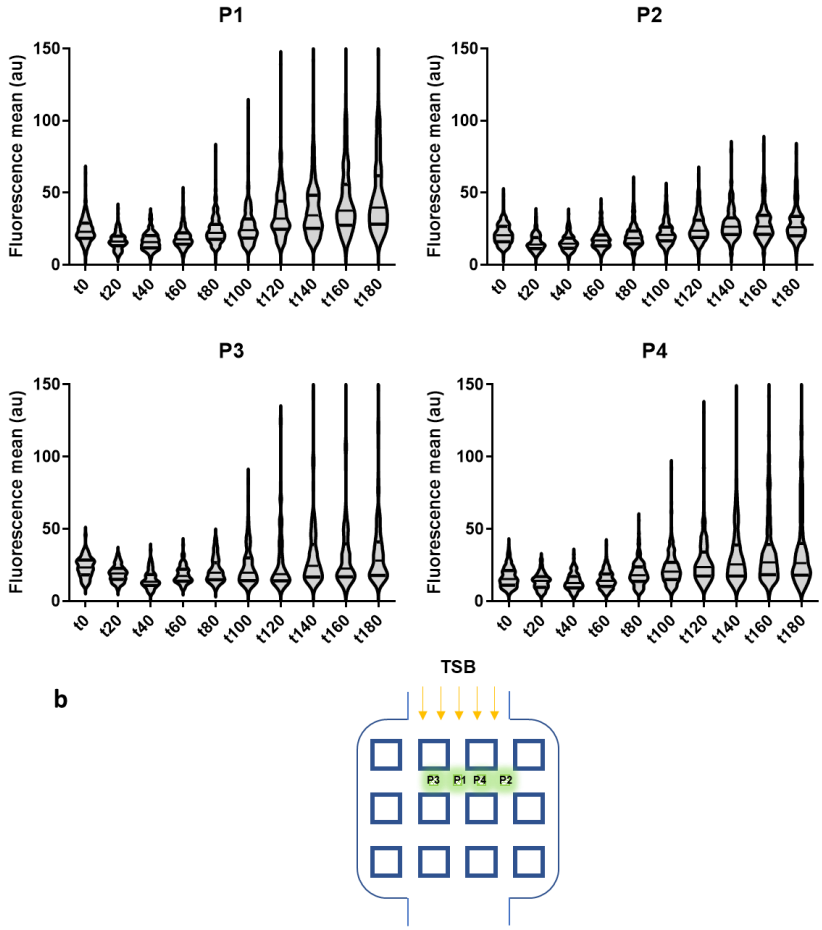

Figure 4. VraTSR activation is position independent. (a) Cells in different positions in the microfluidics chamber were imaged by epifluorescence time-lapse microscopy. Images were captured at 20 min intervals during 180 min. TSB flow was maintained applying a constant pressure of 8 psi. All positions belong to the 0.9 µm section of the chamber. Positions P1 and P2 face the flow directly, while P3 and P4 are regions behind structural columns from the chamber, theoretically protected from the media flow. N > 80 cells for each condition. **(b)** Schematic representation of the microfluidic chamber, with the region where the cells were imaged depicted by the green section. Some positions were facing the TSB flow directly, while others were behind the structural columns, represented by the blue squares.

The pattern of VraTSR activation inside the microfluidic chamber suggested that media flow did not induce *vraTSR*. To further confirm this, we followed the cells inside the microfluidic chamber without media flow *i.e.* no TSB being injected during the whole experiment (Fig. 5).

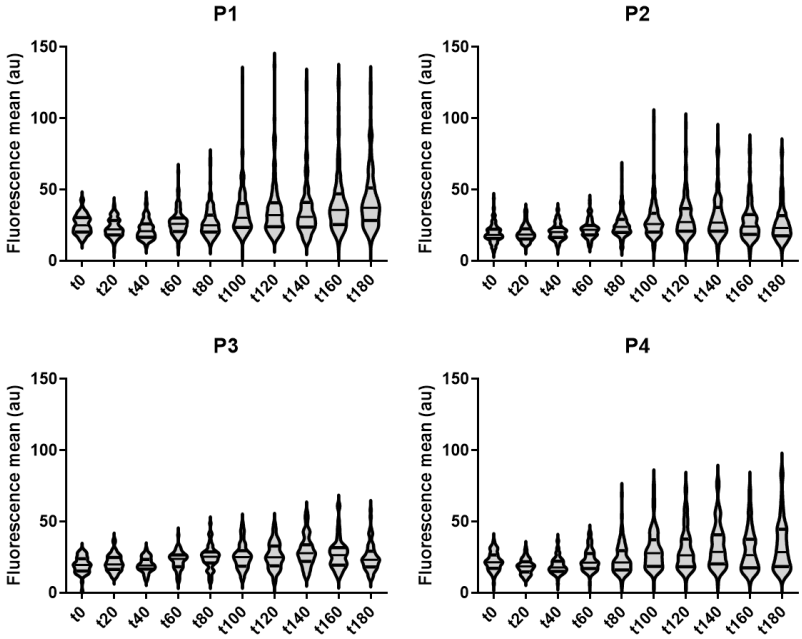

Figure 5. VraTSR is activated without media flowing through the chamber. Cells in different positions in the microfluidics chamber were imaged by epifluorescence time-lapse microscopy. Images were captured at 20 min intervals during 180 min. Growth media injection was stopped after the immobilization of the cells. All positions belong to the 0.9 µm section of the chamber. Positions P1 to P4 are arranged along the horizontal axis of the section. VraTSR activation could be observed in all the monitored positions. N > 50 cells for each condition.

Considering that *vraTSR* was activated in the absence of media flow, we concluded that shear stress was not involved in the mechanism behind VraTSR activation. One alternative hypothesis was that polydimethylsiloxane (PDMS), a polymer that is used to manufacture the microfluidic device, induced the VraTSR system, although it has been described as an non-toxic, biocompatible material[37]. We placed the cells on a PDMS layer and after 120 min no detectable increase in GFP fluorescence could be observed (Fig. 6)

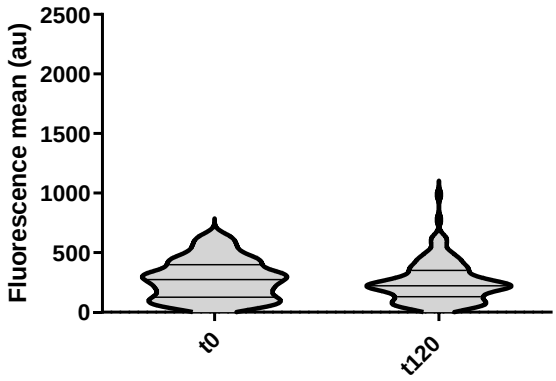

Figure 6. Polydimethylsiloxane (PDMS) does not activate VraTSR system. COL Pvra-sGFP cells were placed on a PDMS slide and followed for 120 min. No detectable fluorescence increase could be observed after the cells were in contact with PDMS. N > 80 cells for each timepoint.

A perhaps more interesting hypothesis is that the physical pressure exerted on the cells when they get trapped by the chamber ceiling, would trigger VraTSR, suggesting a mechano-sensing mechanism behind VraTSR activation. If this was the case, VraTSR regulatory system could respond to fluctuations in the

width of the periplasmic space, triggered by the compression force. VraT and VraS are predicted to be at the membrane and one could conjecture that these proteins may sense variations in the distance between the cell membrane and the CW, by interacting with peptidoglycan or other CW components[23]. To mimic the condition where a physical force is applied on the cells, like what happens inside the microfluidic scaffold (Fig. 7A), we used a PDMS column device developed by the group of Professor Sean Sun, from Johns Hopkins University, that allowed us to exert a constant pressure on the cells, during image acquisition (Fig. 7B). When the cells were compressed by the PDMS device, we could not observe VraTSR activation (Fig.7C). We noted, however, that TSB media was squeezed out of the region immediately below the column, due to the compression force and the compressed cells were not dividing, during the course of the experiment (data not shown). We could not determine whether the lack of growth medium was impairing VraTSR activation, rendering this result inconclusive.

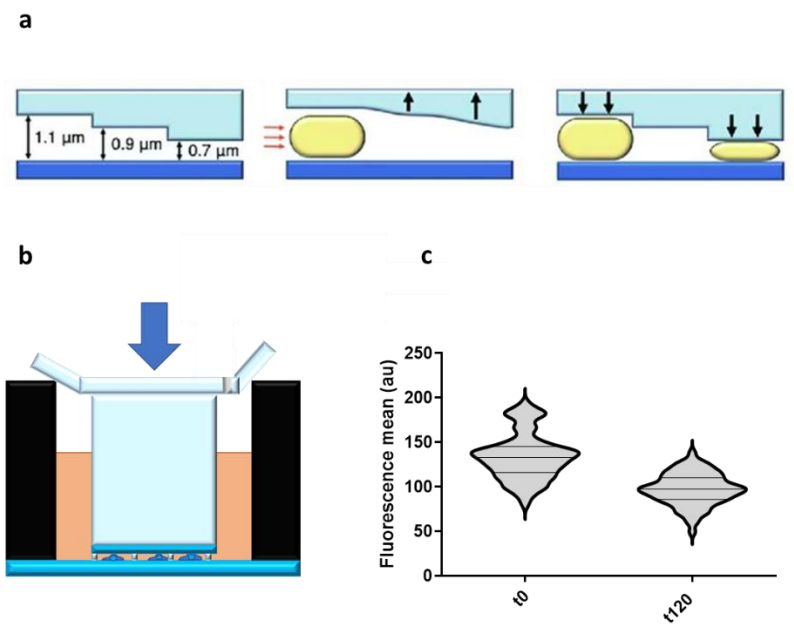

Figure 7. Mechanical compression of *S. aureus* cells did not lead to VraTSR activation. (a) Schematic representation of the trapping mechanism behind cell immobilization in the CellASIC® ONIX Microfluidic Platform (adapted from Chikada T, *et al*, 2021)[38]. **(b)** Schematic representation of the PDMS column device used to compress the cells, during image acquisition by epifluorescence microscopy. A constant mechanical force is applied on the top of the device (see methods), moving the PDMS column (light blue) downwards, thus squeezing the cells between the microscopy slide and the glass on the bottom of the column (blue). During this process, TSB media (depicted in brown) was squeezed out of the imaging region, leaving the cells deprived of nutrients. **(c)** COL Pvra-sGFP cells were compressed on using the device depicted in Figure 7b and followed for 120 min. No GFP fluorescence increase was detected, showing that VraTSR regulatory system was not activated under these conditions. N > 70 cells for each condition.

Despite the results from the compression device being inconclusive, the possibility of VraTSR sensing variations in the

periplasmic space length remained under consideration, since the exposure of *S. aureus* cells to hyperosmotic and hypoosmotic media rendered VraTSR activation (Fig.8). Hyperosmotic shock induces cell plasmolysis, which leads to the cytoplasm losing water as the periplasm gains water[39]. VraTSR system responded to the presence of high concentrations of both sucrose and sorbitol, two compounds known for inducing hyperosmotic shock stress in bacteria[40,41]. On the other hand, a hypoosmotic shock causes the water to flow into the cell thus increasing internal turgor pressure[42]. This flow of water increases the pressure exerted from the cytoplasm on the membrane and peptidoglycan wall[43].

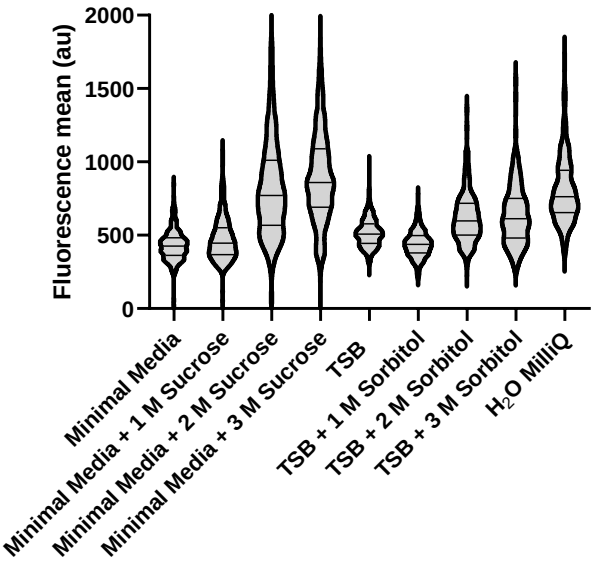

Figure 8. VraTSR responds when *S. aureus* cells experience an osmotic shock. COL Pvra-sGFP cells were incubated with or without osmotic shock inducing media for 60 min. The *vraTSR* expression levels increased after both hyperosmotic shock (sucrose and sorbitol) and hypoosmotic shock (MilliQ water), . N > 296 cells for each condition.

Our observations that VraTSR regulatory system was responding to both hyperosmotic and hypoosmotic shocks are compatible with the hypothesis of this system detecting variations in periplasm width. Nevertheless, we could not establish if VraTSR activation resulted directly from the mechanical compression of the immobilized cells inside the microfluidics device. These results led us to conclude that CellASIC® ONIX Microfluidic Platform was not ideal to study if *vraTSR* expression levels correlated with tolerance to CW targeting antibiotics. We therefore decided to study cells growing on an agarose pad, as described previously in the methods section.

Higher *vraTSR* expression levels do not lead to higher tolerance to CW targeting antibiotics

To study the effect of *vraTSR* expression levels on antibiotic tolerance using agarose pads, we first exposed COL Pvra-sGFP cells to sub-inhibitory concentrations (0.4x MIC) of the CW targeting antibiotic oxacillin to trigger VraTSR, in a liquid culture, and then placed cells on an agarose pad containing an inhibitory concentration of the same antibiotic (4x MIC) and the indicator dye for dead cells, propidium iodide (PI). Cells were then monitored by epifluorescence microscopy for 255 min. For each cell, we measured the GFP fluorescence at t_0 (when cells were placed on the agarose pad) and then followed them until the end of the experiment to evaluate whether they (i) remained alive; (ii) died or (iii) divided. Cells that were dead at t_0 were discarded from the analysis, as no information regarding GFP intensities could be

obtained (left-censored data). Cells that divided during the experiment were also discarded as neither of the two sister cells could be considered as a continued observation of the mother cell (right-censored data).

We applied Cox Proportional Hazards model to estimate the effect of *vraTSR* expression levels, measured as GFP fluorescence intensity, on bacterial survival. This model allows us to evaluate how a specific factor influences the rate at which an event, like cell death, happens over time. The factor we examined here was GFP intensity, a proxy for *vraTSR* expression levels, at t_{0min}. We found a statistically significant correlation between GFP fluorescence intensity and probability of death in the presence of oxacillin ($p < 0.001$, Cox Proportional Hazards model and Wald test). In fact, when dividing the cells into 10% quantiles according to their GFP fluorescence, we observed a pattern where cells with higher GFP fluorescence at t_{0min} (and not lower as we initially predicted) tended to die more during the timelapse (Fig.9). Analysis also revealed that approximately 80% of the cells were alive at the end of the time-lapse, despite the presence of four times the MIC concentrations of oxacillin the in the agarose pad. MICs were determined in liquid cultures, and may not directly translate to the conditions used in these experiments. Previous studies show that *S. aureus* optical density still increases after 2 h incubation at 1x MIC of oxacillin[22].

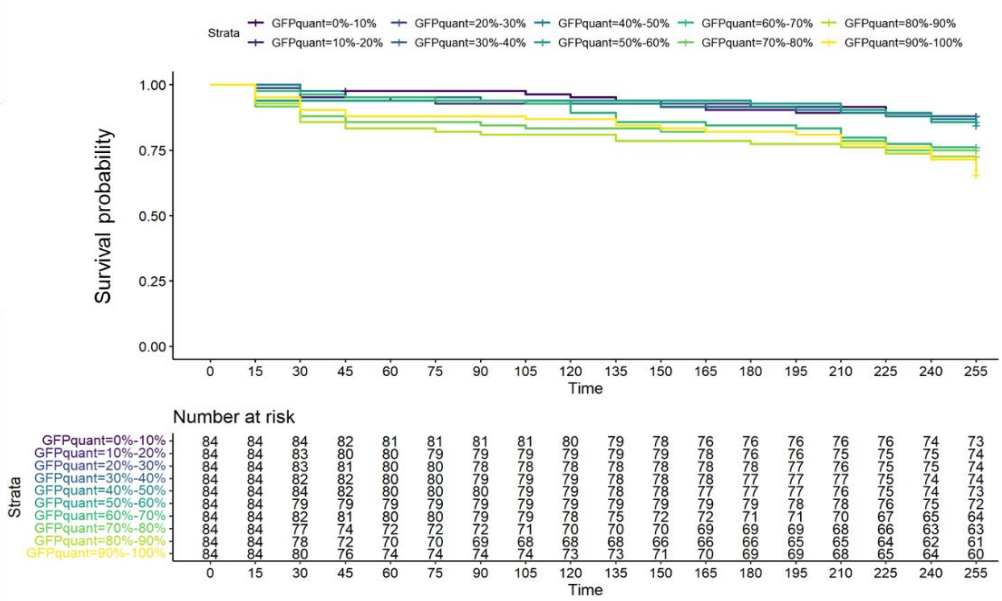

Figure 9. Cells expressing higher levels of *vraTSR* seem to be more susceptible to oxacillin. COL Pvra-sGFP cells were exposed cells to sub-inhibitory concentrations (0.4x MIC) of the CW targeting antibiotic oxacillin to trigger VraTSR, in a liquid culture, and then placed on an agarose pad containing an inhibitory concentration (4x MIC) of the same antibiotic together with the indicator dye for dead cells, propidium iodide (PI). GFP fluorescence was evaluated at t_{0min} and cells were monitored for 255 min to evaluate whether they died or survived antibiotic exposure. Cells were divided into 10% quantiles, according to the GFP fluorescence at t_{0min}. Cells belonging to quantiles of higher GFP intensity had a higher death rate than the ones from lower fluorescence quantiles. Number at risk represents the number of cells alive at that particular timepoint. N = 840 cells.

The fact that cells expressing higher *vraTSR* levels seem to be more susceptible to the antibiotic presence challenges the current view, where VraTSR is essential for the cells to survive antibiotic treatment[44]. Disrupting *vraT*, *vraS* or *vraR* renders a reduction in the levels of resistance to β-lactam antibiotics, like oxacillin[21,25,44]. It is possible that there are optimal expression levels for *vraTSR* and that above a certain threshold, *vraTSR* expression is not advantageous for the cells. Overexpression of certain genes can have deleterious effects on bacterial cells[45,46]. Above a certain threshold *vraTSR* expression is not advantageous for the cells possibly due to deleterious overexpression of specific genes from the CWSS loop[47,48]. Alternatively, cells that express higher *vraTSR* levels may be the ones to which damage inflicted by the antibiotic treatment was more severe. This implies that for inhibitory antibiotic concentrations, VraTSR system cannot efficiently prevent cell death. It should be noticed that we imaged cells after a 120 min incubation with sub-inhibitory antibiotic concentrations to trigger VraTSR, so we did not assess how early each cell activated the system. It is possible that cells that activated this regulatory system sooner were more tolerant to the antibiotic presence, but this information was missed due to the set-up of these experiments.

Final Remarks

Populations of genetically identical cells can display phenotypic differences, even in homogeneous environments[49]. This is especially useful in fluctuating environments[50]. Typically, microorganisms adapt to volatile conditions by sensing environmental stimuli and processing them through signal transduction mechanisms, like TCS, to regulate the genetic expression accordingly. Phenotypic heterogeneity enables bacteria to anticipate abrupt changes in their environment[50]. *vraTSR* expression in *S. aureus* revealed to have high variance in an isogenic population. Its expression levels seemed to influence the capability of cells to survive antibiotic treatment yet, higher expression levels appeared to have a negative impact on the survival ability. Our results also suggest that VraTSR activation mechanism needs to be revisited, since this system was responding, albeit in lowed levels, in a condition where the cells were trapped inside microfluidic chambers, in the absence of CW targeting antibiotics.

References

1. Ventola CL. The antibiotic resistance crisis: causes and threats. *P T J*. 2015;40(4):277-283. PMID: 25859123

2. Golkar Z, Bagasra O, Pace DG. Bacteriophage therapy: a potential solution for the antibiotic resistance crisis. *J Infect Dev Ctries*. 2014;8(2):129-136. doi:10.3855/JIDC.3573

3. Reardon S. WHO warns against "post-antibiotic" era. *Nature*. April 2014. doi:10.1038/nature.2014.15135

4. Deleo FR, Otto M, Kreiswirth BN, Chambers HF. Community-associated meticillin-resistant *Staphylococcus aureus*. *Lancet*. 2010;375:1557-1568. doi:10.1016/S0140

5. Fishovitz J, Hermoso JA, Chang M, Mobashery S. Penicillin-binding protein 2a of methicillin-resistant *Staphylococcus aureus*. *IUBMB Life*. 2014;66(8):572–577. doi:10.1002/iub.1289

6. Westblade LF, Errington J, Dörr T. Antibiotic tolerance. *PLOS Pathog*. 2020;16(10):e1008892. doi:10.1371/JOURNAL.PPAT.1008892

7. Balaban NQ, Helaine S, Lewis K, et al. Definitions and guidelines for research on antibiotic persistence. *Nat Rev Microbiol*. 2019;17(7):441-448. doi:10.1038/s41579-019-0196-3

8. Levin-Reisman I, Brauner A, Ronin I, Balaban NQ. Epistasis between antibiotic tolerance, persistence, and resistance mutations. *Proc Natl Acad Sci U S A*. 2019;116(29):14734-14739. doi:10.1073/pnas.1906169116

9. Lewis K. Persister cells. *Annu Rev Microbiol*. 2010;64:357-372. doi:10.1146/annurev.micro.112408.134306

10. Smits WK, Kuipers OP, Veening JW. Phenotypic variation in bacteria: The role of feedback regulation. *Nat Rev Microbiol*. 2006;4(4):259-271. doi:10.1038/nrmicro1381

11. Vázquez-Jiménez A, Santillán M, Rodríguez-González J. How the extrinsic noise in gene expression can be controlled? *IFAC-PapersOnLine*. 2017;50(1):15092-15096. doi:10.1016/j.ifacol.2017.08.2236

12. Sumner ER, Avery AM, Houghton JE , Robins RA, Avery

SV. Cell cycle- and age-dependent activation of Sod1p drives the formation of stress resistant cell subpopulations within clonal yeast cultures. *Mol Microbiol*. 2003;50(3):857-870. doi:10.1046/J.1365-2958.2003.03715.X

13. Corona F, Martinez JL. Phenotypic resistance to antibiotics. *Antibiotics*. 2013;2(2):237-255. doi:10.3390/antibiotics2020237

14. Raser JM, O'Shea EK. Molecular biology - Noise in gene expression: Origins, consequences, and control. *Science*. 2005;309(5743):2010-2013. doi:10.1126/science.1105891

15. Wang JD, Levin PA. Metabolism, cell growth and the bacterial cell cycle. *Nat Rev Microbiol*. 2009;7(11):822-827. doi:10.1038/nrmicro2202

16. Windels EM, Michiels JE, van den Bergh B, Fauvart M, Michiels J. Antibiotics: Combatting tolerance to stop resistance. *MBio*. 2019;10(5):e02095-19. doi:10.1128/mBio.02095-19

17. Windels EM, Michiels JE, Fauvart M, Wenseleers T, Van den Bergh B, Michiels J. Bacterial persistence promotes the evolution of antibiotic resistance by increasing survival and mutation rates. *ISME J*. 2019;13(5):1239-1251. doi:10.1038/s41396-019-0344-9

18. Walsh C. Molecular mechanisms that confer antibacterial drug resistance. *Nature*. 2000;406(6797):775-781. doi:10.1038/35021219

19. Epand RM, Walker C, Epand RF, Magarvey NA. Molecular mechanisms of membrane targeting antibiotics. *Biochim Biophys Acta - Biomembr*. 2016;1858(5):980-987. doi:10.1016/J.BBAMEM.2015.10.018

20. Utaida S, Dunman PM, Macapagal D, *et al*. Genome-wide transcriptional profiling of the response of *Staphylococcus aureus* to cell-wall-active antibiotics reveals a cell-wall-stress stimulon. *Microbiology*. 2003;149(10):2719-2732. doi:10.1099/mic.0.26426-0

21. Kuroda M, Kuroda H, Oshima T, Takeuchi F, Mori H, Hiramatsu K. Two-component system VraSR positively modulates the regulation of cell-wall biosynthesis pathway in

Staphylococcus aureus. *Mol Microbiol*. 2003;49(3):807-821. doi:10.1046/j.1365-2958.2003.03599.x

22. Dengler V, Meier PS, Heusser R, Berger-Bächi B, McCallum N. Induction kinetics of the *Staphylococcus aureus* cell wall stress stimulon in response to different cell wall active antibiotics. *BMC Microbiol*. 2011;11:16. doi:10.1186/1471-2180-11-16

23. Boyle-Vavra S, Yin S, Jo DS, Montgomery CP, Daum RS. VraT/YvqF is required for methicillin resistance and activation of the VraSR regulon in *Staphylococcus aureus*. *Antimicrob Agents Chemother*. 2013;57(1):83-95. doi:10.1128/AAC.01651-12

24. Yin S, Daum RS, Boyle-Vavra S. VraSR two-component regulatory system and its role in induction of *pbp2* and *vraSR* expression by cell wall antimicrobials in *Staphylococcus aureus*. *Antimicrob Agents Chemother*. 2006;50(1):336–343. doi:10.1128/AAC.50.1.336-343.2006

25. McCallum N, Stutzmann Meier P, Heusser R, Berger-Bächi B. Mutational analyses of open reading frames within the *vraSR* operon and their roles in the cell wall stress response of *Staphylococcus aureus*. *Antimicrob Agents Chemother*. 2011;55(4):1391–1402. doi:10.1128/AAC.01213-10

26. Oshida T, Tomasz A. Isolation and characterization of a Tn551-autolysis mutant of *Staphylococcus aureus*. *J Bacteriol*. 1992;174(15):4952-4959. doi:10.1128/JB.174.15.4952-4959.1992

27. Monk IR, Shah IM, Xu M, Tan MW, Foster TJ. Transforming the untransformable: Application of direct transformation to manipulate genetically *Staphylococcus aureus* and *Staphylococcus epidermidis*. *MBio*. 2012;3(2):e00277-11. doi:10.1128/mBio.00277-11

28. Nair D, Memmi G, Hernandez D, et al. Whole-genome sequencing of *Staphylococcus aureus* strain RN4220, a key laboratory strain used in virulence research, identifies mutations that affect not only virulence factors but also the fitness of the strain. *J Bacteriol*. 2011;193(9):2332-2335. doi:10.1128/JB.00027-11

29. Gill SR, Fouts DE, Archer GL, *et al*. Insights on evolution of virulence and resistance from the complete genome analysis

of an early methicillin-resistant *Staphylococcus aureus* strain and a biofilm-producing methicillin-resistant *Staphylococcus epidermidis* strain. *J Bacteriol*. 2005;187(7):2426-2438. doi:10.1128/JB.187.7.2426-2438.2005

30. Huber J, Donald RGK, Lee SH, *et al*. Chemical genetic identification of peptidoglycan inhibitors potentiating carbapenem activity against methicillin-resistant *Staphylococcus aureus*. *Chem Biol*. 2009;16(8):837-848. doi:10.1016/j.chembiol.2009.05.012

31. Reed P, Atilano ML, Alves R, *et al*. *Staphylococcus aureus* survives with a minimal peptidoglycan synthesis machine but sacrifices virulence and antibiotic resistance. *PLoS Pathog*. 2015;11(5):e1004891. doi:10.1371/journal.ppat.1004891

32. Gander MJ, Mazza C, Rummler H. Stochastic gene expression in switching environments. *J Math Biol*. 2007;55(2):249-269. doi:10.1007/s00285-007-0083-9

33. Millipore M. CellASIC ™ ONIX Microfluidic Platform. 2012. http://www.merckmillipore.com/GB/en/product/CellASIC-ONIX-Microfluidic-Platform,MM_NF-C117908. Accessed May 30, 2022.

34. Sutlief AL, Valquier-Flynn H, Wilson C, *et al*. Live cell analysis of shear stress on *Pseudomonas aeruginosa* using an automated higher-throughput microfluidic system. *J Vis Exp*. 2019;143. doi:10.3791/58926

35. Edwards N, Beeton S, Bull AT, Merchuk JC. A novel device for the assessment of shear effects on suspended microbial cultures. *Appl Microbiol Biotechnol*. 1989;30(2):190-195. doi:10.1007/BF00264010

36. Lange H, Taillandier P, Riba JP. Effect of high shear stress on microbial viability. *J Chem Technol Biotechnol*. 2001;76(5):501-505. doi:10.1002/jctb.401

37. Wipff PJ, Majd H, Acharya C, Buscemi L, Meister JJ, Hinz B. The covalent attachment of adhesion molecules to silicone membranes for cell stretching applications. *Biomaterials*. 2009;30(9):1781-1789. doi:10.1016/j.biomaterials.2008.12.022

38. Chikada T, Kanai T, Hayashi M, Kasai T, Oshima T, Shiomi

D. Direct observation of conversion from walled cells to wall-deficient L-form and vice versa in *Escherichia coli* indicates the essentiality of the outer membrane for proliferation of L-form cells. *Front Microbiol*. 2021;12:537. doi:10.3389/fmicb.2021.645965

39. Sochacki KA, Shkel IA, Record MT, Weisshaar JC. Protein diffusion in the periplasm of *E. coli* under osmotic stress. *Biophys J*. 2011;100(1):22-31. doi:10.1016/j.bpj.2010.11.044

40. Rojas ER, Huang KC, Theriot JA. Homeostatic cell growth is accomplished mechanically through membrane tension inhibition of cell-wall synthesis. *Cell Syst*. 2017;5(6):578-590.e6. doi:10.1016/j.cels.2017.11.005

41. Chang J, Coleman S, Lee YE, Schellenberg-beaver T. Differential effects of sucrose or NaCl osmotic shock on β -galactosidase activity in *Escherichia coli* BW25993 is dependent on normalization method by total viable count or total protein content. *J Exp Microbiol Immunol*. 2014;18:54-59.

42. Rojas ER, Huang KC. Regulation of microbial growth by turgor pressure. *Curr Opin Microbiol*. 2018;42:62-70. doi:10.1016/j.mib.2017.10.015

43. Booth IR, Louis P. Managing hypoosmotic stress: Aquaporins and mechanosensitive channels in *Escherichia coli*. *Curr Opin Microbiol*. 1999;2(2):166-169. doi:10.1016/S1369-5274(99)80029-0

44. Gardete S, Wu SW, Gill S, Tomasz A. Role of VraSR in antibiotic resistance and antibiotic-induced stress response in *Staphylococcus aureus*. *Antimicrob Agents Chemother*. 2006;50(10):3424-3434. doi:10.1128/AAC.00356-06

45. Myrbråten IS, Stamsås GA, Chan H, et al. SmdA is a novel cell morphology determinant in *Staphylococcus aureus*. Foster SJ, Pujol N, eds. *MBio*. 2022;13(2):e0340421. doi:10.1128/mbio.03404-21

46. Bhattacharyya S, Bershtein S, Yan J, *et al*. Transient protein-protein interactions perturb *E. coli* metabolome and cause gene dosage toxicity. *Elife*. 2016;5:e20309. doi:10.7554/eLife.20309

47. Belcheva A, Golemi-Kotra D. A close-up view of the VraSR two-component system: A mediator of *Staphylococcus*

aureus response to cell wall damage. *J Biol Chem*. 2008;283(18):12354-12364. doi:10.1074/jbc.M710010200

48. Belcheva A, Verma V, Golemi-Kotra D. DNA-binding activity of the vancomycin resistance associated regulator protein VraR and the role of phosphorylation in transcriptional regulation of the *vraSR* operon. *Biochemistry*. 2009; 48(24):5592-5601. doi:10.1021/bi900478b

49. Ackermann M. A functional perspective on phenotypic heterogeneity in microorganisms. *Nat Rev Microbiol 2015 138*. 2015;13(8):497-508. doi:10.1038/nrmicro3491

50. Thattai M, Oudenaarden A. Stochastic gene expression in fluctuating environments. *Genetics*. 2004;167(1):523-530. doi:10.1534/GENETICS.167.1.523

Chapter IV

Revisiting the role of VraTSR in *Staphylococcus aureus* response to cell wall targeting antibiotics

Chapter contents

Abstract 166
Introduction 167
Experimental Procedures 169
Bacterial growth conditions 169
Construction of *S. aureus* strains 174
Minimum inhibitory concentration (MIC) assays 179
Fluorescence-Activated Cell Sorting (FACS) analysis 179
S. aureus imaging by fluorescence microscopy 180
Determination of VraT topology, using PhoB fusions 181
Results 181
VraT is a membrane localized protein with an extracellular C-terminal domain 181
VraTSR does not sense an intermediate in peptidoglycan synthesis 183
Inhibition of transglycosylase activity induces VraTSR 186
Discussion 192
References 196

Author contributions

P.B. Fernandes performed all experiments shown, except strains COLΔ*pbpB*, which was constructed by Patricia Reed. Plasmid pVraS-mCherry was constructed by João M. Monteiro.

Acknowledgments

We thank Terry Roemer (Merck) for the generous gift of CDFI and Sérgio Filipe (FCT-NOVA) for helpful discussions. We thank Nathalie Reichmann (ITQB) for the plasmid pCNX-pbp2TP.

This chapter contains unpublished data, part of a manuscript under review.

Abstract

Exposure of *Staphylococcus aureus* to cell wall inhibitors leads to the activation of the VraTSR three-component sensory regulatory system. This system is composed of VraS, a membrane histidine kinase, VraR, its cognate response regulator and VraT, a protein required for the full activity of VraTSR. The exact function of VraT remains mostly uncharacterized, although it has been proposed to detect the unknown stimulus sensed by the VraTSR system. Here we elucidate the topology of VraT, showing that its C-terminal domain is extracellular. We also demonstrate that the signal sensed by VraTSR is not an intermediate in the peptidoglycan synthesis pathway, as previously suggested. Instead, the specific inhibition of the penicillin-binding protein (PBP)2 leads to strong activation of the system.

Introduction

Staphylococcus aureus is a Gram-positive bacterial pathogen responsible for worldwide nosocomial and community-acquired infections. Methicillin-resistant *S. aureus* (MRSA) strains in particular are currently the second most frequent cause of global deaths associated with antibiotic resistance[1]. *S. aureus* can cause a variety of infections in the human body, ranging from mild skin infections to life-threatening diseases[2]. The versatility of this pathogen is partially due to its capacity to cope with changing environmental conditions, with adaptative responses coordinated by its 16 two-component systems (TCS)[3].

Bacterial TCS sense various environmental cues, including different chemical and physical stimuli such as ions, gases, antibiotics, osmotic pressure or metabolites[4,5]. This allows bacterial cells to mount the appropriate response via changes in metabolism, cell division, antibiotic resistance and pathogenicity, amongst other functions[6].

Among the several TCS present in *S. aureus*, the vancomycin resistance-associated regulatory system, also known as VraTSR, coordinates the bacterial response to cell wall (CW) synthesis disruption[7]. VraTSR was initially identified due to its role in vancomycin resistance. However, it is also involved in the response to several other compounds that target CW synthesis[8,9,10]. Accordingly, disrupting this system increases the susceptibility of *S. aureus* towards several CW targeting compounds[8].

VraTSR is encoded by the *vraUTSR* operon[7]. VraS is a membrane histidine kinase belonging to the intramembrane-sensing histidine kinases (IMHKs) family, since it is predicted to lack an extracellular sensing domain, which is characteristic of

most histidine kinases[7,11,12]. Upon detecting a still unknown stimulus, that presumably results from *S. aureus* exposure to CW targeting compounds, VraS undergoes autophosphorylation at a conserved histidine residue, likely to be Histidine 156[11,13]. VraR is the cognate response regulator that is phosphorylated by VraS[11]. Phosphorylated VraR dimerizes and binds to its own *vraUTSR* promoter, as well as to the promoters of several other genes, activating or repressing their transcription[11,14]. These genes, that constitute the VraR regulon, also known as the cell wall stress stimulon (CWSS)[15], belong to different functional categories, including lipid and carbohydrate metabolism, DNA replication and repair, and importantly, cell envelope biogenesis. The latter encompasses genes involved in peptidoglycan biosynthesis such as *pbpB*, encoding the major *S. aureus* peptidoglycan synthase Penicillin-Binding Protein 2 (PBP2), *mgt*, encoding a monofunctional glycosyltransferase or *murZ,* that encodes a UDP-N-acetylglucosamine enolpyruvyl transferase[8,9].

The role of VraT is less clear. Boyle-Vavra and colleagues have proposed that VraT (previously named YvqF) is the protein that detects the unknown stimulus sensed by the VraTSR system, promoting autophosphorylation of VraS, through a still elusive mechanism[7]. Accordingly, deletion of *vraT* affects resistance of *S. aureus* to several CW targeting antibiotics, similarly to what was observed for *vraS* and *vraR* deletion mutants[7,16]. Deletion of *vraT* also impairs VraTSR-dependent activation of the CWSS, showing its relevant role in this process[7,16]. VraT is predicted to be a membrane protein, described as interacting with VraS, but not VraR[7,16]. Its structure and topology are not known, and therefore the cellular localization of the C-terminal region, speculated to be the sensor domain, is yet to be determined[7,16].

In this work, we aimed at unveiling the identity of the stimulus responsible for VraTSR activation and specifically to determine if this stimulus was an intermediate in the peptidoglycan synthesis pathway that would accumulate, or be depleted, in the presence of various CW targeting antibiotics.

Experimental Procedures

Bacterial growth conditions

Plasmids and strains used in this study are listed in Table 1 and Table 2. *S. aureus* strains were grown in tryptic soy broth (TSB, Difco) with aeration at 37 °C or on tryptic soy agar (TSA, Difco) at 30 °C or 37 °C. For microscopy experiments, overnight cultures of *S. aureus* strains were diluted 1:200 in TSB medium and allowed to grow at 37 °C until an $OD_{600\ nm}$ of approximately 0.5. Cells were then harvested and resuspended in the same medium. *Escherichia coli* strains were grown in Luria-Bertani broth (LB, Difco) with aeration, or LB agar (LA, Difco) at 30 °C. Culture medium was supplemented with appropriate antibiotics (100 µg ml^{-1} ampicillin, 10 µg ml^{-1} erythromycin, 10 µg mL^{-1} chloramphenicol or 50 µg ml^{-1} of both kanamycin and neomycin; Sigma-Aldrich), with 100 µg ml^{-1} 5-bromo-4-chloro-3-indolyl-β-D-galactopyranoside (X-Gal; VWR) or with cadmium chloride (0.1 µM, Sigma-Aldrich), when required. Cell wall targeting antibiotics were used at their minimum inhibitory concentrations: 2 µg mL^{-1} for vancomycin, 800 µg mL^{-1} for oxacillin, 1.5 µg mL^{-1} for CDFI, 40 µg mL^{-1} for bacitracin, 125 µg mL^{-1} for D-cycloserine, 300 µg mL^{-1} for fosfomycin and 1 µg mL^{-1} for PC190273.

Table 1. Plasmids used in this study

Plasmids	Description	Source or reference
pCN51	Shuttle vector containing a cadmium inducible P_{cad} promoter; Amp^R Ery^R	[17]
pCNX	Shuttle vector containing a cadmium inducible P_{cad} promoter; Amp^R Kan^R	[18]
pMAD	*E. coli-S. aureus* shuttle vector with a thermosensitive origin of replication for Gram-positive bacteria; Amp^R Ery^R *lacZ*	[19]
pBCB4-ChE	*S. aureus* integrative vector for N- and C-terminal mCherry fusions; Amp^R Ery^R	[20]
pFAST3	*S. aureus* integrative vector that allows for C-terminal sGFP fusions; Amp^R Ery^R	[21]
pPvra-pFAST3	*S. aureus* integrative vector with *vraTSR* promoter upstream of sfgfp-p7	This study
pPBP2	pCNX derivative containing *pbpB* under the control of P_{cad} promoter; Amp^R Kan^R	This study
pPBP2TG	pCNX derivative containing *pbpB*TG (E114Q) under the control of P_{cad} promoter; Amp^R Kan^R	This study
pCNX-pbp2TP	pCNX derivative containing *pbp2*TP (S398G) under the control of P_{cad} promoter; Amp^R Kan^R	This study
pPBP2TGTP	pCNX derivative containing pbp2TGTP (E114Q and S398G) under the control of P_{cad} promoter; Amp^R Kan^R	This study
pVraT-GFP	pMAD with s*gfp* 5´ fusion to *vraT*, Amp^R, Ery^R	This study
pVraS-mCherry	pMAD with *mCherry* 3’ fusion to *vraS,* Amp^R, Ery^R	This study
pVraT-PhoB	pCN51 derivative containing *phoB* 3´ fusion to *vraT* under the control of P_{cad} promoter, Amp^R, Ery^R	This study

pPhoB_VraT	pCN51 derivative containing *phoB* 5' fusion to *vraT* under the control of P_{cad} promoter, Amp^R, Ery^R	This study

Table 2. Strains used in this study.

Strains	Description	Source or reference
Escherichia coli		
DC10B	Δ*dcm* in the DH10B background; Dam methylation only	[22]
Staphylococcus aureus		
COL	HA-MRSA	[23]
RN4220	Restriction-deficient derivative of NCTC8325-4	R. Novick
COL Pvra-sGFP	COL with pFAST3-Pvra; Ery^R	This study
ColPBP1TP	COL tet^S *pbpA*::*pbpA*^{S314A}	[24]
COLΔ*pbpB*	*pbpB* deletion in COL	This study
COLΔ*pbp3*	*pbp3* deletion in COL	[24]
COLΔ*pbpD*	*pbpD* deletion in COL	[25]
COLΔ*mgt*	*mgt* deletion in COL	[26]
COLlΔ*sgtA*	*sgtA* deletion in COL	[26]
COLΔ*mecA*	*mecA* deletion in COL	[27]
ColPBP1TP_Pvra-sGFP	COL *tet*^{S} *pbpA::pbpA*^{S314A} with pPvra-pFAST3; Ery^R	This study
COLΔ*pbpB*_Pvra-sGFP	COLΔ*pbpB* with pPvra-pFAST3; Ery^R	This study
COLΔ*pbp3*_Pvra-sGFP	COLΔ*pbpC* with pPvra-pFAST3; Ery^R	This study
COLΔ*pbpD*_Pvra-sGFP	COLΔ*pbpD* with pPvra-pFAST3; Ery^R	This study

COLΔ*mgt*_Pvra-sGFP	COLΔ*mgt* with pPvra-pFAST3; Ery^R	This study
COLΔ*sgtA*_Pvra-sGFP	COLΔ*sgtA* with pPvra-pFAST3; Ery^R	This study
COLΔ*mecA*_Pvra-sGFP	COLΔ*mecA* with pPvra-pFAST3; Ery^R	This study
COLΔ*pbpB*_Pvra-sGFPpCNX	COL*ΔpbpB*_Pvra-sGFP with pCNX; Ery^R, Kan^R, Neo^R	This study
COLΔ*pbpB*_Pvra-sGFPpPBP2	COL*ΔpbpB*_Pvra-sGFP with pPBP2; Ery^R, Kan^R, Neo^R	This study
COLΔ*pbpB*_Pvra-sGFPpPBP2TG*	COLΔ*pbpB*_Pvra-sGFP with pPBP2TG; Ery^R, Kan^R, Neo^R	This study
COLΔ*pbpB*_Pvra-sGFPpPBP2TP*	COLΔ*pbpB*_Pvra-sGFP with pCNX-pbp2TP; Ery^R, Kan^R, Neo^R	This study
COLΔ*pbpB*_Pvra-sGFPpPBP2TG*TP*	COLΔ*pbpB*_Pvra-sGFP and pPBP2TGTP, Ery^R, Kan^R, Neo^R	This study
BCBPM073	COL *pbpB*::*sgfp-pbpB*	[28]
COLsGFP_VraT	COL *vraT*::*sgfp-vraT*	This study
COLsGFP-VraTVraS-mCherry	COL *vraT*::*sgfp-vraT, vraS::vraS-mcherry*	This study
COLΔ*phoB*	*phoB* deletion in COL	Veiga *et al*, submitted
COLΔ*phoB*pCN51	ColΔ*phoB* with pCN51; Ery^R	This study
COLΔ*phoB*pVraT-PhoB	ColΔ*phoB* with pVraT_PhoB; Ery^R	This study
COLΔ*phoB*pPhoB-VraT	ColΔ*phoB* with pPhoB_VraT; Ery^R	This study

Table 3. Oligonucleotides used in this study

Primer name	Sequence (5'-3')
PVraSR_P1_KpnI	gctgcggtacccggtgctatttctgcgcc
PVraSR_P2_New_Xho	cgcgctcgagttataataagttttaaaataccaaatgcgc
PBP2KO-P1	acgacgaattctcaaatacacttctgctg
PBP2KO-P2	tagttgaatatatccgtcatacgcggtcctcactttc
PBP2KO-P3	tgaggaccgcgtatgacggatatattcaactaatc
PBP2KO-P4	acgcaggattctgtccactattagaagattg
PBP2muts_P1	ggtcgactctagaggatccccgttgatattagatga aagtgaggaccgcgtatgacggaaaacaaaggatc
PBP2muts_P2	gcctgaattcgagctcggtacccttagttgaatatacctgttaatcc
P1pMADpbp2TP	gcgcccgggcattcaaatacgttttatc
P2pMADpbp2TP	cgcggatccaccagtagggtgaggatc
P3pMADpbp2TP	cgcggatccttaaaacctttcttagcg
P4pMADpbp2TP	cgcgtcgacgaattttaaagaaagatatg
P1pCNXpbp2	caggtcgacaaaaaataaggaggaaaaaaaatgacggaaaacaaaggatc ttctc
P2pCNXpbp2	cgcatggtaccttagttgaatatacctgttaatccaccgctgtttc
E114Q fw	gtactcgcgactcaagacaatcgtttctacgaacatg
E114Q rev	cgattgtcttgagtcgcgagtactgcgtctttc
VraSCterfwdNcoI	cgcgcgccatggggtactcgcttacaaaatcaatcagc
VraSmchMLbwd	agaaccagcagcggagccagccgaatttaaaggtgctttcacc
mCherryMLfwd	tccgctgctggttctggcgagttcatgattgtgagcaagg
mCherrybwd2	atacgaatcctccttctagtacagctcgtccatgccaccgg
Vrasfwd3	aaggaggattcgtatgacgattaaagtattgtttgtggatg
VraRbwdBamHI	gcgcgcggatcctatcatgttgatgaacatcctagtgatacc
orf1_fw_EcoRI	gcgcgaattcaaggtgatagttatgaactatgttgaacg
orf1_rev_link_sgfp	ctatgccacagcgttcatataatttattagatacg
sgfp_fw_link_orf1	gaacgctgtggcataggatatcataaggaggattcg
sgfp_rev_link_vraT	gaactcgccagaaccagcagcggagccagccgaatgatggtgatggtcgact ttg
vraT fw_link_sgfp	tcggctggctccgctgctggttctggcgagttcatgacacacaaatatatatc
vraT rev bamHI	gcgcggatcctcatcgataaatcacctctacgtctccgataaacg

phoB_vraT_P1	gtcgactctagaggatccccctcaggaggatgtcttatgcaatccgataaaagtt ctaaagatg
phoB_vraT_P2	catggaggcgccgcaggacttgaatatatcaaatattatttttgcgc
phoB_vraT_P3	caagtcctgcggcgcctccatgacacacaaatatatatcaacg
phoB_vraT_P4	cctgaattcgagctcggtaccctcaactcatcgataaatcacctctacgtc
vraT_phoB_P1	ggtcgactctagaggatccccgaacgctgtggcatagaaaggcggcgaaac
vraT_phoB_P2	cggattgggaggcgccgcaggatcgataaatcacctctacgtctcc
vraT_phoB_P3	cgatcctgcggcgcctcccaatccgataaaagttctaaag
vraT_phoB_P4	gcctgaattcgagctcggtacccttacttgaatatatcaaatattatttttgcgc

Construction of *S. aureus* strains

Sequence of primers used for strain construction as listed in Table 3.

To construct the *vraTSR* promoter fusion, an 814 bp DNA fragment containing the *vraTSR* promoter region was amplified from COL genomic DNA using the primers PvraSR_P1_KpnI and PvraSR_P2_New_XhoI, digested with KpnI and XhoI, and cloned into KpnI/XhoI digested pFAST3, upstream of sfgfp-p7, resulting in plasmid pPvra-pFAST3, confirmed by DNA sequencing. pPvrap-FAST3 was electroporated into the *S. aureus* RN4220 strain and integrated into the chromosome at the *vraTSR* promoter site by homologous recombination, as confirmed by PCR and sequencing; the resulting strain was named RN Pvra-sGFP. Strain COL Pvra-sGFP was constructed by transducing the integrated plasmid pPvra-pFAST3 from RN Pvra-sGFP into COL using phage 80α, as previously described[29].

To construct the *S. aureus* Δ*pbpB* null mutant, lacking PBP2, we amplified 1 kb DNA fragments from *S. aureus* COL genomic DNA corresponding to the upstream (primers PBP2_KO-P1 and PBP2_KO-P2) and downstream (primers PBP2_KO-P13 and PBP2_KO-P4) regions of the *pbpB* gene. The resulting PCR products were joined by overlap PCR using primers PBP2_KO-P1 and PBP2_KO-P4. The overlap PCR product was digested with EcoRI and BamHI and cloned into the thermosensitive plasmid pMAD[19], producing plasmid pΔ*pbpB*. The plasmid was sequenced and introduced into RN4220 by electroporation[30]. Following electroporation, the plasmid was transduced into COL using phage 80α as previously described[29]. Insertion and excision of pΔ*pbpB* was performed as previously described[19], except the integration steps were performed at 37 ^{o}C instead of 43 ^{o}C, resulting in strain COLΔ*pbpB.* Deletion of the target gene was verified by PCR and resulting strains were verified by whole genome sequencing.

To monitor *vraTSR* expression levels in the mutants lacking different enzymes involved in the last stages of peptidoglycan synthesis, pPvra-pFAST3 was transduced into the mutant strains using phage 80α, with erythromycin selection, resulting in strains: ColPBP1TP_Pvra-sGFP, COLΔ*pbpB*_Pvra-sGFP, COLΔ*pbp3*_Pvra-sGFP, COLΔ*pbpD*_Pvra-sGFP, COLΔ*mgt*_Pvra-sGFP, COLΔ*sgtA*_Pvra-sGFP and COLΔ*mecA*_Pvra-sGFP.

To investigate the mechanism behind PBP2-dependent VraTSR activation, COLΔ*pbpB*_Pvra-sGFP was complemented with plasmids encoding different alleles of PBP2. For that, a 2214 bp fragment encompassing the wild type *pbpB* allele was amplified

using primers PBP2muts_P1 and PBP2muts_P2 from *S. aureus* COL genomic DNA. The same pair of primers were used to amplify a fragment, coding for the glycosyltransferase-inactive PBP2^{E114Q} from COLTG42[31] genomic DNA. These fragments were introduced into SmaI-digested pCNX using the Gibson assembly® cloning kit (NEB), originating plasmids pPBP2 and pPBP2TG. Transduction of these plasmid into COLΔ*pbpB*_Pvra-sGFP gave COLΔ*pbpB*_Pvra-sGFPpPBP2 and COLΔ*pbpB*_Pvra-sGFPpPBP2TG*, respectively. To construct plasmid pCNX-pbp2TP, a full copy of *pbpB* allele encoding for PBP2^{S398G} (pbp2TP) was cloned into the pCNX plasmid, downstream of the cadmium inducible P_{cad} promoter. The pbp2TP sequence was amplified from pMAD-pbp2TPbig which was constructed by amplifying two PCR fragments encompassing 1.7 kb upstream or downstream of nucleotide T1192 of *pbpB* using primers P1pMADpbp2TP/ P2pMADpbp2TP and P3pMADpbp2TP/ P4pMADpbp2TP, respectively. The two fragments were joined by overlap PCR using primers pair P1pMADpbp2TP and P4pMADpbp2TP, digested with BglII and SmaI and cloned into pMAD, creating plasmid pMADpbp2TPbig. This plasmid contains the nucleotide exchanges T1192G and C1193G which switch the catalytic serine from the TP domain of PBP2 to a glycine (S398G) and a silent mutation (T1197C) that introduces a BamHI restriction site to facilitate screening of clones. The pMAD-PBP2TPbig plasmid served as a template to amplify the full pbp2TP allele using primers P1pCNXpbp2 and P2pCNXpbp2. The resulting PCR fragment was cloned downstream of the P_{cad} promoter of pCNX plasmid, after digesting with SalI and KpnI, resulting in plasmid pCNX-pbp2TP. pCNX-pbp2TP was then transduced to COLΔ*pbpB*_Pvra-sGFP, originating strain COLΔ*pbpB*_Pvra-sGFPpPBP2TP*. To construct pPBP2TGTP, the mutation coding

for glycosyltransferase-inactive PBP2^{E114Q} was inserted into plasmid pCNX-pbp2TP, via site-directed mutagenesis, using primers E114Q fw and E114Q rev. The resulting plasmid was transduced to COLΔ*pbpB*_Pvra-sGFP, giving strain COL*pbpB*_Pvra-sGFPpPBP2TG*TP*.

To localize VraT and VraS, an N-terminal fusion of VraT to the P7 variant of superfast GFP (sfGFP)[32] and a C-terminal fusion of VraS to mCherry were constructed. A 409 bp fragment encoding the upstream region of *vraT* was amplified by PCR from *S. aureus* COL genomic DNA, using primers orf1_fw_EcoRI and orf1_rev_link_sgfp. Primers sgfp_fw_link_orf1 and sgfp_rev_link_vraT were used to amplify *gfp* from pFAST3. A third 744 bp fragment containing *vraT* and a sequence encoding an 11 amino acid linker was amplified using primers vraT fw_link_sgfp and vraT rev BamHI. The fragments were joined by overlap PCR using the primers orf1_fw_EcoRI and vraT rev BamHI. The resulting fragment was digested with EcoRI and BamHI restriction enzymes and cloned into pMAD, giving pVraT-GFP. The plasmid was sequenced and then electroporated into *S. aureus* RN4220 strain at 30 °C, using erythromycin and X-gal selection, and transduced to COL using phage 80α. Integration and excision of the plasmid into the chromosome was performed as previously described[19], giving COLsGFP_VraT. An 862 bp fragment encoding VraS, excluding the stop codon, and a sequence encoding an 11 amino acid linker was amplified by PCR from *S. aureus* COL genomic DNA, using primers VraSCterfwdNcoI and VraSmchMLbwd. Primers mCherryMLfwd and mCherrybwd2 were used to amplify *mCherry* from pBCB4-Cherry. A third 860 bp fragment containing the downstream region of *vraS* was amplified

using primers Vrasfwd3 and VraRbwdBamHI. The fragments were joined by overlap PCR using the primers mCherryMLfwd and VraRbwdBamHI. The resulting fragment was digested with NcoI and BamHI restriction enzymes and cloned into pMAD, giving pVraS-mCherry. The plasmid was sequenced and then electroporated into *S. aureus* RN4220 strain at 30 °C, using erythromycin selection in the presence of X-gal, and transduced into COLsGFP_VraT, using phage 80α. Integration and excision of the plasmid into the chromosome was performed as described[19], resulting in strain COLsGFP-VraTVraS-mCherry.

To determine the topology of VraT, PhoB fusions to VraT were made at both N and C-terminal ends. For the N-terminal fusion to VraT a 1389 bp fragment encompassing *phoB* allele and a 5 amino acid linker was amplified using primers phoB_vraT_P1 and phoB_vraT_P2 from *S. aureus* COL genomic DNA. Another fragment with 748 bp with *vraT* coding sequence was amplified from the same genomic DNA, using primers phoB_vraT_P3 and phoB_vraT_P4. These fragments were introduced into SmaI-digested pCN51 using the Gibson assembly® cloning kit (NEB), originating plasmid pPhoB_VraT. For the C-terminal PhoB fusion to VraT, a 772 bp fragment with *vraT* coding sequence and encoding a 5 amino acid linker was amplified from *S. aureus* COL genomic DNA, using primers vraT_phoB_P1 and vraT_phoB_P2. Primers vraT_phoB_P3 and vraT_phoB_P4 were used to amplify a 1376 bp DNA fragment with *phoB* coding sequence, from the same genomic template. These fragments were introduced into SmaI-digested pCN51 using the Gibson assembly® cloning kit (NEB), originating plasmid pVraT-PhoB. Plasmids pCN51, pPhoB_VraT and pVraT-PhoB were transduced to COLΔ*phoB*, giving strains

COLΔ*phoB*pCN51, COLΔ*phoB*pPhoB-VraT and COLΔ*phoB*pVraT-PhoB, respectively.

Minimum inhibitory concentration (MIC) assays

MICs of relevant antimicrobial compounds were determined by broth microdilution in sterile 96-well plates. Series of two-fold dilutions of each compound were performed in TSB. Cultures of *S. aureus* strains and mutants were added at a final density of ~$5x10^5$ CFU ml^{-1} to each well. In each plate, some wells were not inoculated, for sterility control, and cell viability was assessed in wells with TSB to which no compound was added. Plates were incubated at 37 °C. Endpoints were assessed visually after 24 and 48 h and the MIC was determined as the lowest compound concentration that inhibited growth. All assays were performed in triplicate.

Fluorescence-Activated Cell Sorting (FACS) analysis

Overnight TSB cultures of *S. aureus* strains to be tested were diluted 1:200 in TSB and grown at 37 °C to exponential growth phase ($OD_{600\ nm}$ of 0.5-0.7). The appropriate antibiotic was then added and cells were incubated for 1 h. After antibiotic incubation, cells were collected by centrifugation, washed once with PBS (phosphate buffered saline, NaCl 137 mM, KCl 2.7 mM, Na_2HPO_4 10mM, KH_2PO_4 1.8 mM) and resuspended in PBS. Samples were filtered with a 40 µm strainer and diluted 1:50 in PBS. Flow cytometry data were collected on a S3e cell sorter (Bio-Rad) using a target flow rate of 500 events per second and collecting 5,000 events for each sample. A 100 mW 488 nm laser line was used for excitation, with amplification settings of 350 forward scattering

(FSC) and 950 (FL1, 525/30 nm). Acquisition was triggered by forward scattering with a threshold of 1.15.

S. aureus imaging by fluorescence microscopy

For fluorescence microscopy experiments, *S. aureus* cultures were grown to mid-exponential phase ($OD_{600\ nm}$ of 0.5-0.7) and 1 ml was collected by centrifugation. Cells were suspended in the same volume of PBS and 1 µL was placed on a thin layer of agarose (1.2% in PBS). When incubation with antibiotics was required prior to imaging, *S. aureus* cells were grown to an $OD_{600\ nm}$ of 0.3-0.4 at which point appropriate compounds were added. Cells were further incubated at 37 ºC, before being collected by centrifugation.

To evaluate septal enrichment when studying protein localization, we determined the fluorescence ratio (FR) calculated as the ratio of the median fluorescence of the 25% brightest pixels of the septum *versus* median fluorescence at the cell periphery, both corrected for background fluorescence. To measure FRs and cytoplasm fluorescence in two different strains, strains were imaged on the same microscopy slide. For this one strain was labelled with DNA dye Hoechst 33342, both cultures were washed with TSB, and then the two cultures were mixed prior to visualization by epifluorescence microscopy using a Zeiss Axio Observer microscope with a Plan-Apochromat 100x/1.4 oil Ph3 objective. Images were acquired with a Retiga R1 CCD camera (QImaging) using Metamorph 7.5 software (Molecular Devices).

Determination of VraT topology, using PhoB fusions

Overnight cultures of wild-type (wt) COL, COLΔ*phoB*, COLΔ*phoB*pCN51, COLΔ*phoB*pVraT-PhoB and COLΔ*phoB*pPhoB-VraT were diluted in TSB to a final $OD_{600\ nm}$ of 0.05 and grown to mid-exponential phase ($OD_{600\ nm}$ ~ 0.5). Subsequently 1 ml of culture was harvested by centrifugation and resuspended in the same volume of TSB. Serial ten-fold dilutions of each strain were made and 20 µl of 10^0, 10^{-2}, 10^{-4} and 10^{-6} dilutions were plated onto tryptic soy agar plates containing BCIP (5-bromo-4-chloro-3-indolyl phosphate, toluidine salt, 100 µg ml^{-1}, Sigma), supplemented with erythromycin 10 µg ml^{-1} and 2 µM of cadmium chloride (Sigma-Aldrich), when appropriate. Plates were incubated at 37 °C for 24 h.

Results

VraT is a membrane localized protein with an extracellular C-terminal domain

The role of VraT has remained elusive, but it was suggested to be involved in stimulus perception of the VraTSR regulatory system[7]. We confirmed that both VraT and VraS localize to the membrane using fluorescent fusions to both proteins (Figure 1). This result indicates that, as expected, CW damage is perceived either at the cell surface or at the cell membrane[11].

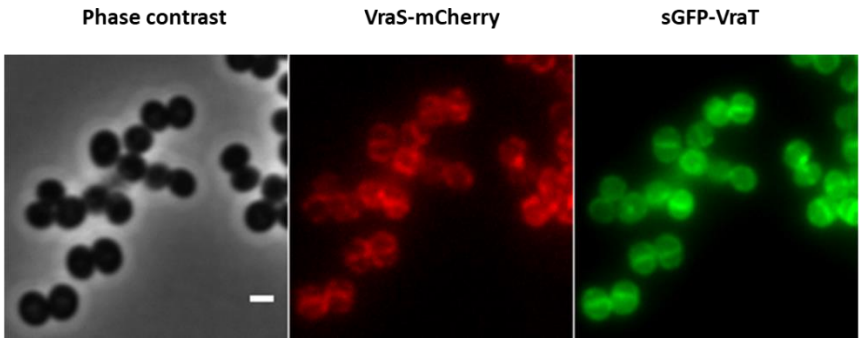

Figure 1. VraT and VraS localize at the cell membrane. Epifluorescence microscopy images of *S. aureus* COL expressing a mCherry-tagged derivative of VraS (red) and a sGFP-tagged derivative of VraT (green). The VraTSR system was induced by incubating the cells, for 60 min, with 0.5 µg ml^{-1} of CDFI, an inhibitor of the lipid II flippase MurJ.

Given that VraS, initially thought to be the sensor of the VraSR two-component system, does not display a clear extracellular sensing domain, characteristic of most histidine kinases, Boyle-Vavra and colleagues suggested that VraT was responsible for perception of CW damage on the outer surface of the cell[7,12]. However, VraT topology remained unclear, with different authors suggesting that its C-terminal domain lies intracellularly or extracellularly[7,16]. To examine the topology of VraT, we fused the *phoB* gene, encoding staphylococcal alkaline phosphatase, lacking its native export signal peptide, to either end of *vraT* and evaluated the enzymatic activity, as previously described[33]. Alkaline phosphatase PhoB is active only in the extra-cytoplasmic environment, where it can process the chromogenic alkaline phosphatase substrate BCIP (5-Bromo-4-chloro-3-indolyl phosphate), generating a blue colour. As shown in Figure 2, only the PhoB C-terminal fusion to VraT showed some PhoB activity, indicating that the C-terminal domain of VraT is extracellular, while

the N-terminal region is intracellular. This topology is compatible with a sensor function for the C-terminal domain of VraT.

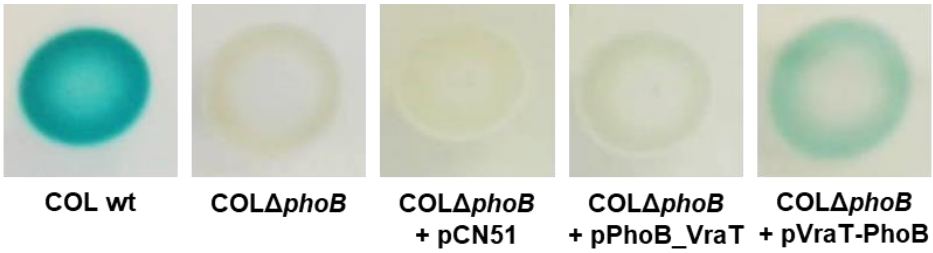

Figure 2. C-terminal domain of VraT is extracellular. VraT topology was assessed by fusing the *phoB* gene to *vraT,* at either end. The *phoB* fusions to *vraT* were expressed from the pCN51 plasmid, under the control of a cadmium inducible promoter, in the background of a *phoB* deletion mutant (COLΔ*phoB*). An empty pCN51 plasmid was also introduced into COLΔ*phoB* (COLΔ*phoB* + pCN51) and used as a negative control. The wild type strain COL was used as positive control. The strains were grown on plates containing cadmium chloride and chromogenic BCIP (5-Bromo-4-chloro-3-indolyl phosphate), a substrate that, when processed by the alkaline phosphatase PhoB, an enzyme active only in the extra-cytoplasmic environment, gives a blue coloration to the colonies[34]. Only COL and COLΔ*phoB* carrying the *vraT-phoB* fusion (COLΔ*phoB* + pVraT-PhoB) showed alkaline phosphatase activity, indicating that the C-terminal, but not the N-terminal domain of VraT faces the extra-cytoplasmic environment.

VraTSR does not sense an intermediate in peptidoglycan synthesis

CW synthesis is a multi-enzymatic, sequential process that leads to the formation of the lipid II molecule (Figure 3)[35]. Lipid II is subsequently flipped to the extracellular space and inserted in the peptidoglycan (PG) mesh[35]. Thus, the accumulation or depletion of an intermediate molecule in this enzymatic pathway, particularly

lipid II, would be a good candidate for the signal sensed by VraTSR.

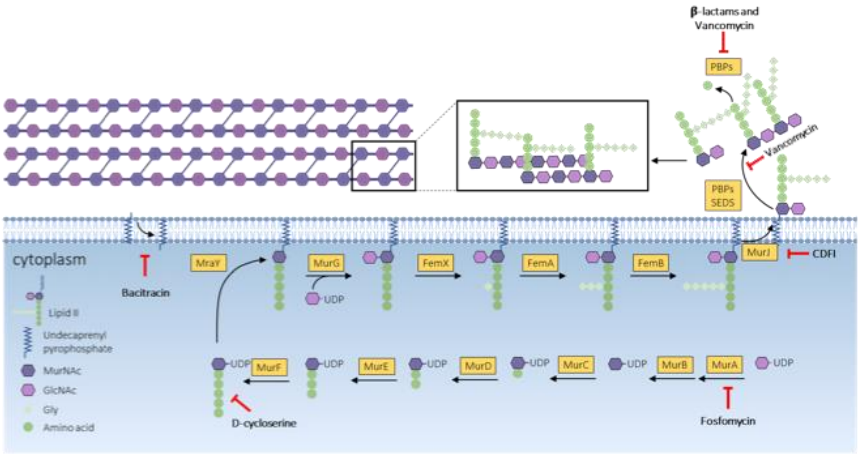

Figure 3. Schematic representation of peptidoglycan synthesis pathway, indicating the targets of cell wall active antibiotics. Fosfomycin inhibits the enzyme MurA (UDP-N-acetylglucosamine-3-enolpyruvyl transferase) that performs the addition of phosphoenolpyruvate to UDP-N-acetyl-glucosamine (GlcNAc), generating UDP-N-acetyl-muramic acid (UDP-MurNAc)[36]. D-cycloserine inhibts the addition of D-alanine to the peptidoglycan precursor by inhibiting D-alanine:D-alanine ligase A and alanine racemase[37]. CDFI (2-(2-Chlorophenyl)-3-[1-(2,3-dimethylbenzyl)piperidin-4-yl]-5-fluoro-1H-indole)[38] inhibits MurJ, the lipid II flippase. Bacitracin blocks dephosphorylation and the recycling of the lipid carrier undecaprenyl pyrophosphate, preventing the membrane steps of peptidoglycan synthesis[39]. Glycopeptide antibiotics, like vancomycin, bind to the D-Ala-D-Ala motif of lipid II blocking the access of enzymes performing transglycosylase and/or transpeptidase activity[40]. ß-lactam antibiotics, such as oxacillin, mimic the D-Ala-D-Ala end of lipid II stem peptide, forming an acyl-enzyme complex with PBPs, inhibiting their activity[41].

We tested the effect of various antibiotics, blocking initial or final steps of the PG synthesis pathway (Figure 3) and determined that in all cases the VraTSR response was triggered (Figure 4), confirming previous work[10]. Antibiotics blocking the early stages of CW synthesis, like fosfomycin, are expected to inhibit the formation

of all subsequent lipid precursors including lipid II, while antibiotics blocking the late steps of this process, like vancomycin, were previously shown to accumulate lipid II [42,43]. Considering that these antibiotics produce opposite effects on PG precursor levels, but all result in the activation of the VraTSR response, it seems unlikely that VraTSR is sensing the accumulation or depletion of lipid-linked precursors.

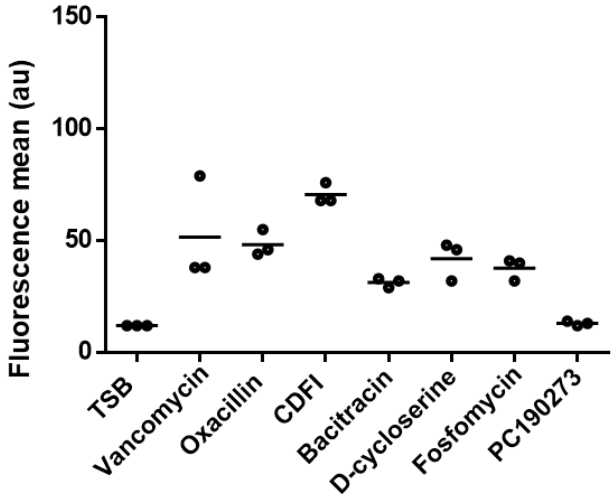

Figure 4. VraTSR responds to various CW targeting antibiotics. COL Pvra-sGFP cells were incubated with 1 X MIC of different CW targeting antibiotics for 60 min prior to being analysed by Fluorescence-Activated Cell Sorting (FACS). All tested CW targeting antibiotics activated the VraTSR regulatory system, independently of the step of the PG synthesis pathway that was blocked. Incubation with the FtsZ inhibitor PC190273, an antibiotic that does not target the CW synthesis, was included as a negative control. TSB indicates growth in the absence of antibiotics. N = 5000 cells for each replicate, experiments were performed in triplicate. Each point represents the median of one FACS experiment.

Inhibition of transglycosylase activity induces VraTSR

Given that we were unable to identify one specific CW synthesis precursor as the signal that triggers VraTSR system, we decided to investigate whether the system was triggered by lack of activity of a particular enzyme or set of enzymes involved in CW synthesis. We started by focusing on the late stages of CW synthesis performed by PBPs (1-4), the exogenous PBP (PBP2A) and monofunctional glycosyltransferases MGT and SgtA[44]. Two of these enzymes, the bifunctional transpeptidase-transglycosylase PBP2 and the monofunctional transglycosylase MGT, have their genetic expression upregulated by the response regulator VraR, as part of the CWSS[8,9]. Deletion of the gene encoding PBP2, but not the other PBPs, led to the activation of VraTSR (Figure 5). PBP2 is the only bifunctional PBP in *S. aureus*, while the remaining PBPs display monofunctional transpeptidase activity[44]. These results are in line with previous work showing that decreasing levels of *pbpB* (encoding PBP2) transcription lead to increasing levels of *vraTSR* transcripts[45].

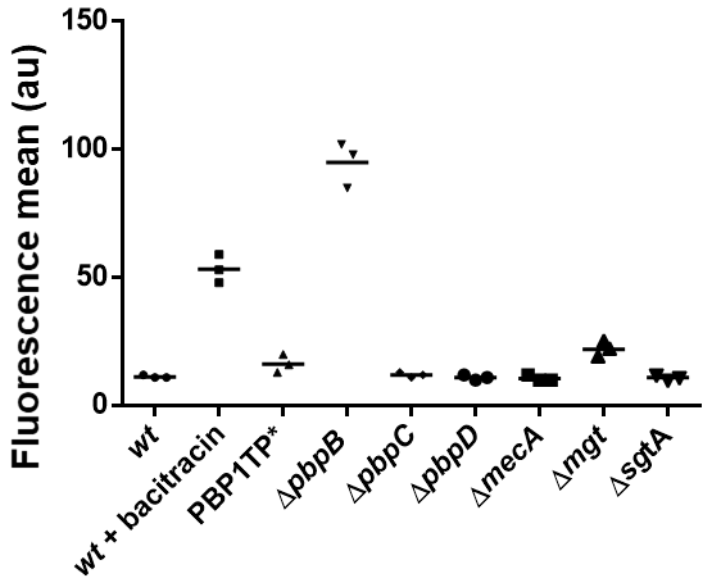

Figure 5. Depletion of PBP2, but not of the remaining CW synthesis enzymes, leads to VraTSR activation. *S. aureus* mutants lacking different CW synthesis enzymes: PBP2 (Δ*pbpB*), PBP3 (Δ*pbpC*), PBP4 (Δ*pbpD*), PBP2A (Δ*mecA*), MGT (Δ*mgt*), SgtA (Δ*sgtA*) or encoding a transpeptidase mutant of the essential PBP1 (PBP1TP*), and expressing GFP under the control of the *vraTSR* promoter were analysed by FACS. Only the cells lacking PBP2 (Δ*pbpB*) showed strong VraTSR activation while the Δ*mgt* mutant showed low activation levels. Control experiments, where COL Pvra-sGFP cells were grown in the absence (wt) or in the presence of bacitracin (wt+bacitracin), which induces the VraTSR response, were performed as negative and positive controls, respectively. N = 5000 cells for each replicate, experiments were performed in triplicate. Each point represents the median of one FACS experiment.

To explore the mechanism behind PBP2-dependent VraTSR activation, we evaluated if the delocalization of PBP2 from the division septum was the signal detected by VraTSR. PBP2 is recruited to the division septum by binding to its substrate, lipid II [46],

and the presence of CW synthesis inhibitors causes PBP2 delocalization (Figure 6) in agreement with previous observations[46,47].

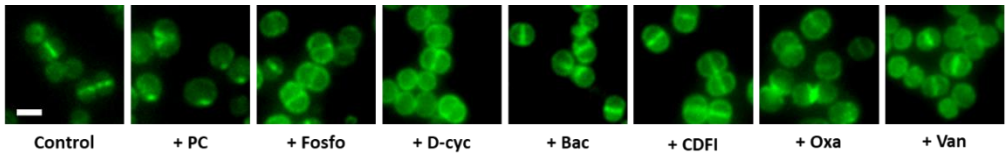

Figure 6. PBP2 delocalizes in the presence of tested cell wall targeting antibiotics. COL *pbpB*::*sgfp-pbpB* (BCBPM073) cells were imaged by epifluorescence microscopy after incubation for 60 min with 1 x MIC of PC190273 (+ PC), Fosfomycin (+Fosfo), D-cycloserine (+D-cyc), Bacitracin (+Bac), 2-(2-Chlorophenyl)-3-[1-(2,3-dimethylbenzyl)piperidin-4-yl]-5-fluoro-1H-indole (+CDFI), Oxacillin (+ Oxa) and Vancomycin (+Van). Incubation in TSB without antibiotics was used as negative control. In the presence of all antibiotics tested, septal enrichment of PBP" is lost or decreased and the protein becomes dispersed over the membrane. Scale bar = 1 µm

To test that hypothesis, we incubated cells expressing a fluorescent derivative of PBP2 (strain BCBPM073) and cells expressing GFP under the control of the *vraTSR* promoter (COL Pvra-sGFP) with increasing concentrations of vancomycin. Interestingly, we observed that PBP2 delocalized with concentrations as low as 1 µg ml^{-1} of vancomycin, while VraTSR remained untriggered at that concentration (Figure 7). In the experimental settings tested, we could only observe VraTSR activation when we incubated the cells with 10 µg ml^{-1}, a concentration ten-fold higher than that required to delocalize PBP2 from the septum (Figure 7), indicating that PBP2 delocalization alone is not the trigger for the VraTSR system.

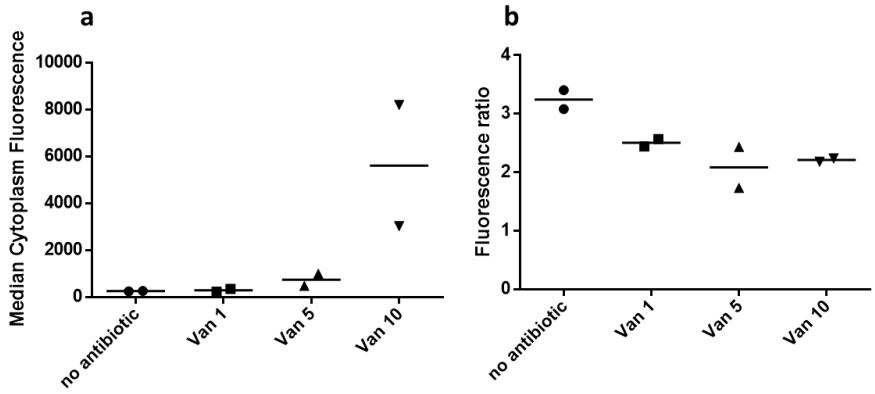

Figure 7. PBP2 delocalization does not correlate with VraTSR activation. Strains COL Pvra-sGFP and BCBPM073 (expressing a GFP fluorescent derivative of PBP2) were both incubated in the presence of increasing vancomycin concentrations (Van 1, 5 and 10 µg ml^{-1}) for 45 min. COL Pvra-sGFP cells were then stained with DNA dye Hoechst 33342, to differentiate the two populations, and mixed with BCBPM073 cells just prior to imaging on the same microscope slide **(a)** GFP fluorescence of COL Pvra-sGFP cells showing that VraTSR activation occurs only when in the presence of 10 µg ml^{-1} of vancomycin. N > 277 cells for each condition in each replicate **(b)** PBP2 septal enrichment was evaluated measuring the fluorescence ratio of GFP-PBP2 fluorescence at the septum *versus* at the cell periphery, both corrected for background fluorescence in BCBPM073 cells. PBP2 delocalized from the septum at the lowest vancomycin concentration tested. N between 62 and 90 for each condition in each experiment, experiments performed in duplicate.

As PBP2 delocalization was not the trigger for VraTSR activation, we further explored if lack of this protein or of one of its two enzymatic activities (transpeptidation and transglycosylation) activated the VraTSR system. For that purpose, the strain lacking PBP2 and containing the *vraTSR* GFP reporter (COLΔ*pbpB*_Pvra-sGFP) was complemented with plasmid-encoded PBP2, as well as plasmid-encoded alleles of PBP2, with point mutations to individually ablate transglycosylation or transpeptidation activities,

or both activities simultaneously. When COLΔ*pbpB*_Pvra-sGFP was complemented with an empty plasmid, VraTSR remained activated (Figure 8), in agreement with the data shown in Figure 5 for the *pbpB* mutant. Complementation with the double mutant of *pbpB* had similar results, indicating that it is the lack of PBP2 activity and not of the protein itself that signals CW damage. As expected, complementation with the wild type *pbpB* allele lowered *vraTSR* expression to levels equivalent to those of the parental strain COL Pvra-sGFP. We then focused on which PBP2 activity was relevant for VraTSR activation. Complementation with the construct coding for the glycosyltransferase inactive PBP2^{E114Q} resulted in induced VraTSR, suggesting that lack this activity could be key to activate the system. However, complementation with the transpeptidase-inactive PBP2^{S398G} also induced VraTSR, suggesting that either both activities are required to turn off the system or that a mutation in one domain may be compromising the activity of the other domain. In fact, the MIC of moenomycin, an antibiotic that inhibits transglycosylase activity[48], for the mutant complemented with the PBP2 lacking transpeptidase activity, showed increased susceptibility towards this antibiotic when compared with COL Pvra-sGFP, although not to the same level as the strain complemented with the PBP2 transglycosylase mutant (Figure 8b). This indicates that the mutation in the transpeptidase domain of PBP2 may be partially impairing transglycosylation activity.

a

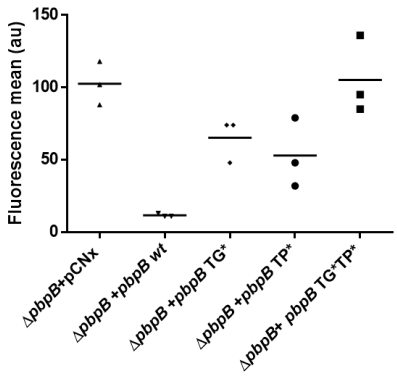

b

Strain	Moenomycin MIC
Col Pvra-sGFP	0.08 µg mL^{-1}
Δ*pbpB* +pCNx	0.0032 µg mL^{-1}
Δ*pbpB* + *pbpB* TG*	0.0032 µg mL^{-1}
Δ*pbpB* + *pbpB* TP*	0.02 µg mL^{-1}
Δ*pbpB* + *pbpB wt*	0.16 µg mL^{-1}

Figure 8. Both PBP2 activities are important for preventing VraTSR activation. (a) Strain COLΔ*pbpB*_Pvra-sGFP was complemented with plasmids encoding either the wild type allele of *pbpB* (Δ*pbpB* + *pbpB wt*), or mutated alleles encoding a glycosyltransferase inactive PBP2^{E114Q} (Δ*pbpB* + *pbpB* TG*), a transpeptidase inactive PBP2^{S398}(Δ*pbpB* + *pbpB* TP*) or a double mutant PBP2$^{E114Q\ S398}$ (Δ*pbpB* + *pbpB* TG*TP*). A control complemented with an empty vector, lacking PBP2 (Δ*pbpB* +pCNX), was also included. The VraTSR system was induced in the absence of PBP2 or in the presence of any of the tested PBP2 mutants. N = 5000 cells for each experiment, experiments performed in triplicate. Each point represents the median of one FACS experiment. **(b)** Moenomycin MICs for strains from panel (a), as well as the control strain COL Pvra-sGFP.

Taken together, these results suggest that inhibition of transglycosylase activity seems to be key in triggering the VraTSR regulatory system. We cannot discard a role for inhibition of transpeptidase activity, but we favour the former hypothesis, since (i) the depletion of the other PBPs (monofunctional transpeptidases) did not activate VraTSR and (ii) COLΔ*mgt*, a strain lacking the monofunctional transglycosylase MGT, showed VraTSR activation, albeit to low levels.

Discussion

Two-component and three-component systems (TCS) are incredibly versatile systems, capable of detecting a wide variety of stimuli[49]. Among the 16 two-component systems described in *S. aureus*, VraTSR is responsible for detecting CW damage, although the exact signal that is detected remains unknown[7,9]. Other *S. aureus* TCS, GraXSR and BraSR, also respond to damage inflicted on the CW[50,51], with additional partners being required for full activity. In the GraXSR system, which responds to antimicrobial peptides (CAMPs), the sensing mechanism depends on the ABC transporter VraFG, encoded by an operon located directly downstream of *graXRS*[50,52]. CAMPs are sensed by VraFG and the signal is transduced to GraS through a possible interaction between VraG and GraS[50]. BraSR, which responds to bacitracin, upregulates the transcription of two operons encoding ABC transporters, *braDE* and *vraDE,* which act as sensing partner and detoxification module, respectively[51]. Interestingly, both GraXSR and BraSR have IMHKs, a feature shared with the VraTSR system[50]. The putative sensing partner in the VraTSR regulatory system has been proposed to be the membrane protein VraT, though its structure and function remain undetermined[7]. Here we have shown that VraT localizes at the cell membrane, like the histidine kinase VraS, and that its C-terminal domain is extracellular. Since VraS lacks a typical histidine kinase extracellular sensing domain, the signal detection by VraTSR may be performed by VraT, as previously suggested[7].

Given the importance of VraTSR in antibiotic resistance of MRSA strains, there is great interest in identifying the signal sensed by this system. It was clear early on that the system does not directly

sense antibiotic molecules, given that structurally different molecules that target CW synthesis are capable of inducing VraTSR. The best candidate so far for the CW damage signal has been the accumulation or depletion of the peptidoglycan precursor lipid II[53]. This molecule is synthesized on the inner side of the cytoplasmic membrane and then flipped to the outer side of the membrane[35]. If accumulation of lipid II triggered the VraTSR system, then one would expect its activation in the presence of antibiotics such as vancomycin, that lead to lipid II accumulation[43], but not in the presence of antibiotics such as fosfomycin or D-cycloserine, that lead to its depletion. The reverse would be expected if depletion of lipid II was the CW damage signal. However, all tested CW targeting antibiotics triggered the VraTSR system, indicating that neither the accumulation nor the depletion of any peptidoglycan synthesis precursor is likely to correspond to this signal.

A common effect of all CW targeting antibiotics tested is the depletion of the substrate for PBPs. *S. aureus* has four native PBPs (PBP1-4), with one extra PBP (PBP2A) from an exogenous origin, with low affinity to beta-lactam antibiotics, present in MRSA strains[44]. PBP2 is the only bifunctional PBP, with both transglycosylase and transpeptidase activities, while the others are monofunctional TPases[54,55,56,24,25]. Two *S. aureus* monofunctional PBPs, namely the essential PBP1 and the non-essential PBP3, which only have transpeptidase activity, interact with cognate SEDS transglycosylases, FtsW and RodA respectively, to synthesize PG[24]. Monofunctional glycosyltransferases are also present in *S. aureus*, namely MGT and SgtA, both of which are non-essential for cell viability[57,26]. Here we showed that when we individually depleted various PG synthases, only the absence of

PBP2 led to strong VraTSR activation, while lack of MGT lead to low level activation of VraTSR. This is in accordance with previous work showing that reducing the levels of *pbpB* transcription led to higher levels of *vraTSR* transcripts[45]. PBP2 is the only PBP whose expression is directly regulated by VraR, a feature shared with MGT[9,58]. This indicates that PBP2 activity is crucial to maintain the VraTSR system in the OFF state. A second common effect of all CW targeting compounds tested, besides depletion of substrate for PBPs, is the delocalization of PBP2 from the division septum (Figure 6)[46,47]. Therefore, one possibility for the mechanism mediating the role of PBP2 in VraTSR activation could be a direct interaction between this protein and VraT/VraS, disrupted upon PBP2 delocalization in the presence of CW targeting compounds. However, this is unlikely to be the case, as we showed that PBP2 delocalization does not correlate with VraTSR activation: the former was observed in the presence of low (1 μg ml^{-1}) concentrations of vancomycin, which were insufficient for VraTSR activation (see Figure 7). In contrast, inactivation of either the transglycosylase or the transpeptidase domain of PBP2 lead to a strong activation of the VraTSR system. Unfortunately, we could not pinpoint which of the two activities had a major role, because inactivation of the transpeptidase domain of PBP2 impaired the activity of the transglycosylase domain, leading to an increased susceptibility to the transglycosylase inhibitor moenomycin. It is possible that processivity of the transglycosylase activity of PBP2 is impaired if the resulting glycans cannot be incorporated into the peptidoglycan mesh via transpeptidation. We favour the hypothesis that it is the decrease of transglycosylase activity that signals cell wall damage because removal/inactivation of the other transpeptidases (PBP1, PBP3 and PBP4) did not result in VraTSR activation, in particular

of PBP4, whose absence leads to a major decrease in peptidoglycan cross-linking[25]. Additionally, lack of MGT, and not of any of the other peptidoglycan synthases tested, also led to VraTSR activation, albeit to a lower level. A decrease of PBP2 transglycosylase activity leads to shorter glycans and therefore to an increase in the number of extremities of glycan strands, which could be sensed by VraT[31]. Alternatively, a reduction in transglycosylase activity without concomitant reduction of the activity of peptidoglycan hydrolases could lead to an increase in the concentration of a peptidoglycan hydrolysis product that could be sensed as CW damage by VraTSR. Identifying the exact CW damage signal is key to fully understanding the response of MRSA strains to beta-lactam antibiotics.

References

1. Murray CJ, Ikuta KS, Sharara F, et al. Global burden of bacterial antimicrobial resistance in 2019: a systematic analysis. *Lancet*. 2022;399(10325):629-655. doi:10.1016/S0140-6736(21)02724-0
2. Lowy FD. *Staphylococcus aureus* Infections. *N Engl J Med*. 1998;339(8):520-532. doi:10.1056/nejm199808203390806
3. Ji Q, Chen PJ, Qin G, et al. Structure and mechanism of the essential two-component signal-transduction system WalKR in *Staphylococcus aureus*. *Nat Commun*. 2016;7(1):1-11. doi:10.1038/ncomms11000
4. Krell T, Lacal J, Busch A, Silva-Jiménez H, Guazzaroni ME, Ramos JL. Bacterial sensor kinases: Diversity in the recognition of environmental signals. *Annu Rev Microbiol*. 2010;64:539-559. doi:10.1146/annurev.micro.112408.134054
5. Jacob-Dubuisson F, Mechaly A, Betton JM, Antoine R. Structural insights into the signalling mechanisms of two-component systems. *Nat Rev Microbiol*. 2018;16:585–593. doi:10.1038/s41579-018-0055-7
6. Zschiedrich CP, Keidel V, Szurmant H. Molecular Mechanisms of Two-Component Signal Transduction. *J Mol Biol*. 2016; 428(19):3752-75. doi:10.1016/j.jmb.2016.08.003
7. Boyle-Vavra S, Yin S, Jo DS, Montgomery CP, Daum RS. VraT/YvqF is required for methicillin resistance and activation of the VraSR regulon in *Staphylococcus aureus*. *Antimicrob Agents Chemother*. 2013;57(1):83-95. doi:10.1128/AAC.01651-12
8. Kuroda M, Kuroda H, Oshima T, Takeuchi F, Mori H,

Hiramatsu K. Two-component system VraSR positively modulates the regulation of cell-wall biosynthesis pathway in *Staphylococcus aureus*. *Mol Microbiol*. 2003;49(3):807-821. doi:10.1046/j.1365-2958.2003.03599.x

9. Yin S, Daum RS, Boyle-Vavra S. VraSR two-component regulatory system and its role in induction of *pbp2* and *vraSR* expression by cell wall antimicrobials in *Staphylococcus aureus*. *Antimicrob Agents Chemother*. 2006;50(1):336–343. doi:10.1128/AAC.50.1.336-343.2006
10. Dengler V, Meier PS, Heusser R, Berger-Bächi B, McCallum N. Induction kinetics of the *Staphylococcus aureus* cell wall stress stimulon in response to different cell wall active antibiotics. *BMC Microbiol*. 2011; 11,16. doi:10.1186/1471-2180-11-16
11. Belcheva A, Golemi-Kotra D. A close-up view of the VraSR two-component system: A mediator of *Staphylococcus aureus* response to cell wall damage. *J Biol Chem*. 2008;283(18):12354-12364. doi:10.1074/jbc.M710010200
12. Mascher T. Intramembrane-sensing histidine kinases: A new family of cell envelope stress sensors in Firmicutes bacteria. *FEMS Microbiol Lett*. 2006; 264(2):133-44. doi:10.1111/j.1574-6968.2006.00444.x
13. Galbusera E, Renzoni A, Andrey DO, et al. Site-specific mutation of *Staphylococcus aureus* VraS reveals a crucial role for the VraR-VraS sensor in the emergence of glycopeptide resistance. *Antimicrob Agents Chemother*. 2011;55(3):1008-1020. doi:10.1128/AAC.00720-10
14. Belcheva A, Verma V, Korenevsky A, Fridman M, Kumar K, Golemi-Kotra D. Roles of DNA sequence and sigma A factor in transcription of the VraSR operon. *J Bacteriol*.

2012;194(1):61-71. doi:10.1128/JB.06143-11

15. Utaida S, Dunman PM, Macapagal D, et al. Genome-wide transcriptional profiling of the response of *Staphylococcus aureus* to cell-wall-active antibiotics reveals a cell-wall-stress stimulon. *Microbiology*. 2003;149(10):2719-2732. doi:10.1099/mic.0.26426-0
16. McCallum N, Stutzmann Meier P, Heusser R, Berger-Bächi B. Mutational analyses of open reading frames within the *vraSR* operon and their roles in the cell wall stress response of *Staphylococcus aureus. Antimicrob Agents Chemother*. 2011;55(4):1391–1402. doi:10.1128/AAC.01213-10
17. Charpentier E, Anton AI, Barry P, Alfonso B, Fang Y, Novick RP. Novel cassette-based shuttle vector system for gram-positive bacteria. *Appl Environ Microbiol*. 2004;70(10):6076-6085. doi:10.1128/AEM.70.10.6076-6085.2004
18. Monteiro JM, Fernandes PB, Vaz F, et al. Cell shape dynamics during the staphylococcal cell cycle. *Nat Commun*. 2015; 6,8055. doi:10.1038/ncomms9055
19. Arnaud M, Chastanet A, Débarbouillé M. New vector for efficient allelic replacement in naturally nontransformable, low-GC-content, gram-positive bacteria. *Appl Environ Microbiol*. 2004;70(11):6887-6891. doi:10.1128/AEM.70.11.6887-6891.2004
20. Pereira PM, Veiga H, Jorge AM, Pinho MG. Fluorescent reporters for studies of cellular localization of proteins in *Staphylococcus aureus*. *Appl Environ Microbiol*. 2010;76(13):4346-4353. doi:10.1128/AEM.00359-10
21. Nair DR, Monteiro JM, Memmi G, et al. Characterization of a novel small molecule that potentiates β-lactam activity against gram-positive and gram-negative pathogens.

Antimicrob Agents Chemother. 2015;59(4):1876-1885. doi:10.1128/AAC.04164-14

22. Monk IR, Shah IM, Xu M, Tan MW, Foster TJ. Transforming the untransformable: Application of direct transformation to manipulate genetically *Staphylococcus aureus* and *Staphylococcus epidermidis*. *MBio*. 2012;3(2). doi:10.1128/mBio.00277-11
23. Gill SR, Fouts DE, Archer GL, et al. Insights on evolution of virulence and resistance from the complete genome analysis of an early methicillin-resistant *Staphylococcus aureus* strain and a biofilm-producing methicillin-resistant *Staphylococcus epidermidis* strain. *J Bacteriol*. 2005;187(7):2426-2438. doi:10.1128/JB.187.7.2426-2438.2005
24. Reichmann NT, Tavares AC, Saraiva BM, et al. SEDS–bPBP pairs direct lateral and septal peptidoglycan synthesis in *Staphylococcus aureus*. *Nat Microbiol*. 2019;4(8):1368-1377. doi:10.1038/s41564-019-0437-2
25. Memmi G, Filipe SR, Pinho MG, Fu Z, Cheung A. *Staphylococcus aureus* PBP4 is essential for β-lactam resistance in community-acquired methicillin-resistant strains. *Antimicrob Agents Chemother*. 2008;52(11):3955-3966. doi:10.1128/AAC.00049-08
26. Reed P, Veiga H, Jorge AM, Terrak M, Pinho MG. Monofunctional transglycosylases are not essential for *Staphylococcus aureus* cell wall synthesis. *J Bacteriol*. 2011;193(10):2549-2556. doi:10.1128/JB.01474-10
27. Reed P, Atilano ML, Alves R, et al. *Staphylococcus aureus* survives with a minimal peptidoglycan synthesis machine but sacrifices virulence and antibiotic resistance. *PLoS Pathog*. 2015;11(5):e1004891. doi:10.1371/journal.ppat.1004891

28. Tan CM, Therien AG, Lu J, et al. Restoring methicillin-resistant *Staphylococcus aureus* susceptibility to β-lactam antibiotics. *Sci Transl Med*. 2012;4(126):126ra35. doi:10.1126/scitranslmed.3003592
29. Oshida T, Tomasz A. Isolation and characterization of a Tn551-autolysis mutant of *Staphylococcus aureus*. *J Bacteriol*. 1992;174(15):4952-4959. doi:10.1128/JB.174.15.4952-4959.1992
30. Kraemer GR, Iandolo JJ. High-frequency transformation of *Staphylococcus aureus* by electroporation. *Curr Microbiol*. 1990;21(6):373-376. doi:10.1007/BF02199440
31. Pinho MG, De Lencastre H, Tomasz A. An acquired and a native penicillin-binding protein cooperate in building the cell wall of drug-resistant staphylococci. *Proc Natl Acad Sci U S A*. 2001;98(19):10886-10891. doi:10.1073/pnas.191260798
32. Fisher AC, DeLisa MP. Laboratory evolution of fast-folding green fluorescent protein using secretory pathway quality control. *PLoS One*. 2008;3(6):e2351. doi:10.1371/journal.pone.0002351
33. Liu Q, Cho H, Yeo WS, Bae T. The extracytoplasmic linker peptide of the sensor protein SaeS tunes the kinase activity required for staphylococcal virulence in response to host signals. *PLoS Pathog*. 2015. doi:10.1371/journal.ppat.1004799
34. Manoil C, Beckwith J. A genetic approach to analyzing membrane protein topology. *Science*. 1986;233(4771):1403-1408. doi:10.1126/science.3529391
35. van Heijenoort J. Assembly of the monomer unit of bacterial peptidoglycan. *Cell Mol Life Sci C*. 1998;54(4):300-304. doi:10.1007/s000180050155

36. Kahan FM, Kahan JS, Cassidy PJ, Kropp H. The mechanism of action of fosfomycin (phosphonomycin). *Ann N Y Acad Sci*. 1974;235(1):364-386. doi:10.1111/j.1749-6632.1974.tb43277.x

37. Lambert MP, Neuhaus FC. Mechanism of D-cycloserine action: alanine racemase from *Escherichia coli* W. *J Bacteriol*. 1972;110(3):978-987. doi:10.1128/jb.110.3.978-987.1972

38. Huber J, Donald RGK, Lee SH, et al. Chemical Genetic Identification of Peptidoglycan Inhibitors Potentiating Carbapenem Activity against Methicillin-Resistant *Staphylococcus aureus*. *Chem Biol*. 2009;16(8):837-848. doi:10.1016/j.chembiol.2009.05.012

39. Stone KJ, Strominger JL. Mechanism of action of bacitracin: complexation with metal ion and C 55 -isoprenyl pyrophosphate. *Proc Natl Acad Sci U S A*. 1971;68(12):3223-3227. doi:10.1073/pnas.68.12.3223

40. Beauregard DA, Williams DH, Gwynn MN, Knowles DJC. Dimerization and membrane anchors in extracellular targeting of vancomycin group antibiotics. *Antimicrob Agents Chemother*. 1995;39(3):781-785. doi:10.1128/AAC.39.3.781

41. Ghuysen JM. Serine β-lactamases and penicillin-binding proteins. *Annu Rev Microbiol*. 1991;45:37-67. doi:10.1146/annurev.mi.45.100191.000345

42. Schirner K, Eun YJ, Dion M, et al. Lipid-linked cell wall precursors regulate membrane association of bacterial actin MreB. *Nat Chem Biol*. 2015;11(1):38-45. doi:10.1038/nchembio.1689

43. Qiao Y, Srisuknimit V, Rubino F, et al. Lipid II overproduction allows direct assay of transpeptidase inhibition by β-lactams.

Nat Chem Biol. 2017;13(7):793. doi:10.1038/nchembio.2388

44. Scheffers D-J, Pinho MG. Bacterial cell wall synthesis: New insights from localization studies. *Microbiol Mol Biol Rev*. 2005;69(4):585-607. doi:10.1128/mmbr.69.4.585-607.2005
45. Gardete S, Wu SW, Gill S, Tomasz A. Role of VraSR in antibiotic resistance and antibiotic-induced stress response in *Staphylococcus aureus*. *Antimicrob Agents Chemother*. 2006;50(10):3424-3434. doi:10.1128/AAC.00356-06
46. Pinho MG, Errington J. Recruitment of penicillin-binding protein PBP2 to the division site of *Staphylococcus aureus* is dependent on its transpeptidation substrates. *Mol Microbiol*. 2005;55(3):799-807. doi:10.1111/j.1365-2958.2004.04420.x
47. Mann PA, Müller A, Xiao L, et al. Murgocil is a highly bioactive staphylococcal-specific inhibitor of the peptidoglycan glycosyltransferase enzyme MurG. *ACS Chem Biol*. 2013;8(11):2442-2451. doi:10.1021/cb400487f
48. Ostash B, Walker S. Moenomycin family antibiotics: Chemical synthesis, biosynthesis, and biological activity. *Nat Prod Rep*. 2010;27(11):1594-1617. doi:10.1039/c001461n
49. Stock AM, Robinson VL, Goudreau PN. Two-component signal transduction. *Annu Rev Biochem*. 2000;69:183-215. doi:10.1146/annurev.biochem.69.1.183
50. Falord M, Karimova G, Hiron A, Msadeka T. GraXSR proteins interact with the VraFG ABC transporter to form a five-component system required for cationic antimicrobial peptide sensing and resistance in *Staphylococcus aureus*. *Antimicrob Agents Chemother*. 2012;56(2):1047-1058. doi:10.1128/AAC.05054-11
51. Hiron A, Falord M, Valle J, Débarbouillé M, Msadek T. Bacitracin and nisin resistance in *Staphylococcus aureus*: A

novel pathway involving the BraS/BraR two-component system (SA2417/SA2418) and both the BraD/BraE and VraD/VraE ABC transporters. *Mol Microbiol*. 2011; 81(3):602-22. doi:10.1111/j.1365-2958.2011.07735.x

52. Li M, Cha DJ, Lai Y, Villaruz AE, Sturdevant DE, Otto M. The antimicrobial peptide-sensing system aps of *Staphylococcus aureus*. *Mol Microbiol*. 2007;66(5):1136-1147. doi:10.1111/J.1365-2958.2007.05986.X
53. Jordan S, Hutchings MI, Mascher T. Cell envelope stress response in Gram-positive bacteria. *FEMS Microbiol Rev*. 2008;32(1):107-146. doi:10.1111/j.1574-6976.2007.00091.x
54. Murakami K, Fujimura T, Doi M. Nucleotide sequence of the structural gene for the penicillin-binding protein 2 of *Staphylococcus aureus* and the presence of a homologous gene in other staphylococci. *FEMS Microbiol Lett*. 1994;117(2):131-136. doi:10.1111/j.1574-6968.1994.tb06754.x
55. Hartman BJ, Tomasz A. Low-affinity penicillin-binding protein associated with β-lactam resistance in *Staphylococcus aureus*. *J Bacteriol*. 1984;158(2):513-516. doi:10.1128/jb.158.2.513-516.1984
56. Pereira SFF, Henriques AO, Pinho MG, De Lencastre H, Tomasz A. Role of PBP1 in cell division of *Staphylococcus aureus*. *J Bacteriol*. 2007;189(9):3525-3531. doi:10.1128/JB.00044-07
57. Wang QM, Peery RB, Johnson RB, Alborn WE, Yeh WK, Skatrud PL. Identification and characterization of a monofunctional glycosyltransferase from *Staphylococcus aureus*. *J Bacteriol*. 2001;183(16):4779-4785. doi:10.1128/JB.183.16.4779-4785.2001

58. Sengupta M, Jain V, Wilkinson BJ, Jayaswal RK. Chromatin immunoprecipitation identifies genes under direct VraSR regulation in *Staphylococcus aureus*. *Can J Microbiol*. 2012;58(6):703-708. doi:10.1139/W2012-043

Chapter V

Discussion and future perspectives

Chapter contents

Revisiting the *Staphylococcus. aureus* cell cycle 207
Heterogeneity in *S. aureus* response to β-lactams 212
VraTSR activation mechanism: an unsolved puzzle 215
Final Remarks 218

Revisiting the *Staphylococcus aureus* cell cycle

Cell biology studies of *Staphylococcus aureus*, an important pathogen known for its ability to resist antibiotic treatment, are difficult because of the small size of its cells, which are around 1 µm in diameter. This small size has impaired a detailed analysis of the morphology of these bacteria during the cell cycle, due to resolution limit of conventional light microscopy. However, over recent years, new microscopy techniques have enabled a more detailed analysis of this pathogen, allowing us to get a clearer picture of how it grows and divides. Here, we used super-resolution microscopy to study in detail how this microorganism grows and divides, which is essential to better understand how it resists antibiotics and to think of innovative strategies to develop new antimicrobial compounds.

The first studies regarding the *S. aureus* cell cycle concluded that staphylococcal cells divided in three successive perpendicular planes over three consecutive division cycles and remained spherical until the moment of division[1]. The use of light microscopy did not enable an accurate measurement of morphological changes and volume variations during the whole cycle. Interestingly, though, even early works mention that cells “swell” before each division and that separation of the two daughter cells is preceded by an abrupt popping event[1]. When we reassessed this process, using Super-Resolution Structured Illumination Microscopy (SR-SIM), we found that cells gradually increase their volume throughout the cell cycle, from an average volume of 0.47 μm^3, at the beginning of the cycle to 0.91 μm^3, immediately before splitting of the mother cell. We evaluated these data in light of the different models for cell size

regulation in bacteria[2,3,4,5,6]. Briefly, the “sizer” model postulates that reaching a specific cell size triggers initiation of chromosome replication, while the “timer” model states that cell division is dependent on the age of the cell[2,3,4,5]. More recently, a third model, called “adder, was proposed in which cells would add a constant size between their size at birth and size at division, for a specific growth condition[6]. *S. aureus* cells displayed relatively constant sizes at birth (0.47 ±0.07 μm^3) and immediately before division (0.91±0.12 μm^3), which could be compatible with a model that exclusively depends on the absolute size of the cell to determine the timing of division[4]. However, the fact that we did not follow each cell for a complete cycle, to avoid photodamage bias, impaired an accurate analysis of the size added to each cell individually, during that cycle. Therefore, we could not determine if the cell size increment was conserved between different cells, the fundamental basis of the ”adder” model, where the size added to each cell, in each generation, is independent of the cell size at birth[6]. Our data from time-lapse experiments was also not ideal to test the timer model because photodamage is cumulative and could introduce a bias towards longer duration of growth phases. Nevertheless, we noticed that the period comprised between mother cell division and the beginning of the next round of division was not constant amongst cells (31±6 min), with some outliers taking considerably longer to divide, which is not in agreement with the “Timer” model.

One interesting observation was that the continuous cell growth observed during the whole cycle was accompanied by a slight cell elongation, which had not been previously described for *S. aureus*. However, differently from rod-shaped bacteria such as *B. subtilis,* volume increase in *S. aureus* results from an increase of cell length

and width, while the growth in rods volume increase during the cell cycle is due to cell elongation with width remaining constant[7].

We characterised the staphylococcal cell cycle in three different phases: Phase 1 (P1) includes cells that have recently divided and have not started the synthesis of the new septum; Phase 2 (P2) includes cells that are undergoing septum formation; Phase 3 (P3) cells have a septum fully closed, undergoing maturation, before dividing into the two daughter cells. *S. aureus* cells typically spend approximately half of their cycle in P1 and the other half distributed equally between P2 and P3[8]. Immediately after the splitting of the mother cell, daughter cells tend to be more spherical in shape and as P1 progresses they become slightly more elongated. This elongation is halted when cells are synthesizing the new septum and is restarted in P3, when volume increase was also more pronounced, before the next splitting event[8]. These observations questioned the existing model, that postulated that *S. aureus* cells would only experience a more pronounced variation in cell volume during splitting of the septum in the mother cell, when the flat surface of the newly exposed septum is reshaped into a curved surface to generate one hemisphere of each daughter cell. The underlying fundament of this model was that the localization of CW synthesis machinery is localized mostly at the division septum, where most cell wall synthesis takes place, so no cell surface enlargement would occur due to insertion of new cell wall material at the cell periphery[9,10,11,12]. The volume increase would happen during the reshaping of the flat septum into a curved hemisphere through the reorganization of the elastic PG mesh, thus increasing the cell surface area. However, an abrupt change in volume upon septum splitting would result in a massive fluctuation in the

concentration of metabolites and other cellular compounds, which seems incompatible with cellular homeostasis. This model seemed even less likely, when we found that the time period comprised between the splitting of the mother cell and the reshaping of the flat septum is extremely short, less than 2 ms[8]. Our measurements of the cell volume immediately after cell splitting also showed that daughter cells (0.47 μm^3) had, on average, nearly half the volume of the mother cell (0.91 μm^3), implying that the reshaping of the flat septum was not accounting for the volume duplication[8].

We also observed that the CW material originated from the septum accounted only for roughly a third of the total surface area of each new daughter cell and that low levels of PG incorporation can occur around the entire cell surface, mediated by the activity of PG synthase PBP4. PG synthases are not the only enzymes responsible for PG remodelling, because PG growth or elongation requires the cleavage of covalent bonds by PG hydrolases to allow the incorporation of the newly attached material, thus preserving the thickness and integrity of the CW[13,14]. Depletion of the major autolysin (Atl) in *S. aureus* leads to larger and more spherical cells, suggesting a role of this enzyme in shape maintenance and size regulation[8]. Atl is an enzyme known to be required for cell separation and localises in rings at the division site[15,16]. Previous studies using atomic force microscopy imaging have shown the presence of holes around the bacterial circumference at the division site, that enlarge until they merge generating a single larger perforation[17]. It was suggested that these holes are the result of autolytic activity to prepare for cell splitting[17]. Sle1 and LytN hydrolases were also shown to localise in the vicinity of the cross-wall, the mid-cell compartment in the septum, processing PG to

allow for daughter cell separation[18]. Although the role of autolysins is crucial for cell splitting, it does not explain how septum splitting occurs in an extremely fast manner, in less than 2 ms. This may be explained by a mechanical mechanism, where the splitting is driven by circumferential mechanical stress originating from turgor pressure[19]. Thus, we decided to explore the dynamics of cell splitting and reshaping of the flat septum, likely driven by turgor pressure[8]. In agreement with that hypothesis, we observed that septum reshaping was impaired in high osmolarity conditions. On the other hand, we also found that mutants lacking autolysins, such as Sle1 and LytM, had an enrichment of cells in which the flat septum remained intact (D-shaped cells), after splitting of the daughter cells[8]. Furthermore, mutants deficient in Sle1 had a longer Phase 3 of the cell cycle, during which cells are preparing for division, after septum closure. Taken together, this suggests a role of Sle1 in both cell separation and reshaping of the flat septum into a new hemisphere. In conclusion, cell separation and reshaping of the flat septum seem to require both mechanical stress and enzymatic activity to be executed.

Our work allowed us to redefine the cell cycle of *S. aureus* and gave crucial contributions to rethink previous models for the mode of division of this important pathogen. *S. aureus* was generally thought to divide in three alternating orthogonal planes over three consecutive division cycles, an assumption that is no longer valid, after we showed that cell surface scars from previous divisions do not divide the cell in equal parts, a feature that had been proposed to contain epigenetic information regarding the previous planes of division[20,21].

Heterogeneity in *S. aureus* response to β-lactams

S. aureus strains have developed resistance to various classes of antibiotics, including β-lactam antibiotics. This is due to the presence of an exogenous transpeptidase called PBP2A[22]. Despite the resistance mechanism being well studied, less is known about antibiotic tolerance and phenotypic variability, heterogeneity in cell behaviour which is not generated by genetic mutations[23]. Fluctuations in transcription and translation can lead to differences in the level of proteins of isogenic cells, in the same environmental conditions[24,25]. Bacterial populations often show unimodal variation in the expression of a given gene, due to these fluctuations, also called genetic noise[26]. Noise can sometimes originate a second pattern of variation that is non-unimodal, where the population bifurcates into subpopulations, a process called "bistability"[26]. One mechanism known to generate this phenotypic phenomenon is positive autoregulation of a gene leading to a non-linear response[26].

In *S. aureus*, the TCS VraTSR is encoded by the operon *vraUTSR*, whose promoter is upregulated by one of the proteins of the complex (VraR)[27]. This fact prompted us to explore whether *vraTSR* expression would lead to the bifurcation of the population, and if one of the sub-populations would have increased tolerance or susceptibility towards cell wall targeting antibiotics. In our work, however, we never observed a bifurcation of the population, but *vraTSR* expression did show high variance, with cells expressing this operon at different levels, after the system was induced with the CW targeting antibiotic CDFI[28]. Our goal was then to see whether these different levels of *vraTSR* expression had any

correlation with tolerance to CW targeting antibiotics. VraTSR is a system responsible for triggering the response of the cells when in the presence of CW targeting antibiotics, and its disruption leads to a decrease in resistance to this group of antibiotics[29,30]. One could expect that, given this biological role, cells expressing higher levels of *vraTSR* could be better protected against antibiotic treatment. To test this idea, we followed the cells expressing GFP under the control of the *vraTSR* promoter in a time-lapse experiment, in the presence of inhibitory concentrations of oxacillin, after previous induction of *vraTSR* with sub-inhibitory concentrations of the same antibiotic. We estimated the survival probabilities for different *vraTSR* levels using the Cox Proportional Hazards model. This model allows the estimation of the effect of a continuous variable, such as *vraTSR* expression (evaluated through GFP signal intensity) on bacterial survival. Interestingly, we saw that cells expressing higher levels of *vraTSR* were slightly more susceptible to antibiotic treatment than those expressing lower levels. We considered the possibility of *vraTSR* requiring an optimal level to be effective, above which it would start to become deleterious for the cell, like gene dosage toxicity[31], as it would lead to imbalance in the pathways involving enzymes regulated by VraR, such as CW synthesis, carbohydrate transport and metabolism or ion transport[32]. It is possible that cells expressing higher levels of *vraTSR* transcription were those to which more damage was inflicted causing then to die at higher rates. A limitation in our studies was that we did not follow cells during the initial incubation with sub-inhibitory concentration of antibiotic, and therefore cannot evaluate the effect of timing of VraTSR production onset on tolerance.

It would be interesting to study the genes under direct control of VraR, such as *pbp2*, a gene coding for a major PG synthase in *S. aureus*[33], to see if the same expression pattern is maintained or if we could detect bistable populations using a different reporter. A strain where *vraTSR* was placed under the control of an inducible promoter would also help to confirm if cells expressing higher levels of *vraTSR* are less tolerant to the presence of β-lactams. We actually tried to construct this strain, without success.

We were initially planning to study the VraTSR response over time, using microfluidic plates, where live cells would be followed during both the pre-treatment with sub-MIC concentration of antibiotic and the above MIC challenge. To our surprise, we saw that cells inside this platform were triggering VraTSR, albeit to low level, even in the absence of antibiotic. We hypothesized ther mechanical forces could disturb CW growth dynamics, as described previously[34], triggering VraTSR. Localisation of some proteins, like MreB, in *E. coli*[35], even depend on cell curvature. The possibility of VraTSR responding to a mechanical force compressing the CW against the cell membrane posed an interesting model. VraT, a membrane-anchored protein, could sense periplasm length variations, by interacting with a CW component, like PG. In fact, we have shown that VraTSR responded to conditions where periplasm length is expected to vary, like during an osmotic shock, but our work was inconclusive in determining a specific mechanism. These unexpected, yet interesting results, led us to revisit the signal behind VraTSR activation, a mechanism that remains elusive[29].

VraTSR activation mechanism: an unsolved puzzle

VraTSR is a TCS in *S. aureus* that works as a sentinel system responsible to detect a perturbation of CW synthesis and to coordinate a cellular response, also known as cell wall stress stimulon (CWSS)[36,37,38]. This response is interpreted as an attempt by the microorganism to defend itself against the action of cell wall targeting antibiotics[38]. From the four genes encoded in the operon: (*vraU*, *vraT*, *vraS* and *vraR*), *vraU* is the only gene whose product has no apparent role in the signal transduction regulatory system[29,30]. Deletion of this gene has no influence on resistance against CW targeting compounds[29,30]. The other three genes encode VraT, VraS and VraR, which are thought to work together, constituting a three component system[29]. VraT, a hypothetical protein, that we've shown localises at the membrane, was proposed to be responsible for the detection of the still unknown stimulus[29] as VraS, the histidine kinase of the regulatory system, lacks an evident extracellular sensing domain, characteristic of IMHKs[39]. VraT homologs in other Gram-positive bacteria, like *Streptococcus suis* or *Staphylococcus epidermidis,* remain poorly studied [40,41]. However, in *B. subtilis*, the VraT homologue LiaF is known to be a repressor of the LiaS kinase, keeping the LiaFSR regulatory system inactive in the absence of CW damage[39].

The stimulus sensed by VraTSR remains unknown. Given that the system is activated by structurally different antibiotic molecules, it seems implausible that it would respond directly to the antibiotics. A better candidate is Lipid II, since it is an essential component of bacterial peptidoglycan synthesis pathway and its synthetic pathway is considered to be the bottleneck of CW biosynthesis[42,43].

However, we showed that VraTSR responds to antibiotics that lead to opposite outcomes regarding lipid II cellular availability, *i.e.* antibiotics that lead to lipid II accumulation and antibiotics that block lipid II synthesis. This suggests that lipid II is unlikely to be the trigger for the cell wall damage response in *S. aureus.*

A common effect to all cell wall targeting antibiotics is the depletion of substrates of PBPs, so we though lack of activity of one or more PBPs could trigger VraTSR. When we deleted various CW synthesis enzymes, we found that depletion of PBP2, the only bifunctional PBP in *S. aureus*, and the monofunctional transglycosylase MGT, activated VraTSR. Interestingly, both belong to the VraR regulon[44,45]. Previous studies had shown that decreasing *pbpB* transcription levels resulted in increasing levels of *vraTSR* expression[36]. Since the activity of PBP2 seemed particularly important for keeping VraTSR in the OFF state, and that this enzyme delocalises with all CW targeting antibiotics that we have tested, we wondered whether the signal sensed by VraTSR could be the delocalisation of PBP2. However, that was not the case, as we could uncouple PBP2 delocalization from VraTSR activation using low concentrations of vancomycin that caused the former but not the latter phenotype. In agreement, the FtsZ inhibitor PC190273, a compound we showed that did not activate VraTSR, was able to delocalise PBP2, in agreement with previous reports[46]. Furthermore, past work from our laboratory showed that a *S. aureus* COL strain containing a minimal PG synthesis machinery, encoding only PBP1 and PBP2, showed upregulation of the *vraTSR*, while displaying correct localization of both enzymes[47]. All these data seem consistent with our findings,

ruling out PBP2 delocalisation as the trigger mechanism behind VraTSR activation.

PBP2 is the only bifunctional CW synthetic enzyme in *S. aureus*, capable of catalyzing both transglycosylation and transpeptidation reactions. We tried to evaluate which activity was more important for keeping VraTSR in the OFF-state, but mutations in either the transglycosylase domain or transpeptidase domain rendered VraTSR activation. We noticed though that the mutation in the transpeptidase domain probably affected TG activity, since it led to an increased susceptibility to the transglycosylase inhibitor moenomycin. This suggests that PG synthesis by PBP2 may need both activities. Without a fully operational TPase, glycan strands continue to be polymerized without being integrated into the PG mesh and that may be deleterious for the cell. In fact, it was reported for *E. coli* that blocking TPase activity by β-lactams generates uncrosslinked glycan strands that are rapidly degraded, setting up a futile cycle of synthesis and degradation[48]. Although we could not identify which activity was more relevant to keep VraTSR OFF, we lean towards transglycosylase activity for two reasons. First, depletion of all the other PBPs, which display monofunctional transpeptidase activity, did not result in VraTSR activation. Specially PBP4, whose absence leads to a major decrease in peptidoglycan cross-linking[49]. Second, the only other enzyme whose depletion led to VraTSR activation (although to lower levels) was the monofunctional transglycosylase MGT. We can conjecture whether VraT/VraS sense the amount of glycan extremities, since lack of transglycosylation was shown to lead to shorter glycans[50]. A pull-down assay to test for interaction between a purified VraT protein with PG would help to shed some light on

this subject. Or even evaluating if VraT was binding or changing conformation, in the presence of different PG components, like N-acetylglucosamine (GlcNAc) or N-acetylmuramic acid (MurNAc) by nuclear magnetic resonance spectroscopy or circular dichroism. Another hypothesis could be that a reduction in transglycosylation could create an imbalance in CW metabolism, between the *de novo* PG synthesis and turnover, accumulating a hydrolysis by-product that could be sensed by VraT/VraS. Analysing the VraTSR response in mutants devoid of different autolysins, such as amidases, glucosaminidases or endopeptidases could help to determine if this is the case. On this matter, it is interesting to note that CW lytic activity is downregulated in response to CW synthesis inhibition by vancomycin, for example[32].

Final Remarks

Our work explored two of the most fascinating topics regarding *S. aureus* biology, its cell cycle, and its ability to tackle antibiotic treatment. We made significant advances in fundamental areas like the cell cycle characterisation, paving the way for further research not only in chromosome segregation, but also cell division mechanics. Understanding these fundamental biological processes and identifying which proteins are involved is crucial to provide new targets for antimicrobial compounds. Regarding antibiotic resistance mechanisms, we were able to gain new insights into the role of a regulatory system which is one of the many strategies used by *S. aureus* to evade antibiotic action, though I regret not identifying the molecular mechanism detected by this sentinel system after so many years dedicated to this research topic. We hope to have that and other answers in the future.

References

1. Tzagoloff H, Novick R. Geometry of cell division in *Staphylococcus aureus*. *J Bacteriol*. 1977;129(1): 343–350. doi:10.1128/jb.129.1.343-350.1977

2. Lotka AJ. The Stability of the Normal Age Distribution. *Proc Natl Acad Sci*. 1922;8(11):339-345. doi:10.1073/pnas.8.11.339

3. Gyllenberg M. Nonlinear age-dependent population dynamics in continuously propagated bacterial cultures. *Math Biosci*. 1982;62(1):45-74. doi:10.1016/0025-5564(82)90062-1

4. Jun S, Si F, Pugatch R, Scott M. Fundamental principles in bacterial physiology-history, recent progress, and the future with focus on cell size control: A review. *Reports Prog Phys*. 2018;81(5):056601. doi:10.1088/1361-6633/aaa628

5. Diekmann O, Lauwerier HA, Aldenberg T, Metz JAJ. Growth, fission and the stable size distribution. *J Math Biol*. 1983;18(2):135-148. doi:10.1007/BF00280662

6. Taheri-Araghi S, Bradde S, Sauls JT, *et al*. Cell-size control and homeostasis in bacteria. *Curr Biol*. 2015;25(3):385-391. doi:10.1016/j.cub.2014.12.009

7. Burdett IDJ, Kirkwood TBL, Whalley JB. Growth kinetics of individual *Bacillus subtilis* cells and correlation with nucleoid extension. *J Bacteriol*. 1986;167(1):219-230. doi:10.1128/jb.167.1.219-230.1986

8. Monteiro JM, Fernandes PB, Vaz F, et al. Cell shape

dynamics during the *staphylococcal* cell cycle. *Nat Commun*. 2015;6(1):8055. doi:10.1038/ncomms9055

9. Pinho MG, Errington J. Dispersed mode of *Staphylococcus aureus* cell wall synthesis in the absence of the division machinery. *Mol Microbiol*. 2003;50(3):871-881. doi:10.1046/J.1365-2958.2003.03719.X

10. Pinho MG, Errington J. Recruitment of penicillin-binding protein PBP2 to the division site of *Staphylococcus aureus* is dependent on its transpeptidation substrates. *Mol Microbiol*. 2005;55(3):799-807. doi:10.1111/j.1365-2958.2004.04420.x

11. Pereira SFF, Henriques AO, Pinho MG, De Lencastre H, Tomasz A. Role of PBP1 in cell division of *Staphylococcus aureus*. *J Bacteriol*. 2007;189(9):3525-3531. doi:10.1128/JB.00044-07

12. Atilano ML, Pereira PM, Yates J, *et al*. Teichoic acids are temporal and spatial regulators of peptidoglycan cross-linking in *Staphylococcus aureus*. *Proc Natl Acad Sci U S A*. 2010;107(44):18991-18996. doi:10.1073/pnas.1004304107

13. Vermassen A, Leroy S, Talon R, Provot C, Popowska M, Desvaux M. Cell wall hydrolases in bacteria: Insight on the diversity of cell wall amidases, glycosidases and peptidases toward peptidoglycan. *Front Microbiol*. 2019;10:331. doi:10.3389/fmicb.2019.00331

14. Vollmer W. Bacterial growth does require peptidoglycan hydrolases. *Mol Microbiol*. 2012;86(5):1031-1035. doi:10.1111/mmi.12059

15. Sugai M, Komatsuzawa H, Akiyama T, *et al*. Identification of

endo-β-N-acetylglucosaminidase and N-acetylmuramyl-L-alanine amidase as cluster-dispersing enzymes in *Staphylococcus aureus*. *J Bacteriol*. 1995;177(6):1491-1496. doi:10.1128/jb.177.6.1491-1496.1995

16. Yamada S, Sugai M, Komatsuzawa H, *et al*. An autolysin ring associated with cell separation of *Staphylococcus aureus*. *J Bacteriol*. 1996;178(6):1565-1571. doi:10.1128/jb.178.6.1565-1571.1996

17. Touhami A, Jericho MH, Beveridge TJ. Atomic force microscopy of cell growth and division in *Staphylococcus aureus*. *J Bacteriol*. 2004;186(11):3286-3295. doi:10.1128/JB.186.11.3286-3295.2004

18. Frankel MB, Schneewind O. Determinants of murein hydrolase targeting to cross-wall of *Staphylococcus aureus* peptidoglycan. *J Biol Chem*. 2012;287(13):10460-10471. doi:10.1074/jbc.M111.336404

19. Zhou X, Halladin DK, Rojas ER, *et al*. Mechanical crack propagation drives millisecond daughter cell separation in *Staphylococcus aureus*. *Science*. 2015;348(6234):574–578. doi:10.1126/science.aaa1511

20. Saraiva BM, Sorg M, Pereira AR, *et al*. Reassessment of the distinctive geometry of *Staphylococcus aureus* cell division. *Nat Commun*. 2020;11(1):1-7. doi:10.1038/s41467-020-17940-9

21. Turner RD, Ratcliffe EC, Wheeler R, Golestanian R, Hobbs JK, Foster SJ. Peptidoglycan architecture can specify division planes in *Staphylococcus aureus*. *Nat Commun*.

2010;1:26. doi:10.1038/ncomms1025

22. Fishovitz J, Hermoso JA, Chang M, Mobashery S. Penicillin-binding protein 2a of methicillin-resistant *Staphylococcus aureus*. *IUBMB Life*. 2014;66(8): 572–577. doi:10.1002/iub.1289

23. Smits WK, Kuipers OP, Veening JW. Phenotypic variation in bacteria: The role of feedback regulation. *Nat Rev Microbiol*. 2006;4(4):259-271. doi:10.1038/nrmicro1381

24. Raser JM, O'Shea EK. Molecular biology - Noise in gene expression: Origins, consequences, and control. *Science*. 2005; 309(5743):2010–2013. doi:10.1126/science.1105891

25. Kærn M, Elston TC, Blake WJ, Collins JJ. Stochasticity in gene expression: from theories to phenotypes. *Nat Rev Genet 2005 66*. 2005;6(6):451-464. doi:10.1038/nrg1615

26. Dubnau D, Losick R. Bistability in bacteria. *Mol Microbiol*. 2006; 61(3):564-72. doi:10.1111/j.1365-2958.2006.05249.x

27. Belcheva A, Golemi-Kotra D. A close-up view of the VraSR two-component system: A mediator of *Staphylococcus aureus* response to cell wall damage. *J Biol Chem*. 2008;283(18):12354-12364. doi:10.1074/jbc.M710010200

28. Huber J, Donald RGK, Lee SH, *et al*. Chemical genetic identification of peptidoglycan inhibitors potentiating carbapenem activity against methicillin-resistant *Staphylococcus aureus*. *Chem Biol*. 2009;16(8):837-848. doi:10.1016/j.chembiol.2009.05.012

29. Boyle-Vavra S, Yin S, Jo DS, Montgomery CP, Daum RS.

VraT/YvqF is required for methicillin resistance and activation of the VraSR regulon in *Staphylococcus aureus*. *Antimicrob Agents Chemother*. 2013;57(1):83-95. doi:10.1128/AAC.01651-12

30. McCallum N, Stutzmann Meier P, Heusser R, Berger-Bächi B. Mutational analyses of open reading frames within the *vraSR* operon and their roles in the cell wall stress response of *Staphylococcus aureus*. *Antimicrob Agents Chemother*. 2011;55(4):1391–1402. doi:10.1128/AAC.01213-10

31. Bhattacharyya S, Bershtein S, Yan J, et al. Transient protein-protein interactions perturb *E. coli* metabolome and cause gene dosage toxicity. *Elife*. 2016;5:e20309 . doi:10.7554/eLife.20309

32. Kuroda M, Kuroda H, Oshima T, Takeuchi F, Mori H, Hiramatsu K. Two-component system VraSR positively modulates the regulation of cell-wall biosynthesis pathway in *Staphylococcus aureus*. *Mol Microbiol*. 2003;49(3):807-821. doi:10.1046/j.1365-2958.2003.03599.x

33. Scheffers D-J, Pinho MG. Bacterial cell wall synthesis: New insights from localization studies. *Microbiol Mol Biol Rev*. 2005;69(4):585-607. doi:10.1128/mmbr.69.4.585-607.2005

34. Si F, Li B, Margolin W, Sun SX. Bacterial growth and form under mechanical compression. *Sci Rep*. 2015;5(1):1-11. doi:10.1038/srep11367

35. Ursell TS, Nguyen J, Monds RD, *et al*. Rod-like bacterial shape is maintained by feedback between cell curvature and cytoskeletal localization. *Proc Natl Acad Sci U S A*.

2014;111(11):1025-1034. doi:10.1073/pnas.1317174111

36. Gardete S, Wu SW, Gill S, Tomasz A. Role of VraSR in antibiotic resistance and antibiotic-induced stress response in *Staphylococcus aureus*. *Antimicrob Agents Chemother*. 2006;50(10):3424-3434. doi:10.1128/AAC.00356-06

37. Dengler V, Meier PS, Heusser R, Berger-Bächi B, McCallum N. Induction kinetics of the *Staphylococcus aureus* cell wall stress stimulon in response to different cell wall active antibiotics. *BMC Microbiol*. 2011;11:16. doi:10.1186/1471-2180-11-16

38. Utaida S, Dunman PM, Macapagal D, et al. Genome-wide transcriptional profiling of the response of *Staphylococcus aureus* to cell-wall-active antibiotics reveals a cell-wall-stress stimulon. *Microbiology*. 2003;149(10):2719-2732. doi:10.1099/mic.0.26426-0

39. Mascher T. Intramembrane-sensing histidine kinases: A new family of cell envelope stress sensors in Firmicutes bacteria. *FEMS Microbiol Lett*. 2006;264(2):133-144. doi:10.1111/j.1574-6968.2006.00444.x

40. Zhong X, Zhang Y, Zhu Y, et al. The two-component signaling system VraSRss is critical for multidrug resistance and full virulence in *Streptococcus suis* serotype 2. *Infect Immun*. 2018;86(7):e00096-18. doi:10.1128/IAI.00096-18

41. Wu Y, Meng Y, Qian L, *et al*. The vancomycin resistance-associated regulatory system VraSR modulates biofilm formation of *Staphylococcus epidermidis* in an *ica*-dependent manner. *mSphere*. 2021;6(5):e00641-21.

doi:10.1128/msphere.00641-21

42. Breukink E, de Kruijff B. Lipid II as a target for antibiotics. *Nat Rev Drug Discov*. 2006;5(4):321-323. doi:10.1038/nrd2004

43. Jordan S, Hutchings MI, Mascher T. Cell envelope stress response in Gram-positive bacteria. *FEMS Microbiol Rev*. 2008;32(1):107-146. doi:10.1111/j.1574-6976.2007.00091.x

44. Yin S, Daum RS, Boyle-Vavra S. VraSR two-component regulatory system and its role in induction of *pbp2* and *vraSR* expression by cell wall antimicrobials in *Staphylococcus aureus*. *Antimicrob Agents Chemother*. 2006;50(1):336–343. doi:10.1128/AAC.50.1.336-343.2006

45. Sengupta M, Jain V, Wilkinson BJ, Jayaswal RK. Chromatin immunoprecipitation identifies genes under direct VraSR regulation in *Staphylococcus aureus*. *Can J Microbiol*. 2012;58(6):703-708. doi:10.1139/W2012-043

46. Tan CM, Therien AG, Lu J, *et al*. Restoring methicillin-resistant *Staphylococcus aureus* susceptibility to β-lactam antibiotics. *Sci Transl Med*. 2012;4(126):126ra35. doi:10.1126/scitranslmed.3003592

47. Reed P, Atilano ML, Alves R, *et al*. *Staphylococcus aureus* survives with a minimal peptidoglycan synthesis machine but sacrifices virulence and antibiotic resistance. *PLoS Pathog*. 2015;11(5):e1004891. doi:10.1371/journal.ppat.1004891

48. Cho H, Uehara T, Bernhardt TG. Beta-lactam antibiotics induce a lethal malfunctioning of the bacterial cell wall synthesis machinery. *Cell*. 2014;159(6):1300-1311.

doi:10.1016/j.cell.2014.11.017

49. Memmi G, Filipe SR, Pinho MG, Fu Z, Cheung A. *Staphylococcus aureus* PBP4 is essential for β-lactam resistance in community-acquired methicillin-resistant strains. *Antimicrob Agents Chemother*. 2008;52(11):3955-3966. doi:10.1128/AAC.00049-08

50. Pinho MG, De Lencastre H, Tomasz A. An acquired and a native penicillin-binding protein cooperate in building the cell wall of drug-resistant *staphylococci. Proc Natl Acad Sci U S A*. 2001;98(19):10886-10891. doi:10.1073/pnas.191260798

ITQB NOVA, Avenida da República, 2780-157 Oeiras, Portugal | Tel +351 214 469 100 | itqb.unl.pt